METAL-BASED CHEMOSENSORS FOR AMINO ACIDS, PEPTIDES, AND NUCLEOTIDES

THÈSE N^{O} 3886 (2007)

PRÉSENTÉE LE 7 SEPTEMBRE 2007

À LA FACULTÉ DES SCIENCES DE BASE
LABORATOIRE DE CHIMIE SUPRAMOLÉCULAIRE
PROGRAMME DOCTORAL EN CHIMIE ET GÉNIE CHIMIQUE

ÉCOLE POLYTECHNIQUE FÉDÉRALE DE LAUSANNE

POUR L'OBTENTION DU GRADE DE DOCTEUR ÈS SCIENCES

PAR

Andrey BURYAK

Diploma of Chemistry, Moscow State University, Russie
et de nationalité russe

acceptée sur proposition du jury:

Prof. P. Vogel, président du jury
Prof. K. Severin, directeur de thèse
Prof. P. J. Dyson, rapporteur
Prof. L. Fabbrizzi, rapporteur
Prof. J.-L. Reymond, rapporteur

ÉCOLE POLYTECHNIQUE
FÉDÉRALE DE LAUSANNE

Suisse
2007

Acknowledgements

I really spent a wonderful time at EPFL and would like to thank cordially:

My supervisor Professor Kay Severin for giving me the opportunity to work on an inspiring project and for keeping his door always open for discussions at any time.

Dr. Alexei Pozdnoukhov for a fruitful collaboration.

Rosario Scopelliti and Euro Solari, who performed all the X-ray crystallographic analysis.

Anita Schori, Patrick Favre, Giovanni Petrucci, Jacque Gremaud, and Gladys Pache for their unresting support.

Our secretary Christina Zamanos for her ready help with all administrative issues (and for speaking Russian with me from time to time).

All my laboratory colleagues Barnali Dutta, Burcak Icli, Christian Albrecht, Céline Olivier, Estelle Burri, Evgeny Kataev, Dalit Rechavi-Robinson, Davinia Fernandez, Frederike Zaubitzer, Isabelle Saur, Joffrey Wolf, Katrin Thommes, Laurent Quebatte, Lionel Tournier, Nicolas Christinat, Marie-Line Lehaire, Sebastien Rochat, Sebastien Gauthier, Sebastian Mirtschin, Thomas Brasey, Vera Janowski, Wang Mang, and Zacharias Grote on whom I could always rely for their ready cooperation and availability, and who have also provided an enjoyable working environment.

People who are not explicitly mentioned here but who helped me one way or another.

Version Abrégée

Le complexe de métal de transition $[Cp^*RhCl_2]_2$ ainsi que des colorants commercialement disponibles, ont été utilisés pour appliquer la méthode d'analyse par déplacement d'indicateur (Indicator Displacement Assay - IDA) pour détecter les peptides, les acides aminés et les nucléotides. Nous avons trouvé que la combinaison de complexe du Cp*Rh avec le colorant azophloxine compose un ensemble senseur pour détecter les peptides contenant une histidine ou une méthionine dans l'eau à pH neutre. Une interaction forte entre le complexe de rhodium et les peptides contenant une histidine ou méthionine dans la position 1 ou 2 a permis de détecter ces peptides jusqu'a une concentration de 0.3 μM.

Le même complexe organométallique et trois colorants commercialement disponible ont été utilisés pour composer un ensemble de senseurs IDA pour détecter les acides aminés. Nous avons trouvé qu'une variation de pH peut être utilisée efficacement pour modifier la sélectivité d'un senseur. Une excellente discrimination de 20 acides aminés a été atteinte.

La combinaison du complexe $[Cp^*RhCl_2]_2$ avec les colorants gallocyanine, evans blue et mordant yellow 10 forme un IDA multicomposant (MIDA) qui peut être utilisé pour detecter des concentrations millimolaires de nucléotides et l'anion pyrophosphate (PPi) en solutions aqueuse tamponée. De plus, le MIDA permet de déterminer simultanément les concentrations d'ATP et PPi/cAMP avec une seule mesure UV-Vis.

Dans la deuxième partie de notre travail, nous avons examiné si les bibliotheques combinatoires dynamiques (BCD) peuvent être utilisées comme senseurs chimiques. Il a été trouvé que les colorants arsenazo I, methylcalcein blue et glycine cresol red, avec les sels $CuCl_2$ et $NiCl_2$ forment une BCD de complexes différemment colorées. L'introduction d'une analyte capable de réagir avec les membres d'une telle BCD résulte en un ré-équilibrage facilement détectable par spectroscopie UV-Vis. Utilisant les dipeptides comme analytes, nous avons constaté que cette façon de détection est très efficace: même des peptides très semblables comme les régioisomères (Ala-Phe vs. Phe-Ala) et stéréoisomères (Phe-Ala vs. D-Phe-Ala) peuvent facilement être discriminées. De plus, nous avons constaté que l'identité du meilleur senseur dépend du problème à résoudre.

Mots-Clés

Organométallique ◦ Senseur Chimique ◦ Rhodium ◦ Acide Aminé

Nucléotide ◦ Peptide ◦ Chimie Combinatoire ◦ Spectroscopie UV-Vis

Abstract

An organometallic 4d transition metal complex $[Cp^*RhCl_2]_2$, together with commercially available dyes, was used to construct indicator displacement assays (IDAs) for the detection of peptides, amino acids, and nucleotides. The combination of the Cp*Rh complex with the dye azophloxine was found to form a chemosensing ensemble for the sequence-selective detection of histidine- and methionine-containing peptides in water at neutral pH. A strong interaction of the rhodium complex with peptides bearing histidine or methionine residue in the position 1 or 2 allowed to detect these peptides down to a concentration of 0.3 μM.

The same organometallic complex and three commercially available dyes were employed to compose an array of IDA chemosensors for the detection of natural amino acids. We found that the variation of the pH can effectively be used to modulate the selectivity of an IDA sensor. An excellent discrimination of 20 amino acids was achieved.

The combination of $[Cp^*RhCl_2]_2$ with the dyes gallocyanine, evans blue, and mordant yellow 10 forms a multicomponent indicator displacement assay (MIDA), which can be used to sense low millimolar concentrations of nucleotides and the pyrophosphate anion in buffered aqueous solution. Moreover, the MIDA allows to simultaneously determine the concentrations of adenosine triphosphate and pyrophosphate/cyclic adenosine monophosphate with a single UV-Vis measurement.

In the second part of our work we investigated whether dynamic combinatorial libraries (DCLs) can be used for sensing purposes. We found that the dyes arsenazo I, methylcalcein blue, and glycine cresol red, in combination with the metal salts $CuCl_2$ and $NiCl_2$, form a DCL of differently colored metal-dye complexes. The addition of an analyte able to interact with a member(s) of such a library, results in a re-equilibraion easily detectable by UV-Vis spectroscopy. Using dipeptides as analytes we demonstrated that this way of sensing is very effective - even closely related peptides such as regio- (Ala-Phe *vs*. Phe-Ala) and stereo- (Phe-Ala *vs*. D-Phe-Ala) isomers can easily be discriminated. Additionally, we found that the identity of the best sensor depends on the problem to be addressed.

Keywords

Organometallic ◦ Chemosensor ◦ Rhodium ◦ Amino Acid

Nucleotide ◦ Peptide ◦ Combinatorial Chemistry ◦ UV-Vis spectroscopy

Table of Content

Chapter 1 *Introduction*

1.1. Chemosensors: short introduction

Chemical sensors are usually understood to be devices that transform chemical information into analytically useful signals. More generally, the term chemosensor has been defined as a molecule of abiotic origin that signals the presence of matter or energy.[1] The development of artificial chemical sensors was largely stimulated by the practical interest in detecting biologically and environmentally important analytes. Though biosensors may have high affinity and selectivity for biological analytes, chemosensors have many potential advantages. Biosensors are sensitive to pH, oxidizing agents and heat, while abiotic sensors can be synthesized from more robust components. Artificial sensors can, in principle, be tailored for various analytes, and their physical properties can be adjusted to meet specific sensor requirements.

The basic design principle of a chemosensor is that the sensing event has to be related to an easy-to-measure signal. In fact, many chemosensors display changes in either color[2,3] or fluorescence[4] in the presence of a certain guest molecule. But changes in electrochemical properties such as the oxidation potential of redox active groups have also been used.[5] Our work focuses on optical chemosensors so for the sake of simplicity we'll discuss only this type of signal generation. Numerous optical chemosensors have been synthesized and the research in the field has extensively been reviewed.[6-10]

Here we will give a short introduction into the development of optical chemical sensors. The design of optical chemosensors has continuously evolved. In the first approach explored, the sensors feature the receptor unit as part of the chromophore/fluorophore.[11] In these systems, which have been named *intrinsic chemosenors*, the interaction between the bound substrate and the dye (chromophore or fluorophore) leads directly to the modification of its emission properties (Scheme 1-1).

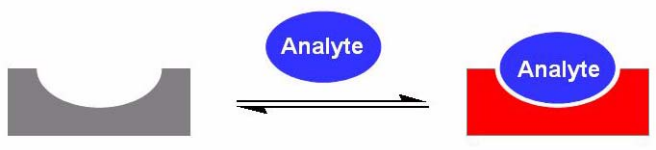

Scheme 1-1 An intrinsic chemosensor.

An example of such sensor, which is able to bind creatinine via three hydrogen bonds, was designed by Bell *et al.*.[12] Creatinine is extracted from buffered water into a chloroform solution of the receptor **1**, producing a proton shift from the phenolic OH group to a naphthyridine nitrogen atom (Scheme 1-2). As a result, a new broad adsorption band in the region 400-500 nm appears. This tautomerisation illustrates how analyte binding can strongly influence an intrinsic chemosensor to produce a large optical response.

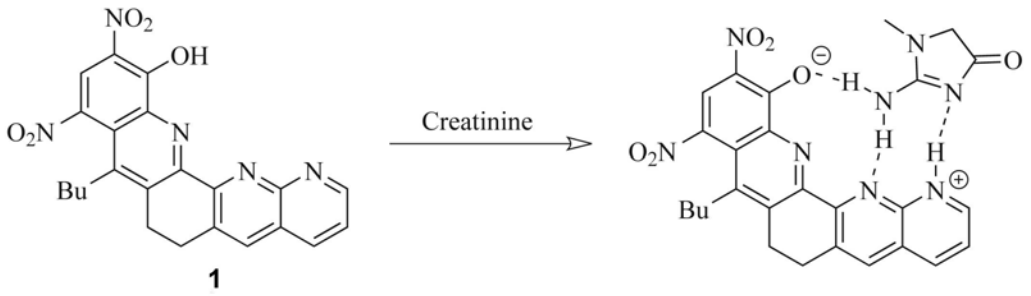

Scheme 1-2 Proton shift in the chemosensor **1** upon binding of creatinine.

In another example by D'Souza *et al.*, the neutral zinc porphyrin **2** was tested as a fluorescencent sensor for nicotine (Figure 1.1).[13] It was observed by both UV-Vis and fluorescence spectroscopy that **2** binds nicotine in toluene solution. The molecular recognition events are believed to involve the pyridyl nitrogen of nicotine axially ligating the zinc ion and the pyrrolidine nitrogen hydrogen bonding to the carboxylic acid group. The result is a batochromic shift of the Soret and visible bands of **2** and a decrease in the intensity of the emission bands of the zinc porphyrin fluorophore at 605 and 650 nm.

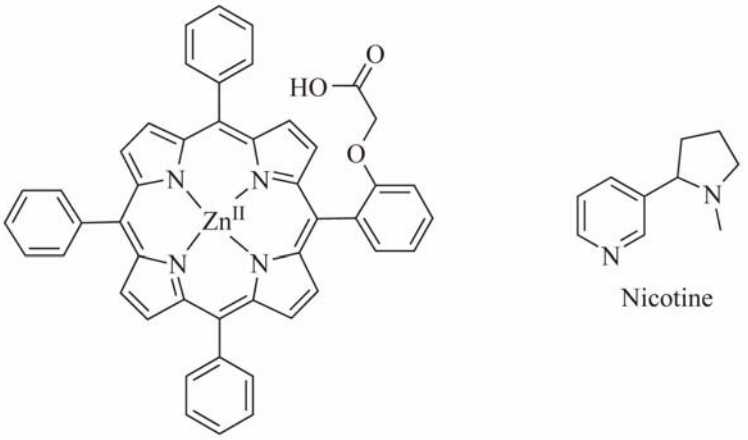

Figure 1.1 A neutral zinc porphyrin complex **2** designed to bind nicotine.

These chemosensors are relatively easy to make, but they are intrinsically rigid as they have to be designed around the substrate; any modification of the binding site, in order to modify its selectivity or affinity for the substrate, may result in a change in emission properties of the dye. For this reason, the evolution and the optimization of this type of sensors may not be easy from the synthetic point of view.

A second strategy, which was largely inspired by the developments in the field of supramolecular chemistry, is based on the construction of a sensor in which the receptor (binding unit) is separated from the dye (signalling unit), although the two subunits are kept in close proximity by means of covalent links (Scheme 1-3). In these kinds of sensors, referred to as *conjugate chemosensors*, the two subunits can be designed, separately optimized, and then eventually connected. Such a modular approach clearly allows more flexibility than the previous one, but still the dye and the receptor must be covalently linked. The overall design of the system must integrate a transduction mechanism, needed to allow proper communication between the two subunit in order to convert the recognition of the analyte into a signal. Below we illustrate the concept of a conjugate chemosensor by a few examples.

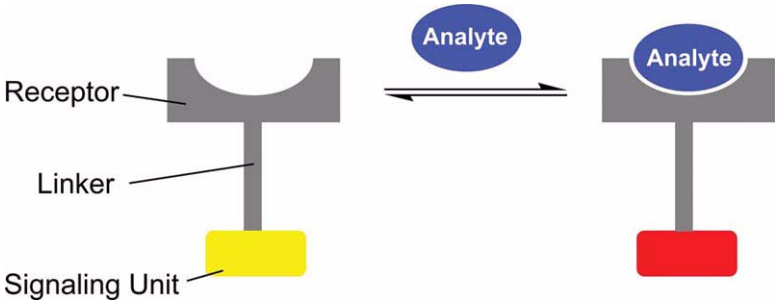

Scheme 1-3 A conjugate chemosensor.

Compound **3**, comprised of an amidobenzocrown ether group as the receptor, a pyrenyl group as a signalling unit, and an alkyl spacer, was studied as a potential chemosensor for alkali metal ions (Figure 1.2).[14] In solution, an intramolecular exciplex between the fluorophore and the receptor is formed and the fluorescence of the former is suppressed due to a photoinduced electron transfer (PET) from the amidobenzocrown moiety. Upon complexation of an alkali metal cation by the receptor, the formation of the intramolecular exciplex becomes impossible and the PET becomes suppressed which results in enhanced fluorescence.

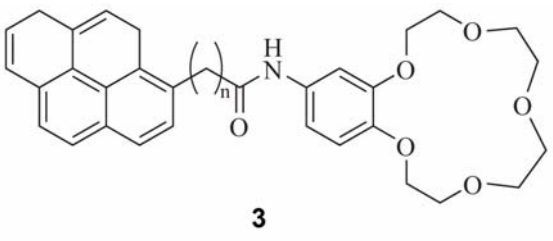

3

Figure 1.2 Fluorescent chemosensor **3** for alkali metal ions.

As an example of a fluorescent sensor for anions, Czarnik *et al.* described the two-component chemosensor **4**, where an antracene fragment serves as a signalling unit and is linked through a methylene group to a branched tetraamine (Scheme 1-4).[15] In an aqueous solution at pH 6, the emission intensity of the antracene subunit is low due to the quenching by the electron pair of the only non-protonated nitrogen. On addition of hydrogenphosphate, the fluorescence of **4** is enhanced. It is suggested that this is due to the coordination of the anion: in

particular, an intracomplex proton transfer occurs between the hydrogenphosphate anion and the non-protonated nitrogen which suppresses the fluorescence quenching.

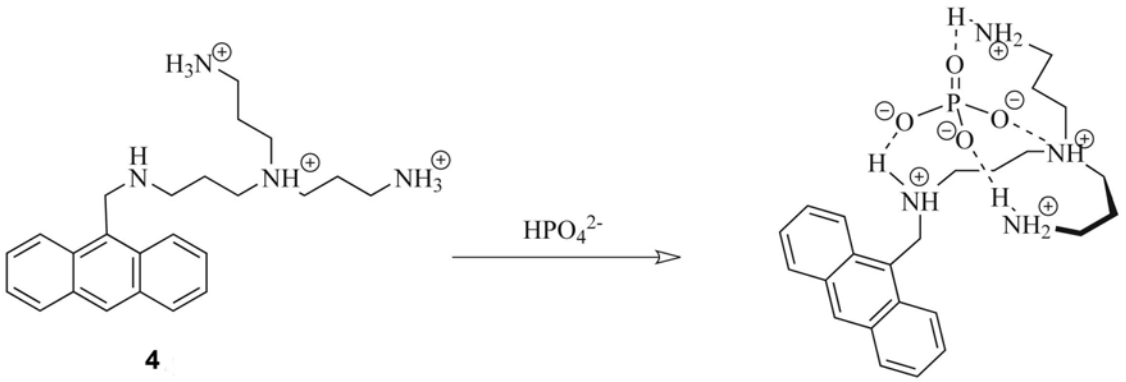

4

Scheme 1-4 Sensing of the HPO_4^{2-} anion by the chemosensor **4**.

Another example of a conjugate chemosensor represents compound **5**, which was designed to bind alkildiammonium ions $H_3N^+(CH_2)_nNH_3^+$ (Figure 1.3).[16] Here, two azocrowns are responsible for the ammonium binding while the antracene part of the sensor signals the binding event. The fluorescence of the antracene moiety is quenched by photoinduced electron transfer (PET) from the two nitrogens. When both nitrogens' electron pairs form hydrogen bonds with the diammonium ion, PET is inhibited, resulting in enhanced fluorescence. As might be expected, the selectivity of the chemosensor is dependent on the distance between the two cations and, in fact, the highest binding constant was found for protonated 1,3-propylenediamine.

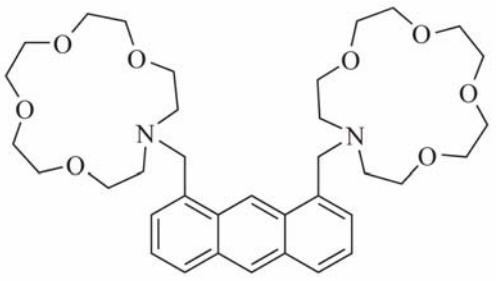

5

Figure 1.3 Fluorescent chemosensor **5** for protonated diamines.

In this section, we described several examples of what can be considered as “classical chemosensors”: intrinsic and conjugate chemosensors. Another approach for making chemical sensors, based on self-assembly methodology, will be discussed in the next section.

1.2. Chemosensing ensembles

Self-assembly and self-organizing processes have attracted increasing attention during the last years in the chemistry of complex systems with functional properties.[17] Indeed, they are at the basis of the so called ‘bottom-up” approach for making complex molecular systems. The building of complex structures, following this strategy, requires the design and synthesis of a limited number of relatively simple building blocks, which are then allowed to self-organize. As a result of the molecular organization into a supramolecular assembly, novel properties and functions may result and lead to possible important applications.

Therefore, self-assembly of receptors and dyes can, at least partially, overcome the synthetic problems connected to classical covalent systems, and provide an efficient strategy for an easy realisation and optimization of optical chemosensors. In this case, there is no need for covalent links between the subunits, they only have to be designed in such a way as to favor their assembly in solution. Among the different strategies[18-21] that can be followed to exploit such principles, at present, one approach appears to be the most promising. It is based on a competitive assay, in which the dye and the substrate compete for the receptor.[10,22,23] The displacement of the dye from the complex results in a change of its optical properties. These self-assembled chemosensors are made by mixing a dye, a substrate, and a receptor which is able to interact with both chemical species, but with different binding strength. Following the design principle, these systems have been named *chemosensing ensembles*.

The chemosensing ensemble strategy is based on a competition assay and works in a manner similar to that of many antibody-based biosensors in competitive immunoassays:[24] a solution containing the unlabelled antigen is added to the antibody receptor that is associated with a labelled antigen. Upon displacement of the latter, a signal modulation is observed. Likewise, the supramolecular version of this assay uses a recognition unit, designed for selective interaction with a desired analyte, along with an external indicator (a UV-Visible chromophore or a fluorescent dye) that associates with the recognition unit in the absence of the analyte. When the analyte is added, the indicator is displaced, thus leading to measurable

changes in its optical properties (Scheme 1-5). This method is also referred to as *indicator displacement assay* (IDA).[10]

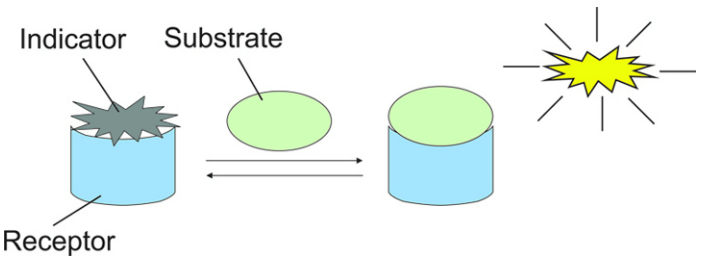

Scheme 1-5 An indicator displacement assay.

This methodology has several advantages in comparison with classical chemosensors. It can be applied to a variety of receptors without the need for covalent attachment of the indicator, which, in turn, can be selected from a large pool of commercially available fluorescent or UV-visible chromophores. The indicators may be chosen on the basis of their optical properties or on their association ability compared with that of the analyte. Additionally, the indicator-receptor ratio can be varied according to specific needs.[25] Moreover, in this set-up, the indicator does not interact directly with the analyte. Upon release from the complex, the indicator experiences a change of interactions, from those within the complex to those with solvent molecules, and such a change of the indicator environment produces a measurable signal. Therefore, the analyte is not involved in the transduction mechanism; this feature is particularly important, because it allows the detection of substrates that do not change directly the optical properties of the indicator.

Although the use of chemosensing ensembles is easy and convenient, it has been developed only in last ten years. After two early examples reported by Inouye[26] and Shinkai[27] and their co-workers, it has been explored by the group of Anslyn, who reported a chemosensing system for the detection of citrate in aqueous media.[28] Receptor **6** was found to be selective for citrate over dicarboxylates, phosphates, sugars, and simple salts in water (Scheme 1-6). Due to the preorganization of the three guanidinium moieties on the same face of the receptor and the ability to form multiple hydrogen-bonding and charge-pairing interactions, it binds citrate better than simple dicarboxylic or monocarboxylic acids by factors of around 35 and 700, respectively. The anionic fluorescent dye 5-carboxyfluorescein (**7**) was used as an indicator in methanol-water solution buffered at pH 7.4. Binding between **6** and **7**

(K_a = 4.7*10^{3}M^{-1}) lowers the pK_a of the phenol moiety of **7** causing its deprotonation. Upon addition of citrate to the ensemble (K_a = 2.9*10^{5}M^{-1}), the carboxyfluorescein is released as a phenol-protonated species, and, as a result, a decrease of the indicator's fluorescence is observed which allows the quantitative detection of citrate. The ensemble was used to determine citrate concentration in commercial beverages that contain high concentrations of potentially competitive anions, including malate, ascorbate, lactate, benzoate and phosphates.

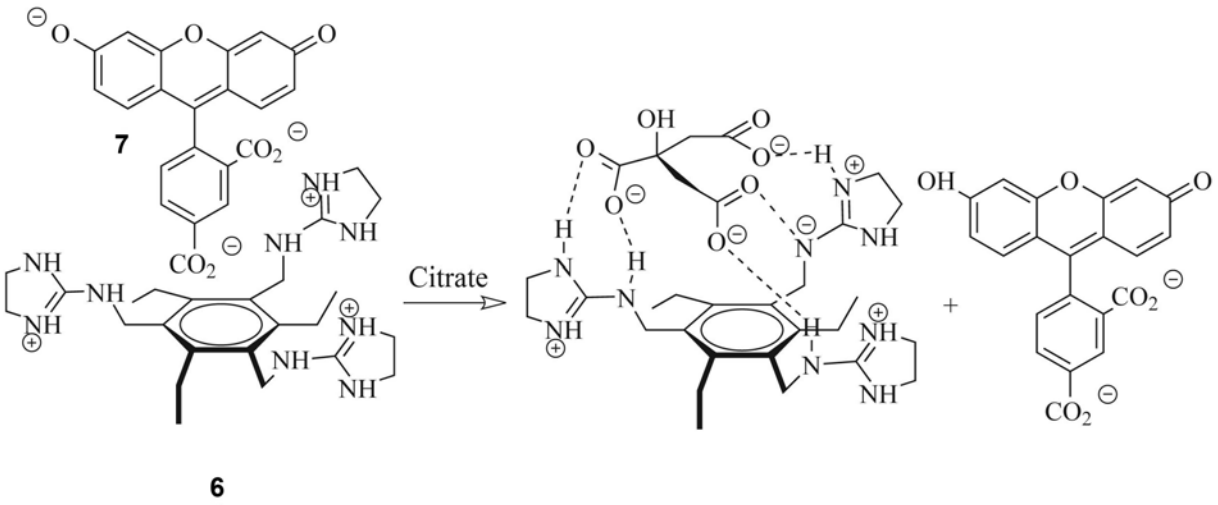

Scheme 1-6 The chemosensing ensemble for the detection of citrate.

The same aromatic scaffold was used to construct the receptor **8** with one pendent boronic acid (Figure 1.4). The receptor was used to analyze tartrate **9**, a natural product in grape juices and wines.[29] Tartrate contains two carboxylates and one diol. The guanidinium moieties and the boronic acid were incorporated into **8** in order to bind the carboxylates and the diol, respectively. From competition experiments with alizarin complexon (**10**), the binding constant between the receptor **8** and the analyte **9** was calculated as 5.5*10^4 M^{-1}.

Receptor **8** was also used in the threshold detection of malate in Pinot Noir grapes.[25] The ratio of the receptor-indicator was adjusted so that it creates significant color changes when *one* equivalent of malate had been added. The same group reported IDA-based chemosensing ensembles for the detection of inositol-1,4,5-trisphosphate,[30] adenosine triphosphate,[31] aspartate,[32] heparin,[33] phosphate,[34] short peptides,[35] α-hydroxyacids,[36] phosphoesters,[37] and amino acids,[38] among others.

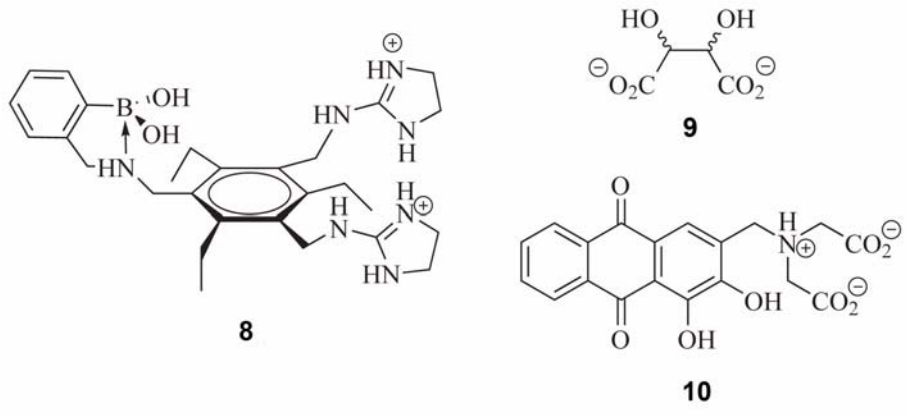

Figure 1.4 A chemosensing ensemble for the detection of tartrate (**9**).

Another example of a successful implementation of the indicator-displacement strategy is Sessler's pyrrolic receptor **11** for halogen anions (Figure 1.5).[39] This meso-octamethylcalix[4]pyrrole has a higher affinity for the fluoride anion than for other halides. It binds to the anion on the basis of H-bonds through the pyrrolic hydrogen atoms. Using the 4-nitrophenolate anion **12** as an indicator, Sessler and co-workers were able to detect the association of fluoride with the receptor based on the color change that results from the displacement of **12**.

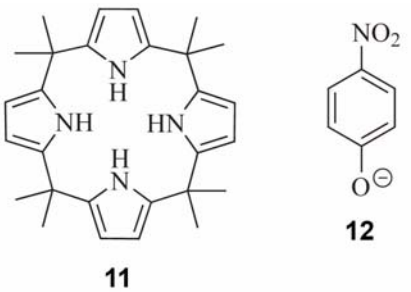

Figure 1.5 A chemosensing ensemble for the detection of the fluoride anion.

The importance of adenosine triphosphate (ATP) in biological systems has inspired many chemists to find suitable sensors. Akkaya and co-workers found that the calixpyridinium receptor **13** has a high affinity for ATP (Figure 1.6).[40] The tetraanionic indicator **14** was used for fluorescence detection. Due to the cationic nature of **13**, indicator **14** was a suitable choice

for ion-pairing interactions. Upon the introduction of ATP, **14** was displaced from **13** and higher fluorescence emission was observed. The binding constant between **13** and ATP was found to be $2.87*10^4$ M^{-1}.

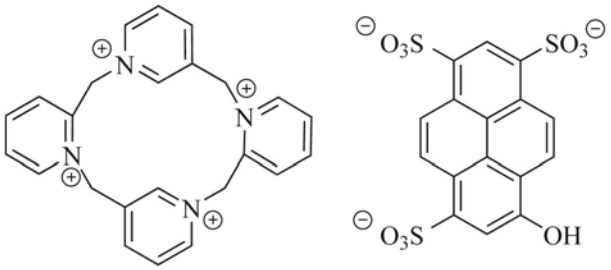

Figure 1.6 A chemosensing ensemble for the detection of ATP.

In the previous examples of indicator-displacement assays, electrostatic interactions, hydrogen bonding or formation of boronic esters have been employed to mediate the interaction between the indicator and the binding site of the receptor. But metal-ligand interactions can be used for this purpose as well. In a metal-based indicator-displacement assay, the receptor is composed from a metal ion(s) coordinated by one or several ligands. An indicator is allowed to coordinate with the metal center and, eventually, the ligand(s). Addition of an analyte to the system causes the displacement of the indicator from the metal and the ligand(s). This results in optical changes that can be measured to derive the binding affinity. Zinc(II) and copper(II) complexes have been used most often though rhodium[41] and ytterbium[42] have been employed as well. The advantage of this approach is that it can operate in highly polar solvents (aqueous ethanol or pure water) and display strong affinity towards anionic substrates. One of the pioneers of this method is the Fabbrizzi group.

In one example, the dicopper(II) cryptate complex **15** forms a long ellipsoidal cavity, in which two copper ions are rigidly held in a distance of 11.3 Å (Figure 1.7).[43] Therefore, **15** is particularly well suited for the inclusion of bidentate anions, such as dicarboxylates, the donor groups of which are well separated and able to interact with both metal ions. Carboxyrhodamine **16**, which contains two carboxylate groups and emits at 571 nm was chosen as the indicator. In water at pH 7, it binds to the receptor (K_a = 10^7 M^{-1}) and its fluorescence is completely quenched, probably through a photoinduced electron transfer or an electronic energy transfer from the metal centre to the excited fluorophore. Addition of

dicarboxylate derivatives, such as phtalate isomers and aliphatic α,ω-dicarboxylate, results in the displacement of the rhodamine dye from the complex and in the recovery of its fluorescence emission. Due to the geometric constrains imposed by the rigid structure of the receptor, the system is able to discriminate between different substrates on the basis of the distance between the two carboxylic functions. Thus, among the phtalate isomers only the 1,4-derivative, binds to the receptor more strongly ($K_a = 10^8\ M^{-1}$) than the dye, and can efficiently displace it from the complex. The other derivatives bind to the receptor more weakly ($K_a < 3.2*10^4\ M^{-1}$) and, as a consequence, the 1,4-derivative can be detected selectively. A similar behavior is observed for aliphatic α,ω-dicarboxylic acids. The derivatives that contain five or six carbon atoms are detected selectively over the shorter or longer analytes. The strong metal-ligand interactions established between the receptor and the anion easily compensate for the unfavourable dehydratation effects and allows recognition in pure water at neutral pH.

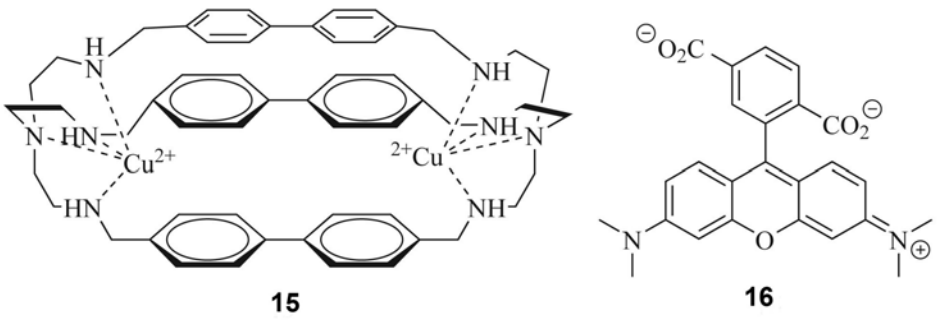

Figure 1.7 A chemosensing ensemble for the detection of dicarboxylates.

The same strategy was applied by Fabbrizzi *et al.* for the detection of pyrophosphate and histidine in water.[44,45] The pyrophosphate anion plays an important role in bioenergetic and metabolic processes.[46] Receptor **17** was designed to incorporate two copper ions in order to gain affinity for analytes (Figure 1.8). Eosine (**18**) was one of the indicators used in this study. Results showed that **17** binds to pyrophosphate better than monophosphate due to the ability of pyrophosphate to coordinate the two copper centres. The same receptor was also able to discriminate histidine from glycine, phenylalanine, valine, leucine, and proline. This is because histidine possesses an imidazole residue which coordinates to dicopper centres resulting in higher selectivity. Similar chemosensing ensembles for citrate[47], carbonate,[48] and glutamate[49] have been developed.

.

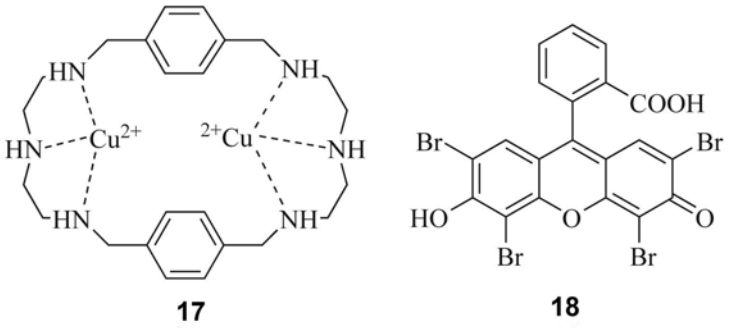

Figure 1.8 A chemosensing ensemble for histidine and pyrophosphate.

Apart from copper and nickel, other metals have been used for metal-complexing indicator-displacement assays as well. One example includes Lippard's dirhodium receptor **19** that incorporates dansylimidazole or dansylpiperazine (Figure 1.9). The complex was used as a nitric oxide sensor.[41] Nitric oxide (NO) is involved in several physiological processes, such as vasodilation,[50] carcinogenesis,[51] and neurodegenerative disorders.[52] In this system, NO displaces the coordinated fluorophore, which restores the fluorescence of the latter. The detection limit for NO was found to be 4-8 μM.

.

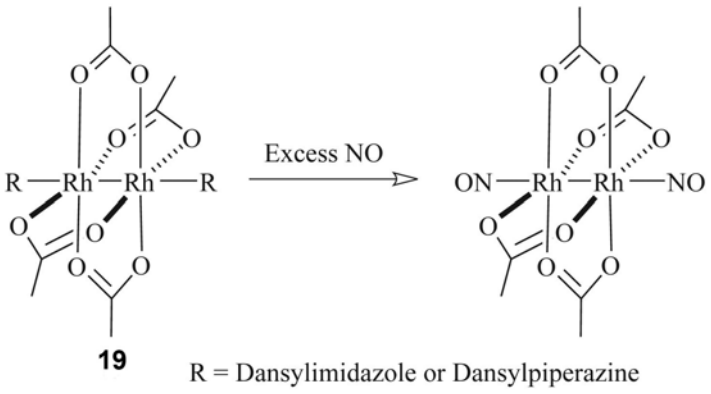

Figure 1.9 A chemosensing ensemble for NO detection.

1.3. Sensor arrays

1.3.1. The concept of sensor arrays

The chemical sensors described in the previous two sections made use of a "lock-and-key" design, where a specific receptor is synthesized in order to strongly and selectively bind the analyte of interest. This type of approach requires the synthesis of a highly selective sensor for each analyte to be detected. Significant rational design and computer modelling, as well as trial and error testing, are successfully being used to optimize the ability of the receptor to recognize the guest. Through this process it is becoming more and more routine to produce synthetic receptors with good selectivities for many classes of small and medium-sized guests, especially those which possess a reasonable number of sites for binding interactions. Despite this progress, it continues to be difficult to design selective receptors for larger and more complex bioanalytes such as proteins, nucleic acids, and complex carbohydrates. In addition, this "lock-and-key" approach is not particularly useful for analysing complex mixtures such as perfumes, drinks, food, mixtures of solvents etc.

But the lock and key type selectivity is not the only method used by nature for the development of receptors and sensors. An emerging strategy, which is complementary to the conventional chemical sensing approach, involves the use of sensor arrays. The utilization of sensor arrays is inspired by the superb performance of the biological olfactory system in odor detection, identification, tracking, and localization tasks. Recent experiments have shown that the olfactory receptors are not highly selective towards specific analytes: in fact, one receptor responds to many analytes and many receptors respond to any given analyte.[53,54] Pattern recognition methods are thus thought to be a dominant mode of olfactory signal processing in the broadly responsive portion of the olfactory system of higher mammals.

In the array approach, the strict "lock-and-key" design criterion of traditional sensing devices is abandoned. Instead, an array of different sensors is used, with every element in the sensor array chosen to respond to a number of different chemicals or classes of chemicals. The elements of such an array need not to be highly selective toward any given analyte. Instead, the collection of sensors should contain as much chemical diversity as possible, so that the array responds to the largest possible cross-section of analytes. In practice, most chemical sensors suffer from some interference by responding to chemical species that are structurally or chemically similar to the desired analyte. This interference is an inevitable consequence of the "lock" being able to fit a number of imperfect "keys". Differentially responsive arrays take advantage of this cross-reactivity by deliberately attempting to use the nonspecific response

patterns for analyte recognition. In this design, identification of an analyte cannot be accomplished from the response of a single sensor element; a distinct pattern of responses produced over the collection of sensors in the array can provide a fingerprint that allows classification and identification of the analyte.

The advantage of this approach is that it can yield responses to a variety of different analytes, including those for which the array was not originally designed. An array of sensors performs an integration to yield a unique signal for a complex but distinctive mixture, such as odors for example, without requiring that the mixture be broken down into its individual components prior to, or during, the analysis. This is a disadvantage when the precise chemical composition of a complex mixture is required but is advantageous when the only required information is the “identity” of the mixture of concern.

1.3.2. Pattern recognition algorithms

An array of chemical sensors creates a distinct pattern for each analyte with the number of dimensions being equal to the number of sensors in the array. Different algorithms used for the pattern-based recognition are presented in this chapter. This area has been thoroughly reviewed by Jurs *et al*..[55]

To analyze data from a chemical sensor array, some characteristics of the data are known, such as the number of observations and the number of variables per observation. The analysis methods and the ways in which they are used can be chosen with such information being taken into account. However, some types of problems cannot be anticipated but are discovered later as data are being analyzed. Therefore, it is not possible to generate a standard procedure for the analysis of data from chemical sensor arrays. Rather it is necessary to have a set of analysis methods available and to tailor the analysis to a particular problem.

There are many tools available for the analysis of data from an array of chemical sensors. The raw sensor responses are often preprocessed, and the preprocessed data are then used in a multivariate analysis. Figure 1.10 shows some of the available methods as either statistical techniques or neural-network based approaches. Further description is based on whether the technique is used for quantification or classification. Additional groupings are defined by the data required for the technique. Those requiring only independent variable information (sensor responses) are called *unsupervised* methods, while those that also use dependent variable information (analyte classes) are called *supervised* methods. Unsupervised

methods are preferred for qualitative applications such as exploring relationships in the data. Supervised methods are used more often for quantitative applications.

The choice of an appropriate data analysis method is highly dependent on the nature of the data and the particular application. There is no universal method which will work in all situations. The steps in a typical analysis, however, are usually similar regardless of the method chosen. First, a data set of sensor array responses for the analytes of interest is assembled. Second, the data are preprocessed appropriately for the application and the chosen method of data analysis. Third, the features to be used are chosen. Frequently, the steady-state response from each sensor is used as input for pattern recognition techniques. Other frequently used options include choosing a subset of sensors to use or doing a principal component analysis (PCA) and then using the components as the input for further analysis. Fourth, analysis is performed using the chosen method. A fifth step is the validation of the model with a training set of data which were not used in creating the model. Among all pattern-recognition methods, linear discriminant analysis (LDA) and principal component analysis are the most frequently used.

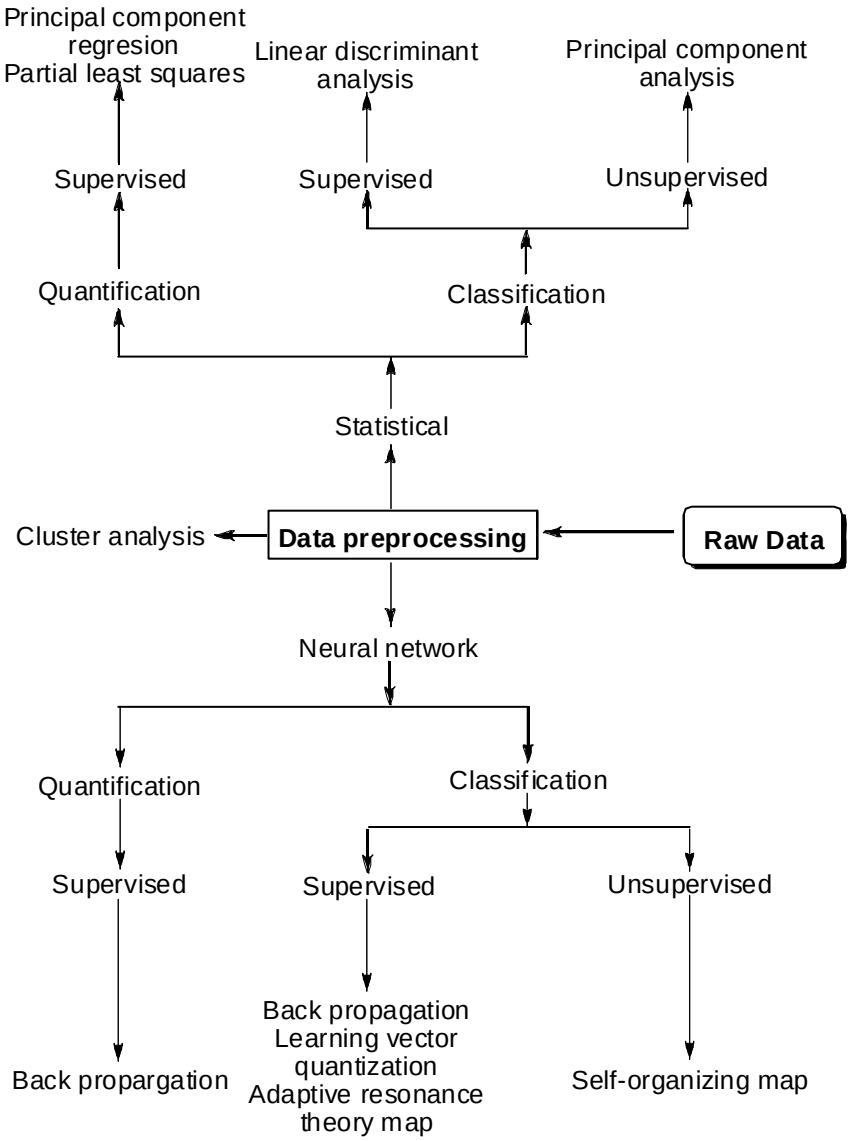

Figure 1.10 Some available methods for the data analysis from sensor arrays.

1.3.3. Selected examples of sensor arrays

In this section we will discuss selected examples of chemical sensor arrays. In first attempts to create sensor arrays scientists used solid materials, mostly for the sensing of gases - so called “chemical noses”. The area of heterogeneous sensor arrays is well established and has recently been thoroughly review by Lewis, Walt and co-workers.[56] The methods described include functional sensors based on surface acoustic wave (SAW) crystals,[57,58] quartz-crystal microbalances (QCM),[59] tin oxide sensors,[60,61] and carbon black composites.[62] One sensor that takes advantage of nonspecific recognition has been called the

"electronic nose" and is commercially available as AromaScan.[63,64] The technology is designed to identify volatile chemicals based on the adsorption of the odors onto an array of semiconducting organic polymers. The adsorption is dynamic, reversible, and is a function of the size of the voids within the individual polymer sensors. It takes only a few seconds for the system to reach an equilibrium. The changes in electrical resistance across each polymer are measured and a fingerprint pattern is created for the particular aroma. This pattern can be stored in a computer and used to identify and quantify further exposures of the array to complex mixtures (Figure 1.11).

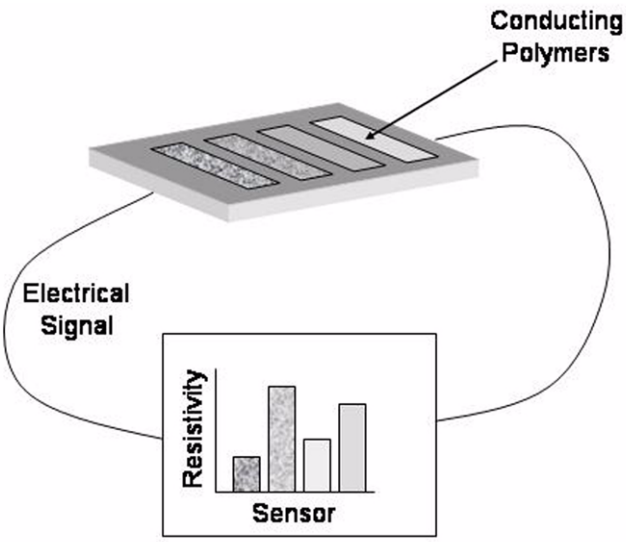

Figure 1.11 Schematic representation of an electronic nose based on semiconducting organic polymer. The resistance of each polymer is affected by adsorption of volatiles into the polymer matrix.

An advantage of this system is that very little chemical design needs to go into the creation of conducting polymers. For example, there are no designed receptors appended to the polymers, and there are no individual specific binding sites designed into the polymer. The lock and key principle has little if any influence on the choice of the conducting polymers. The method simply relies on natural voids within the individual polymers.

As mentioned previously, the area of heterogeneous sensor arrays - "chemical noses" - is already well established. But just recently chemists have started to develop solution-based sensor arrays - "chemical tongues". In the following we will illustrate this concept by a few examples.

To create a sensor array for the detection of proteins, Hamilton and co-workers used tetraphenylporphyrins (TPPs).[65] These porphyrins have large hydrophobic surface areas that are excellent for protein recognition. Derivatization of the TPP periphery with various amino acids and dipeptides resulted in a library of receptors with different charge, size, hydrophobicity, and symmetry, well suited for the recognition of proteins with various surface characteristics. The TPP derivatives are also highly fluorescent that makes signal detection and pattern development easy.

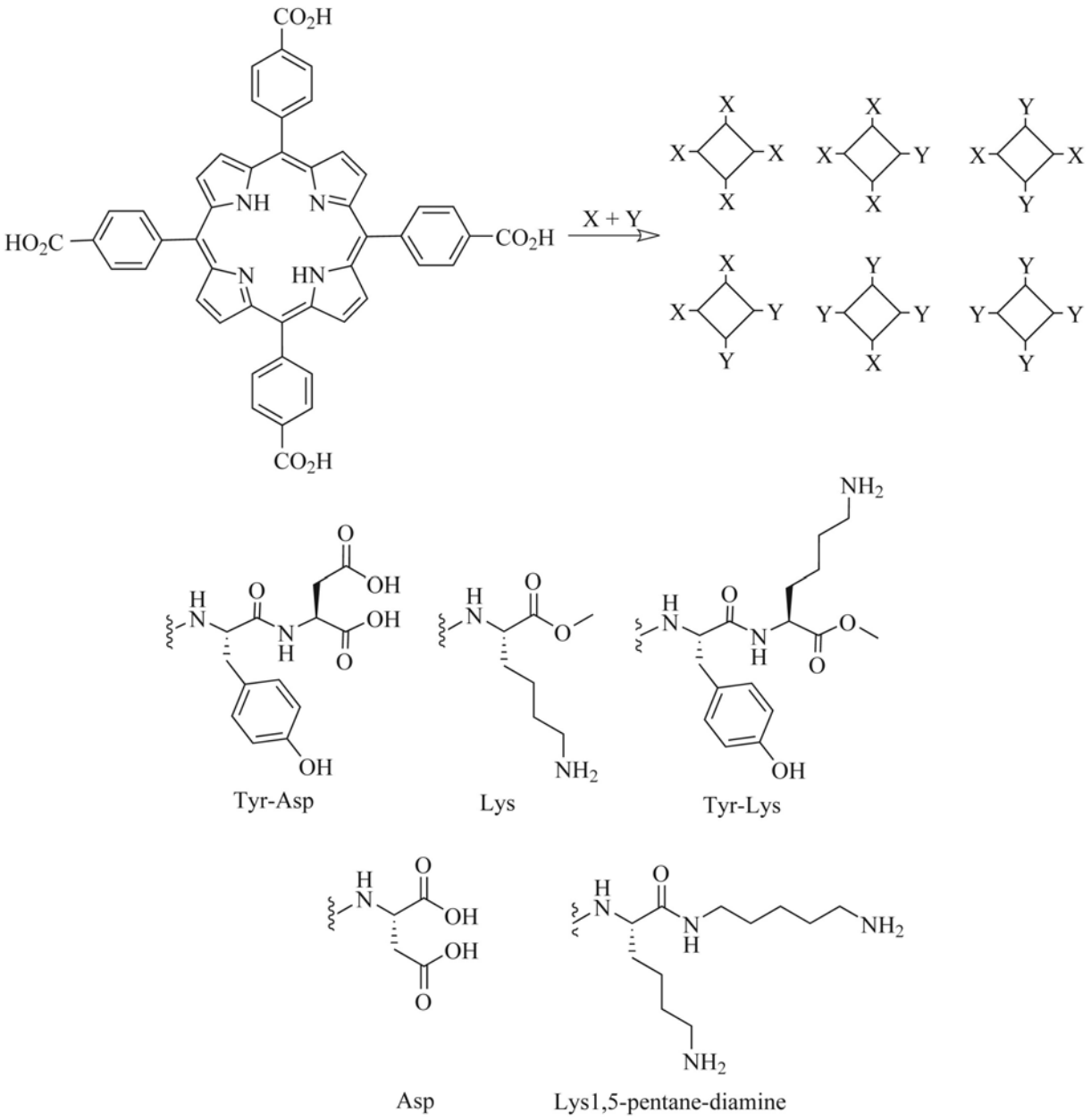

Figure 1.12 Combinatorial synthesis of a TPP library with different peptide components in X and Y positions.

A combinatorial synthesis resulted in a library of 35 members, which were isolated and purified (Figure 1.12). These 35 members were derivatized with four to eight hydrophobic groups and comprised all charge combinations from +8 to -8. Eight of the TPP derivatives were arranged in 8 rows of a 96 well quartz plate. Four proteins (15 μM) with varying pIs (ferredoxin (**21**) (pI 2.75), cytochrome c551 (**22**) (pI 4.7), myoglobin (**23**) (pI 6.8), and

cytochrome c (**20**) (pI 10.6)) were tested against each receptor resulting in various distinguishable quenching patterns (irradiated with UV light at 302 nm) as shown in Figure 1.13. The stronger the interaction between receptor and protein, the greater fluorescence quenching. However, this can not be related to the relative binding affinities as the mechanism of quenching may vary from receptor to receptor based upon the associated protein.

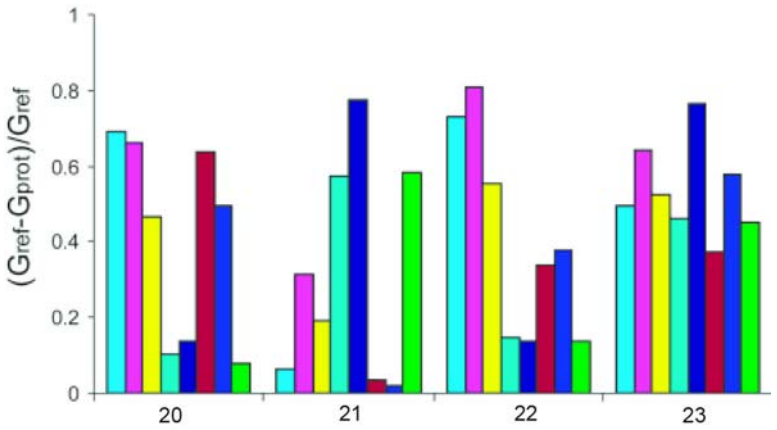

Figure 1.13 Fingerprints of cytochrome c (**20**), ferredoxin (**21**), cytochrome c551 (**22**), and myoglobin (**23**) based on eight porphyrin array. Each bar quantifies the extent of color attenuation measured as the quantity $(G_{ref} - G_{prot})/G_{ref}$, where G_{ref} is the average grey value for the blank well and G_{prot} is the average grey value for the well with protein. @ 2004 American Chemical Society

The response of the array is directly correlated to the charge complementary with the protein. The more basic receptors showed increased fluorescence quenching with the acidic protein ferredoxin, and the more acidic receptors showed increased quenching with basic cytochrome c. The more neutral myoglobin showed interactions with nearly every porphyrin in the array.

A sensor array, which can be used to detect organic compounds in water was described by Suslick *at al.*.[66] Detecting organic compounds in an aqueous environment is inherently difficult due to the high concentration of water. To accomplish this task, a hydrophobic surface was printed with the following: 1) metalloporphyrins which are metal-ion containing dyes that respond to Lewis basicity, 2) derivatives of and precursors to various pH indicators that respond to Bronsted acidity and basicity, 3) conventional solvatochromic dyes with large permanent dipoles that respond to local environment polarity. The arrays were made

of 36 indicators and were used to detect organic compounds (concentration as low as 1 μM) and to analyze a number of soft drinks with colorimetric patterns.

The array was initially saturated in an aqueous solution that does not contain any analytes, and was then imaged by a flatbed scanner. Then an analyte was introduced, and following rapid colorimetric changes, a second image was obtained by the scanner. Each printed receptor on the array was represented by a single spot, the absolute value of the RGB color of which changes upon interaction with an analyte. As illustrated in Figure 1.14, the color change profiles give diagnostic patterns for the organic analytes in aqueous solutions. It should also be mentioned that the pH was set at 7.0, so the pH indicators do not necessarily respond solely to pH, but also to other interactions.

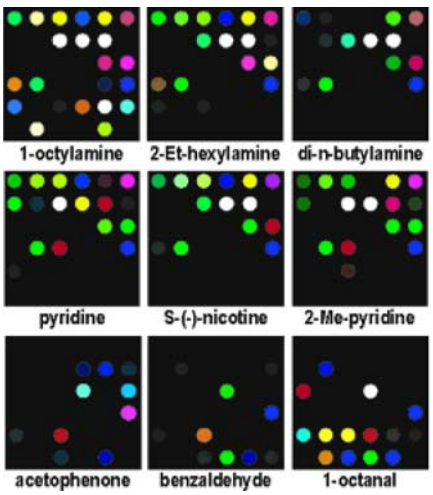

Figure 1.14 A base-sensitive array used to analyze various organic compounds in aqueous solutions (all amines 10 mM, all other analytes 50 mM, in pH 7.0 phosphate buffer). @ 2005 American Chemical Society

The authors used hierarchical cluster analysis (HCA) to identify familial characteristics in the patterns observed. They found that the array of printed receptors was capable of distinguishing such subtle difference as primary versus secondary amines and branched versus cyclic amines. They also determined that the HCA did not have any misclassification out of 144 cases. Finally, it was determined that the limit of discrimination is very large with the possible number of distinct patterns being 34^8.

In addition to the identification of various organics in aqueous solution, color change profiles (as in Figure 1.15) were obtained for a number of soft drinks with an acid-sensitive

array.[66] Though this is not an analysis that identifies the individual components, it does readily distinguish one complex mixture from another. The analysis shows the ability to discriminate analytes in low concentration in the presence of a common high concentration species such as fructose. This is a nice real-world example for employing a sensor array where a facile discrimination of the soft drinks was accomplished.

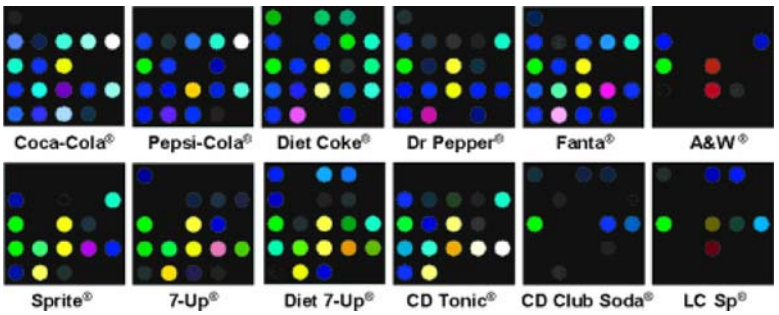

Figure 1.15 Color change profiles with the acid-sensitive array for a series of common soft drinks, chosen as readily available standards for comparisons among complex mixtures. CD: Canada Dry, LCSp: LaCroix Sparkling water. @ 2005 American Chemical Society

The next example describes the use of molecularly imprinted polymers to create sensor arrays for the detection of amines in the solution. Molecularly imprinted polymers (MIPs) are highly crosslinked polymer matrices developed in the presence of a template analyte molecule. After templating, the analyte molecule is removed leaving a binding cavity complementary to the target analyte. MIPs possess high chemical and thermal stability, and can be fashioned to selectively bind a number of different analytes. They can also be rapidly and inexpensively generated making them suitable for an array setting. The drawbacks associated with MIPs - low overall affinities and a high level of cross-reactivity - can actually be advantageous for differential sensor arrays.

An initial demonstration of the utility of MIPs in sensor arrays was demonstrated by Shimizu.[67] In this case, an eight-member sensor array was used to discriminate six different aryl amines.

To test a MIP sensor array using the IDA concept for signal generation, the group of Shimizu[68] templated the six analytes **24**-**29** (Figure 1.16) and included a blank MIP polymer. For the colorimetric signal modulation, indicator **31** was utilized in an IDA format.

Furthermore, the authors showed that a nontemplated analyte, cyclohexylamine (**30**), could be identified by the array using a pattern recognition protocol. Thus, the array strategy allows the detection of analytes not originally used for making the array. The general scheme for generating patterns with a MIP sensor array incorporating a colorimetric IDA for signal modulation is shown in Scheme 1-7.

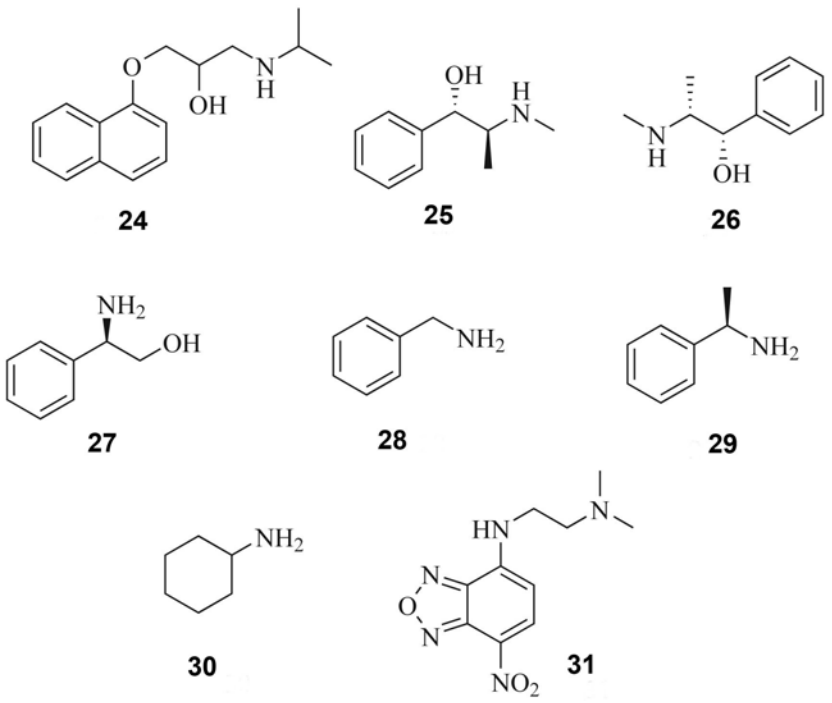

Figure 1.16 The analytes **24**-**30** and the indicator (**31**) tested in the MIP sensor array.

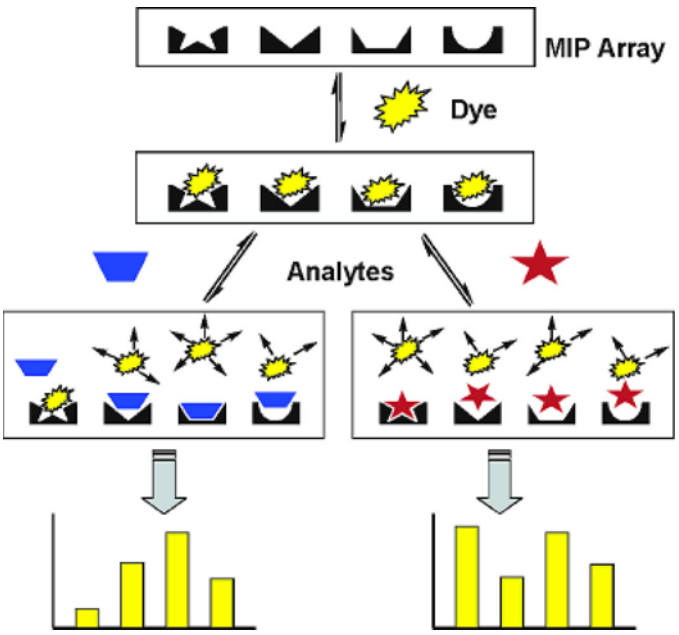

Scheme 1-7 General scheme for a MIP sensor array using a colorimetric IDA. A unique response from each sensor in the array results in a diagnostic pattern for each of the analytes tested. @ 2005 American Chemical Society

The identification of differences in the response patterns was done using linear discriminant analysis (Figure 1.17). Tight clustering of the analytes shows both the recognition capabilities of the array and the reproducibility of the responses. Furthermore, the nontemplated analyte **30** is clearly separated from the other analytes. Using MIP chemistry to access analytes not originally templated is certainly a powerful advance. Further exploration of imprinting technologies may lead to exciting new developments in differential sensing with synthetic arrays.

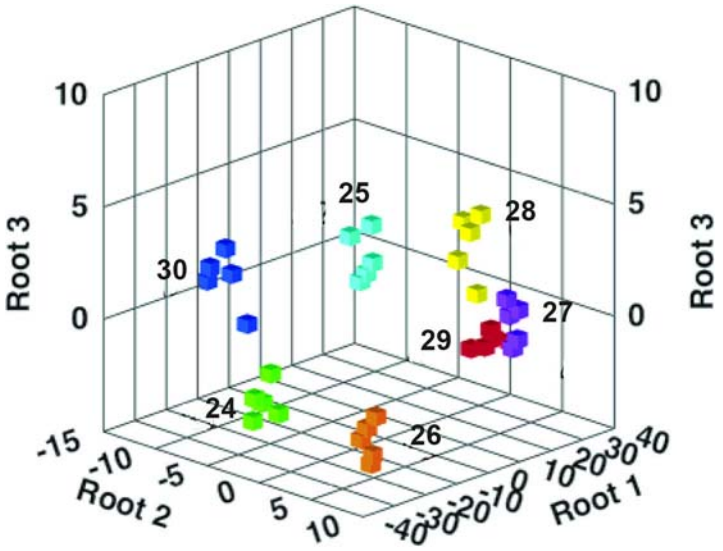

Figure 1.17 A three-dimensional linear discriminant analysis plot that describes 99.7% of the variance of the original data. Response patterns to the seven analytes from the MIP array are demonstrated. @ 2005 American Chemical Society

1.4. The aim of the work

The field of chemosensors has been rapidly growing over the last years. Though interesting new developments have been described in the literature, there is still room for high-impact research. One particular problem to be addressed is the media in which a chemosensor is able to function. In fact, many of the chemosensors described so far bind their respective analyte in organic or water/organic solutions. Real-world applications for the sensing of biologically important analytes would require the analysis to be performed in a purely aqueous solution. We have mentioned in the introduction that the metal-ligand interactions have been employed to design chemosensors able to function in aqueous media. But up to now only simple inorganic metal cations (mostly copper and nickel) have been used for this purpose. Thus, the aims of our research were as following:

- In the first part of our work we investigated whether an organometallic 4d transition-metal complex could offer some advantages in terms of affinity and selectivity. For this we used the complex $[Cp^*RhCl_2]_2$ to design selective chemosensing ensembles for the detection of histidine- or methionine-containing peptides.

- In the next part of our work we developed an array of chemosensing ensembles based on the same organometallic rhodium complex. The arrays were tested for the analysis of natural amino acids and nucleotides.

- Finally, we investigated whether we could extend the concept of sensor arrays by employing dynamic combinatorial libraries for sensing purposes.

Chapter 2

Sequence-selective detection of histidine- and methionine-containing peptides[69]

2.1. Introduction

The binding of small peptides by artificial receptors under physiological conditions (in water) still remains a challenging task. Although early work in this area was limited to peptide recognition in organic solvents,[70,71] some progress has been made in the last few years for peptide binding in more polar solvents. Several examples of peptide binding in aqueous solvents based on metal-ligand[35,72] or hydrophobic interactions[73,74] and, most recently, pure electrostatic interactions[75,76] have been reported.

One example of a receptor, which makes use of hydrophobic interactions for binding of short peptides in aqueous solution is shown below (Figure 2.1). Schmuck *et al.*[74] used a combinatorial approach for the synthesis of a solid-phase bound library of structurally related receptors **32**. The library of 512 members was synthesized and screened for the binding of a fluorophore-labelled derivative of the tetrapeptide N-Ac-Val-Val-Ile-Ala. This peptide represents the C-terminal sequence of the amyloid-β-peptide responsible for the formation of protein plaques within the brains of the patients suffering from Alzheimer's disease. The highest binding constant of $4*10^4$ M^{-1} was achieved for a hydrophobic resin-bound receptor with the first amino acid in the sequence being Lys(Boc), the second being Ser(OtBu) and the third being phenylalanine. The same scaffold was used by the authors to design a receptor (this time, based on electrostatic interactions) for the binding of the D-Glu-L-Lys-D-Ala-D-Ala tetrapeptide.[75,76]

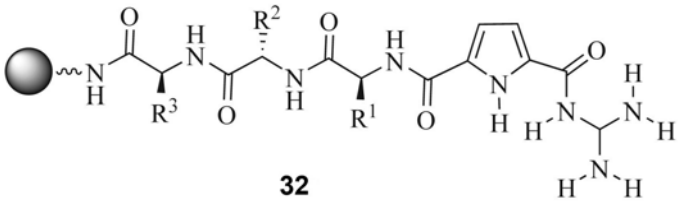

32

Figure 2.1 General structure of the receptor **32** tested for binding of tetrapeptides.

In addition to hydrophobic and electrostatic, metal-ligand interactions were employed to design receptors able to bind small peptides in aqueous solution. One example includes Anslyn's tweezers-like receptor **33** (Figure 2.2), which features a rigid backbone and two flexible peptide arms.[35] The receptor exhibits a selective recognition of short peptides N-terminating in histidine, methionine, and cysteine due to the favorable copper interactions. The

selectivity of the recognition can be modulated by the peptide arms. Among all analytes tested in the study, the highest association constant of 10^6 M^{-1} was found for the tripeptide His-Lys-Lys. In this case, the N-terminal histidine coordinates to the copper while the protonated amino groups of the two lysines ion-pair with the carboxy groups of the peptide arms.

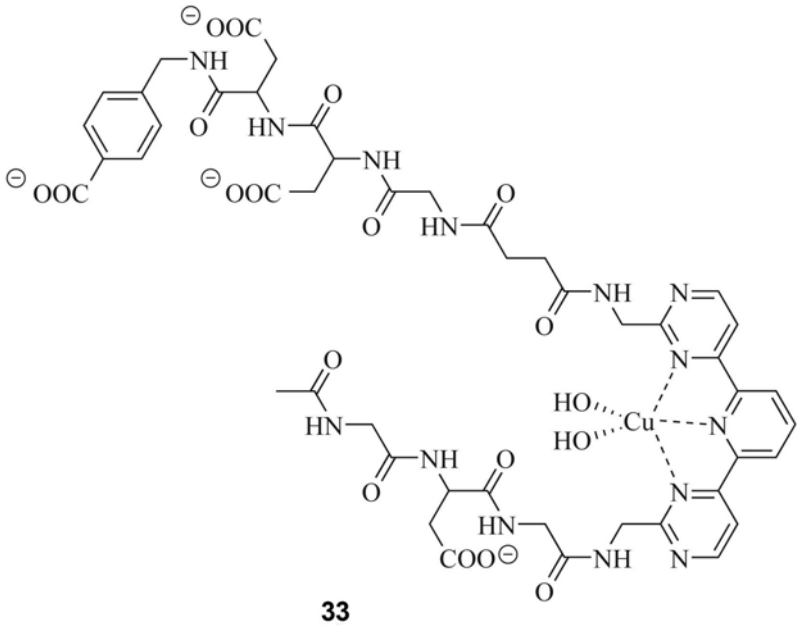

33

Figure 2.2 A tweezers-like receptor **33** developed to bind peptides N-terminated with histidine, methionine or cysteine.

Metal-ligand interactions generally provide higher association constants than hydrophobic and electrostatic ones, especially in polar solvents such as water. So far, 3d-transition metal ions have been used almost exclusively as the metal part of the receptor. At first glance, 4d and 5d transition metals appear to be less suited because they generally display slower exchange kinetics. On the other hand, they may show very high binding constants, which would allow the detection of analytes at low concentrations. Furthermore, they preferentially bind to ligands with “soft” donor groups (e. g. amines) which may be of interest for certain analytes. In this chapter, we demonstrate that the combination of an organometallic Cp^*Rh^{III} complex (**34**) as a receptor with the dye azophloxine (**35**) as an indicator (Figure 2.3) comprises an indicator-displacement assay, which allows the selective detection of histidine- and methionine-containing peptides.

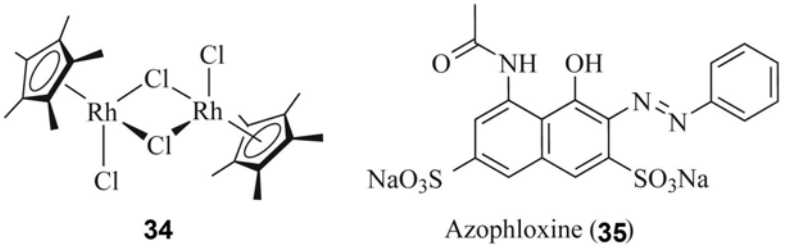

34 Azophloxine (**35**)

Figure 2.3 The structures of the organometallic Rh complex **34** and the indicator azophloxine (**35**).

2.2. Results and discussion

In continuation of our laboratory's research on organometallic receptors,[77-82] we have investigated whether halfsandwich complexes of rhodium(III) can be reversibly attached to indicators in order to build a sensing ensemble. The Cp*Rh complex **34** appeared to be well suited for this purpose because it is soluble in water and because the exchange kinetics for the three facial coordination sites opposite to the π-ligand is fast.[83] Screening of a number of commercially available indicators showed that the dye azophloxine (**35**) undergoes a strong color change upon complexation to Cp*Rh. The UV-Vis absorption spectra of **35** (25 μM) after addition of increasing amounts of **34** is shown in Figure 2.4 (H_2O, 100 mM phosphate buffer, pH 7.0).

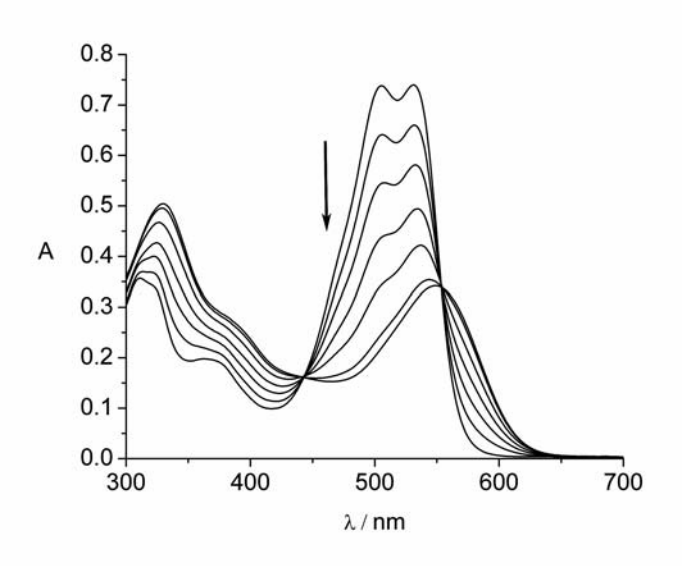

Figure 2.4 UV-Vis absorption spectra of a solution of **35** (25 μM) upon addition of complex **34** (final Rh concentration: 0, 4.8, 9.6, 14.4, 19.2, 24.0 and 26.4 μM). The spectra were recorded in H_2O (100 mM phosphate buffer, pH 7.0) after equilibration.

The complexation of the indicator to the rhodium complex results in a pronounced decrease of the absorption in the region of 500 nm with a new local maximum being found at λ = 549 nm. Clear isosbestic points are observed at λ = 554 and 443 nm indicating that a single species is formed. It appears likely that the indicator is attached to the metal via the diazo- and the phenolate group, since Cp*Rh complexes are known to form stable N,O-chelates with azophenolates.[84] At room temperature, the reaction between **34** (12.5 μM) and **35** (25 μM) proceeds with a half-life of $t_{1/2}$ = 2.5 min; at 50 °C the reaction is complete within 5 min. To determine the binding constant between **34** and **35**, the latter (12.0 μM) was titrated with the Rh-Cp* complex (0-20 μM). The interaction between the indicator and the rhodium complex was found to be very strong: fitting of the titration data to a 1:1 binding algorithm yielded a binding constant of 3.2 (± 1.0)*10^7 M^{-1}.

Having confirmed that the indicator **35** is able to bind to the Cp*Rh complex with a strong concomitant change in color, we investigated whether a mixture of **34** and **35** can be employed to detect histidine- or methionine-containing peptides.[a] The coordination chemistry

a. Redox active cysteine-containing peptides were not included in the study.

of organometallic half-sandwich complexes with amino acids and peptides is well established.[85] It has been demonstrated that peptides preferentially bind to Cp^*Rh^{III}-, Cp^*Ir^{III}- and (arene)Ru^{II}-fragments via the terminal amino group and deprotonated amide group(s). For histidine and methionine, an additional interaction between the N- or S-donor group of the side-chain and the metal is generally observed.[b] In order to determine whether this additional interaction allows a differentiation between peptides, we first examined competition experiments with **34**, **35** and the dipeptides His-Ala or Val-Phe. When a mixture of **34** and **35** ([Rh] = [**35**] = 50 μM) in buffered aqueous solution was mixed with one equivalent of His-Ala, the original red color of free **35** re-appeared. If the indicator **35** was added to a solution of **34** and His-Ala, on the other hand, no color change was observed. This showed that the stability of the complex between Cp*Rh and His-Ala is considerably higher than that of the adduct between **34** and **35**. When the same experiments were performed with Val-Phe instead of His-Ala, one could observe the purple color of the adduct between the receptor **34** and the indicator **35** (Figure 2.5). The affinity of Val-Phe to the Cp*Rh complex is thus not sufficient to replace the indicator **35** to a significant extent. For the "naked-eye" detection of histidine-containing peptides the required minimum concentration is approximately 20 μM.

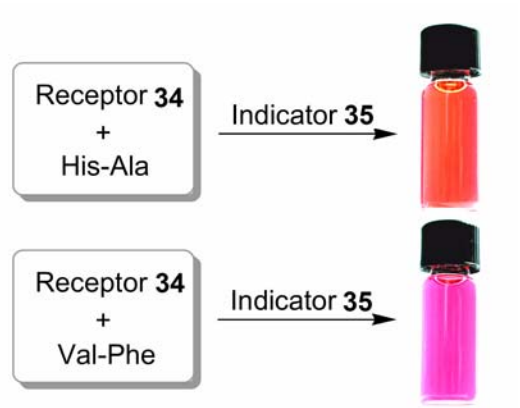

Figure 2.5 "Naked-eye detection of the dipeptide His-Ala by an indicator displacement assay by using a solution of receptor **34** (50 μM), the indicator **35** (100 μM) and the respective dipeptide (100 μM) in water (100 mM phosphate buffer, pH 7.0).

b. We did not succeed in crystallizing the complex of **34** *and a histidine- /methionine-containing peptide. For the crystal structure of [cymeneRu(His)]Cl complex see the Annex.*

A more detailed analysis of competition experiments using UV-Vis spectroscopy was performed to determine the relative binding constants $K_r = K_{peptide}/K_{indicator}$ of the Cp*Rh complex **34** for various peptides. (Where $K_{peptide}$ is defined as: $K_{peptide}$ = [Cp*Rh-peptide complex]/[Cp*Rh(L_n)][peptide] with L_n being aqua, chloro, and/or phosphate ligand; $K_{indicator}$ is defined accordingly). For this purpose, a variable amount of the respective peptide (for histidine- and methionine containing peptides, final concentration: 0 – 26 μM) was mixed with the receptor (final conc. 12 μM) and the indicator (final concentration: 50 μM). After equilibration (50 °C, 10 min), the amount of free indicator was determined using a calibration curve and the resulting data was fitted to calculate K_r. To estimate K_r for peptides without His/ Met residue, a large excess of the respective peptide (final concentration: 300-500 μM) was mixed with the receptor (final concentration: 25 μM) and the indicator (final concentration 25 μM). The results are summarized in Table 2.1.

Table 2.1 Relative binding constants $K_r = K_{peptide}/K_{indicator}$ of the Cp*Rh complex **34** to various peptides.

Entry	Peptide	K_r[a]
1	His-Ala	$> 1*10^3$
2	His-Gly-Gly	$> 1*10^3$
4	Gly-His-Gly	$> 1*10^3$
4	Leu-His-Leu	$> 1*10^3$
5	Gly-Met-Gly	$> 1*10^3$
6	Met-Leu-Phe	$7.4*10^2$ ($\pm 1.5*10^2$)
7	Gly-Gly-His	$1.6*10^1$ ($\pm 0.2*10^1$)
8	Tyr-Gly-Gly-Phe-Met-Arg-Phe	6.9 (± 0.2)
9	Ala-Ser-His-Leu-Gly-Leu-Ala-Arg	$9.1*10^{-1}$ ($\pm 0.2*10^{-1}$)
10	Gly-Gly-Met	$1.7*10^{-1}$ ($\pm 0.2*10^{-1}$)
11	Val-Gly-Gly	$7.4*10^{-2}$ ($\pm 0.2*10^{-2}$)
12	Ala-Ala	$2.2*10^{-3}$ ($\pm 0.3*10^{-3}$)
13	Pro-Glu	$< 1*10^{-3}$

[a] Conditions: phosphate buffer (100 mM), pH 7.0

Table 2.1 Relative binding constants $K_r = K_{peptide}/K_{indicator}$ of the Cp*Rh complex **34** to various peptides.

Entry	Peptide	K_r [a]
14	Val-Phe	$< 1*10^{-4}$
15	Lys-Tyr	$< 1*10^{-4}$

[a] Conditions: phosphate buffer (100 mM), pH 7.0

For peptides containing either His or Met in the position one or two from the N-terminus, we observed nearly complete replacement of the dye upon addition of the peptide (K_r > 740) (entries 1 – 6). This holds true even for peptides such as Leu-His-Leu, in which the His residue is flanked by amino acids with sterically demanding side chains (entry 4). It is reasonable to assume that for peptides with His/Met at – or in direct neighborhood to – the N-terminus, a simultaneous coordination of the amino and the respective side-chain occurs.[c] For tri- or longer peptides with His/Met residues in the middle or at the C-terminus, this is much less favorable and consequently lower relative binding constants are observed (entries 7 – 10). From the values observed for Gly-Gly-His and Gly-Gly-Met (entries 7 and 10), the interaction of the imidazole sidechain of histidine with the Rh-Cp* complex seems to be stronger than the interaction of the thioether sidechain of methionine. The thermodynamic preference for the coordination of N-donor ligands in competition to S-donor ligands has also been observed for a Zn^{II}-containing receptor[35] and is in accordance with theoretical studies of Pt^{II} complexes.[86] Five peptides without His/Met residues were investigated (including dipeptides with basic and acidic side-chains), all of which show a very low relative binding constant (entries 11-15). Remarkably, the substitution of a single His residue with an Ala residue results in a drop of affinity of more than five orders of magnitude (entries 1 and 12).

The high selectivity of the Cp*Rh receptor allows to perform IDAs for the quantitative detection of peptides containing His/Met residues close to the N-terminus. For the detection of His-Ala, for example, the receptor **34** (final Rh concentration: 12 μM) and the indicator **35** (final concentration: 50 μM) were added successively to a solution containing a variable amount of the peptide (0 – 10 μM). The resulting mixture was tempered for 10 min at 50°C and then the absorption at 580 nm was determined.[d] The corresponding calibration curve is depicted in Figure 2.6. The detection limit of this assay was estimated to be 0.3 μM

c. Beside the N-terminal amino group and the sidechain, an amide group can potentially participate in coordination.

(assumed to be $3s_{blank}$ where s stands for the standard deviation). The limit for quantitative detection is approximately 1.0 μM (10 s_{blank}).[87] If similar experiments were performed with Val-Phe instead of His-Ala, no significant change in absorption was observed. This pronounced selectivity allows to sense low micromolar concentrations of His-Ala in the presence of a 100-fold excess of Val-Phe (Figure 2.6).

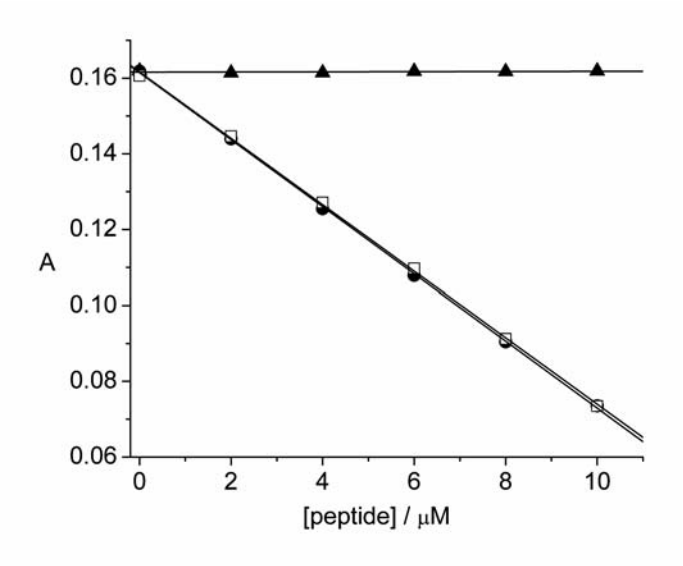

Figure 2.6 Absorbance at 580 nm for solutions containing receptor **34** (12 μM), the indicator **35** (50 μM) and different amounts of His-Ala (circles), Val-Phe (triangles) or His-Ala in the presence of a 100-fold excess of Val-Phe (squares). The data points represent averaged values for three independent experiments; the errors are less than 2%.

A unique advantage of IDAs is the fact that the indicator-receptor ratio can be adjusted for specific sensing problems.[25] It is thus possible to quantify *and* distinguish the tripeptides His-Gly-Gly and Gly-Gly-His in two sets of experiments. If we assume that the peptides are present in concentrations between 0 and 10 μM, one would first have to perform an IDA using an excess of receptor and indicator ([Rh] = 50 μM; [**35**] = 60 μM). Under these conditions, we observe the nearly quantitative replacement of the indicator by both peptides, which allows to determine their concentration without knowing their identity. In a second experiment, the concentration of the receptor is reduced to the value determined in the first

d. Though the largest relative changes in adsorption are observed at 599 nm, owing to reasons of sensitivity (larger absolute changes) it is advantageous to perform the assay at 504 or at 580 nm (see Figure 2.4).

experiment. Because of the excess of the indicator, only the high affinity analyte His-Gly-Gly results in a complete replacement of the indicator whereas for the lower affinity analyte Gly-Gly-His, the response is much smaller. Based on this data it is possible to identify the two peptides. The experimental values for peptide concentrations of 5 μM are given in Table 2.2.

Table 2.2 Differences in the absorbance at 504 nm for solutions of the dipeptides His-Gly-Gly and Gly-Gly-His after addition of various amounts of receptor **34** and indicator **35**.

Peptide	[Peptide][a]	[**34**][a]	[**35**][a]	ΔA
His-Gly-Gly	5.0 μM	25 μM	60 μM	0.108
Gly-Gly-His	5.0 μM	25 μM	60 μM	0.103
His-Gly-Gly	5.0 μM	2.5 μM	60 μM	0.108
Gly-Gly-His	5.0 μM	2.5 μM	60 μM	0.057

[a] Final concentrations are given

Similarly, we attempted to make a fluorescent indicator-displacement assay for the sequence selective detection of peptides. To do so, we synthesized the fluorescent ligand **36** by the reaction of dansyl chloride with 8-aminoquinoline according to a published procedure (Scheme 2-1).[88]

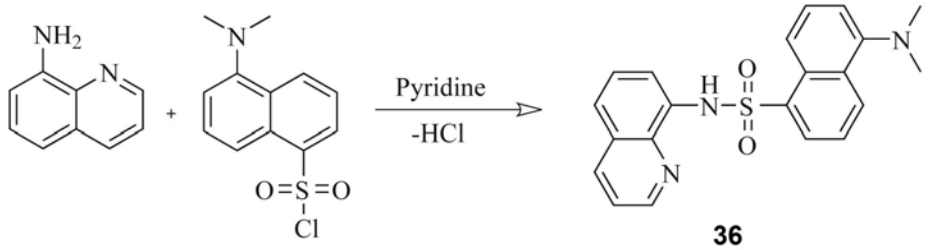

Scheme 2-1 The synthesis of the fluorescent ligand **36**.

Unfortunately, this ligand was found to be insoluble in water and the attempts to use water/organic solvent mixtures were unsuccessful. See the Annex for the crystal structure of the Rh complex **34** with **36**.

2.3. Conclusion

In summary, we have shown that an organometallic 4d transition metal complex can be used to build an IDA for the sequence-specific detection of histidine- and methionine-containing peptides in water at neutral pH. Although the assay is not suited for real-time measurements, it can be completed within a few minutes. The following characteristics make this new system especially appealing: a) the receptor **34** and the indicator **35** are both commercially available; b) the interaction of the receptor with the analyte is very strong, which allows to detect peptides with His/Met residues close to the N-terminus down to a concentration of 0.3 μM; c) the receptor displays a very high selectivity, which allows to perform the analysis in 100 mM phosphate buffer and in the presence of a large excess of competing peptides.

Chapter 3

A chemosensor array for the identification of 20 natural amino acids[89]

3.1. Introduction

In the previous chapter we described an indicator displacement assay for the sequence-selective detection of histidine- and methionine-containing peptides. Though a number of selective IDAs for a variety of analytes has been described so far, the utilization of IDAs for multianalyte sensing[90,91] or for array technologies[68,92] is largely unexplored. In this chapter we describe an IDA-based sensor array, in which the respective sensors are assembled from commercially available building blocks. This array allows differentiation of 20 natural amino acids with high fidelity using UV-Vis spectroscopy in combination with a multivariate analysis.

Over the last years, a number of chemosensors (including IDA-based ones) for amino acids have been described. Some examples are presented below. To make a chemosensor for the aspartate and glutamate anions, Anslyn and co workers designed receptor **37** (Figure 3.1).[32] Here, the Zn^{2+} ion is responsible for the coordination of amino- and carboxy- groups of the amino acids while the two guanidinium groups were incorporated to provide selectivity for the side chains of aspartate and glutamate. Pyrocatechol violet (**38**) was used as the indicator for the analysis to be performed in an IDA format. The dye binds to **37** with an association constant of $3.75*10^5$ M^{-1} and with a concomitant change in color. Upon ligation of an amino acid to the metal ion via a carboxylate and an amine, the guanidinium groups are placed in proximity to the aspartate or glutamate side chains so as to provide hydrogen bonding between the two. It was expected that these additional interactions result in some selectivity for these two amino acids. In fact, a difference of a factor of 7 between aspartate and glutamate, and of a factor of 15 between aspartate and other hydrophobic amino acids was found with the association constant between aspartate and receptor being $1.5*10^5$ M^{-1}. Two more examples of chemosensors selective for aspartate and glutamate can be found in the references [49] and [93].

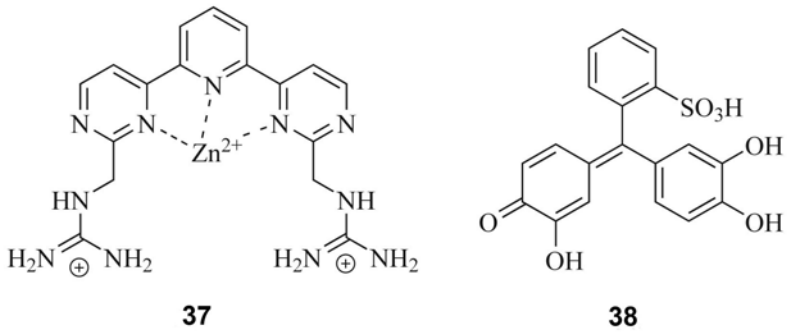

Figure 3.1 A chemosensing ensemble for glutamate and aspartate.

An IDA chemosensor, able to selectively detect cysteine in aqueous solution was designed by Kim *et al.*.[94] Cadmium-containing receptor **39** and the dye pyrocatechol violet (**38**) associate in solution with a binding constant of $2.8*10^5$ M^{-1}. Upon addition of cysteine, a simultaneous coordination of sulthydryl, carboxyl, and amino groups to the both cadmium ions occurs. Consequently, the association constant between cysteine and the receptor is higher than those of all other amino acids which fail to coordinate to both cadmium ions simultaneously. Its exact value was calculated to be $1.6*10^7$ M^{-1}, which is almost two orders of magnitude higher than the K_a of the indicator. Other examples of cysteine-selective chemosensors can be found in references [95-96].

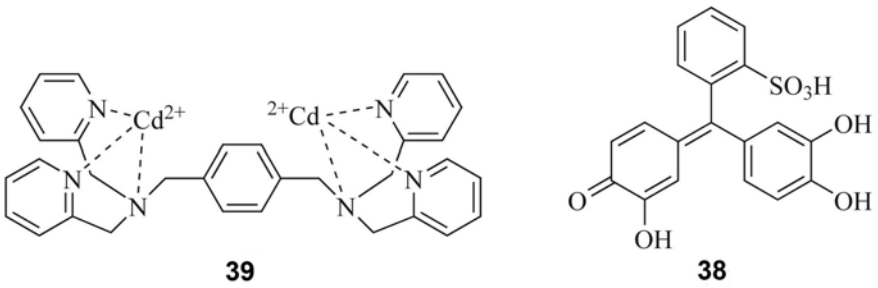

Figure 3.2 A chemosensing ensemble for cysteine.

An example of a chemosensor for the selective detection of histidine was given in chapter 1 (see Figure 1.8 and explanations therein). A few more examples can be found in references [45] and [97]. For a chemosensor, selective for lysine and arginine see reference [98].

In the above-cited examples, the selectivity for a particular amino acid(s) was mainly achieved by using receptors which are able to recognize a certain functional group of an amino acid chain; e.g., imidazole of His,[45,97] thiol of Cys,[94-96] carboxylate of Asp or Glu[32,49,93] or amino groups of Lys and Arg.[98] To distinguish simple, nonfunctionalized amino acids such as Ala or Val, however, a single-sensor approach would be difficult to realize because of the lack of sufficiently specific receptors. We therefore decided to investigate whether an array-based approach would be suitable for achieving the required selectivity.

3.2. Results and discussion

The organometallic Cp*Rh complex **34** was employed as the receptor unit for the array performed in an IDA format. In Chapter 2, we have shown that this complex shows a high affinity for peptides, especially for those bearing His or Met residue close to N-terminus. We therefore decided to investigate whether the same complex can be used for the detection of amino acids. As indicators we employed the commercially available dyes gallocyanine (**40**), xylenol orange (**41**), and calcein blue (**42**) (Figure 3.3).

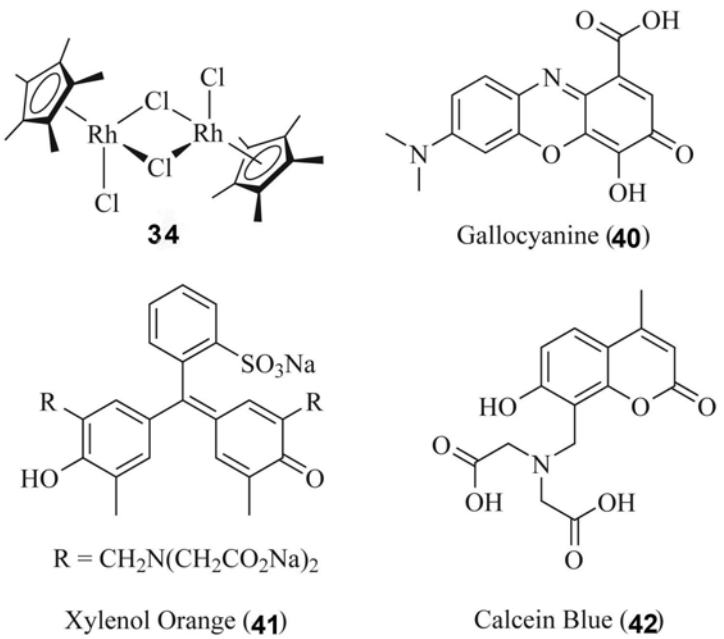

Figure 3.3 Complex **34** and dyes **40**-**42** used to compose IDA sensor array for the identification of 20 natural amino acids.

To determine the association constants between the Rh-Cp* complex and the dyes, UV-Vis titration experiments were performed (Figure 3.4-Figure 3.6). The titration data were fitted to a 1:1 binding algorithm using the program Gepasi, version 3.30.[99,100] The metal binding constant for gallocyanine (**40**) was found to be $K_{(\mathbf{40})}$ = 2.3 (± 0.2)*10^6 M^{-1}.[a] For calcein blue (**42**), a binding constant of $K_{(\mathbf{42})}$ = 7.7 (± 1.6)*10^7 M^{-1} was determined.[b] Xylenol orange (**41**) is able to bind more than one Rh-Cp* complex and a simple 1:1 binding algorithm could not be applied. But due to the similarity of the functional groups of **41** and **42**, the binding constants are expected to be in the same range.

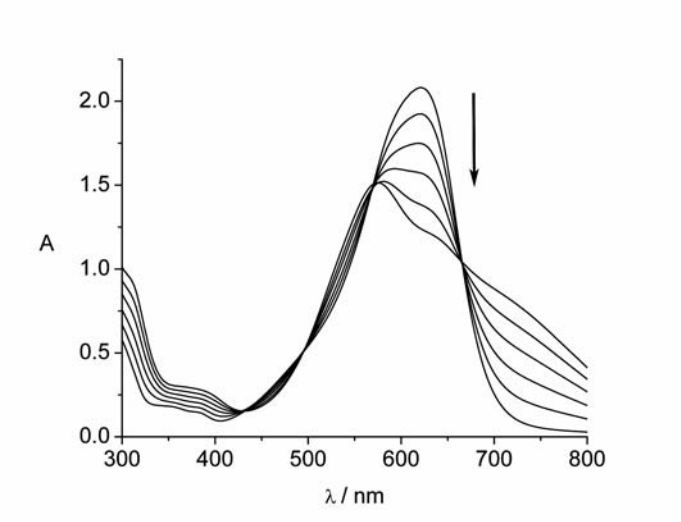

Figure 3.4 UV-Vis adsorption spectra of a solution of **40** (50 μM) upon addition of complex **34** (final Rh concentration: 0, 10, 20, 30, 40, 50 μM). The spectra were recorded in H_2O (100 mM phosphate buffer, pH 7.0) after equilibration.

*a. Experimental conditions: [**40**] = 25 μM, [**34**] = 0-25 μM, 100 mM phosphate buffer, pH 7.0.*
*b. Experimental conditions: [**42**] = 5 μM, [**34**] = 0-5 μM, 100 mM phosphate buffer, pH 7.0.*

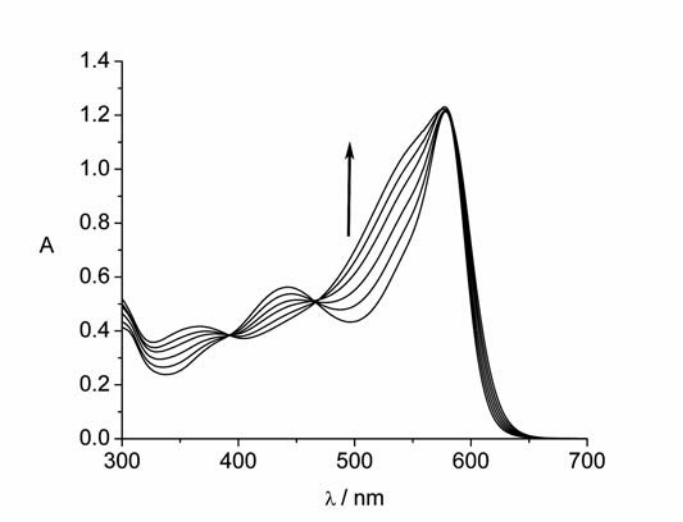

Figure 3.5 UV-Vis adsorption spectra of a solution of **41** (50 μM) upon addition of complex **34** (final Rh concentration: 0, 10, 20, 30, 40, 50 μM). The spectra were recorded in H_2O (100 mM phosphate buffer, pH 7.0) after equilibration.

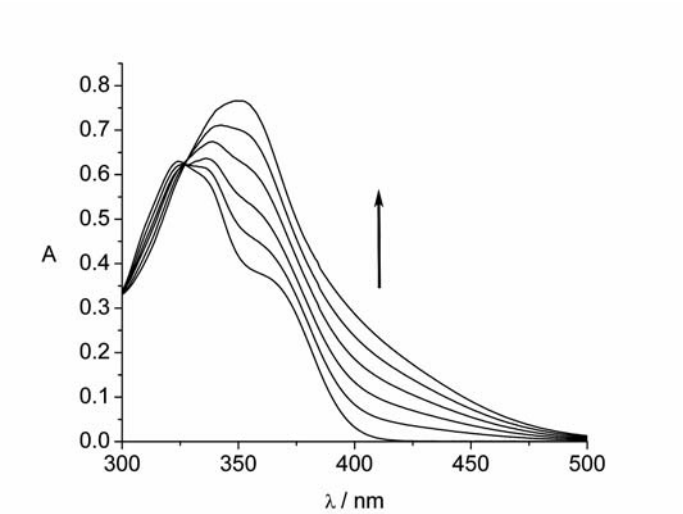

Figure 3.6 UV-Vis adsorption spectra of a solution of **42** (50 μM) upon addition of complex **34** (final Rh concentration: 0, 10, 20, 30, 40, 50 μM). The spectra were recorded in H_2O (100 mM phosphate buffer, pH 7.0) after equilibration.

The binding constants of the amino acids to the Rh-Cp* complex were found to be in the same range as those of the dyes, resulting in a real competition situation for at least one dye - amino acid combination. A key component of our sensor array was the utilization of a

variable pH. The pH was expected to change the selectivity of the IDA because the relative binding affinity of a given dye - amino acid pair depends on the pH.[c] The procedure for the colorimetric identification of 20 natural amino acids using an IDA-based assay is summarized in Scheme 3-1.

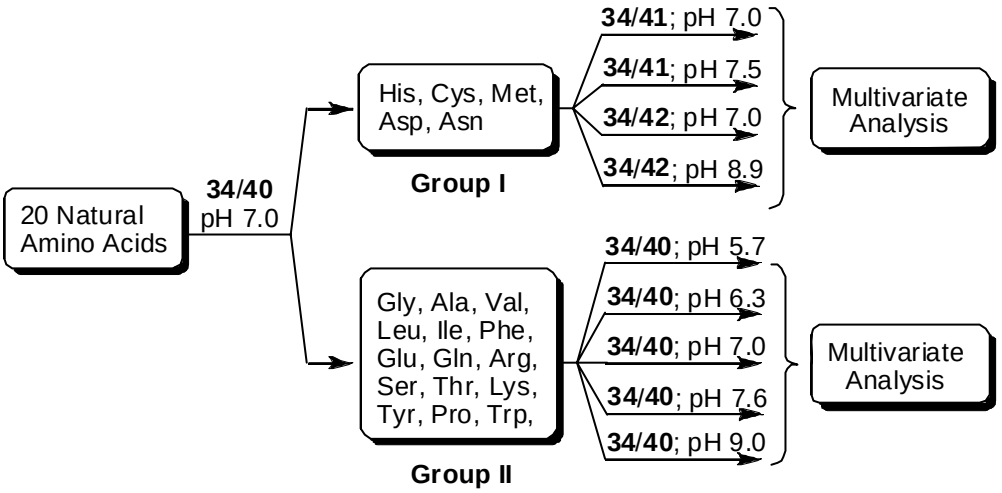

Scheme 3-1 Colorimetric identification of 20 natural amino acids using IDA arrays.

First, the UV-Vis response at 750 nm of an IDA composed of **34** (50 μM) and gallocyanine (**40**) (100 μM) was used to classify the amino acids (750 μM) into a high- and low-affinity group. The high-affinity group consists of His, Cys, Met, Asp and Asn for which a nearly quantitative replacement of the dye **40** from the rhodium complex was observed (ΔA(750 nm) < 0.06, where $\Delta A = A$(**34** +**40** + amino acid) - A(**40**)). The remaining 15 amino acids lead to a partial displacement of the dye (0.55 > ΔA(750 nm) > 0.06) and constitute the second group. After this separation, each member of the first group was analyzed by four IDAs (two different dyes, **41** and **42**, and two different pH values for each dye), and each member of the second group was analyzed by five IDAs (indicator **40** at five different pH values). The UV-Vis absorption was measured at a fixed wavelength for each dye: 750 (**40**), 345 (**41**), and 400 nm (**42**). In each case, the analysis was repeated 12 times with all data being gathered in a highly parallel fashion using a microplate reader.

The data from three selected amino acids of group II (Ala, Phe, Pro) are shown in Figure 3.7. Despite the fact that these amino acids do not possess additional functional groups

c. A behavior of this kind is expected for ligand with metal binding groups, which have a different pK_a.

on their side chains, a unique adsorption patterns was obtained. To evaluate whether this "fingerprint" can be used for the identification of the amino acids, a linear discriminant analysis (LDA) was performed.[55]

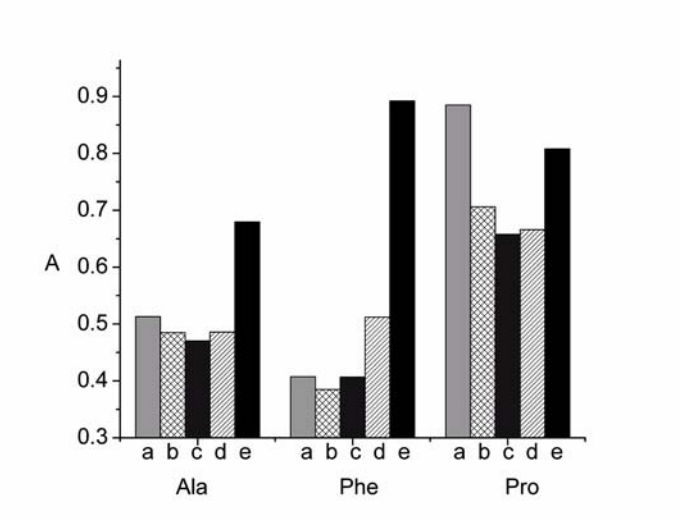

Figure 3.7 Absorbance at 750 nm for mixtures containing the dye **40** (100 μM), the receptor **34** (50 μM), and the respective amino acids (750 μM) determined at five different pH values: 5.7 (a), 6.3 (b), 7.0 (c), 7.6 (d), and 9.0 (e)(MES, phosphate or CHES buffer, 85 mM).

The predictive ability of our sensor array was determined by a cross-validation routine, in which randomly one measurement was omitted. The remaining data were used as the training set for the LDA, and the omitted observation was classified. The data of group I and II were treated separately. For group I, all data were assigned accurately, and for group II, 1 misclassification out of 180 observations was obtained (99.4% accuracy). If only 50% of the data were used as the training set, group I was still assigned with 100% accuracy. For group II, 174 out of 180 observations were classified correctly (96.7% accuracy). The amino acids that gave rise to these occasional mismatches were valine and isoleucine.

To visualize the clustering of the data, a principal component analysis (PCA) was performed.[55] The results of the amino acids of groups I and II are depicted in Figure 3.8 and Figure 3.9 respectively.

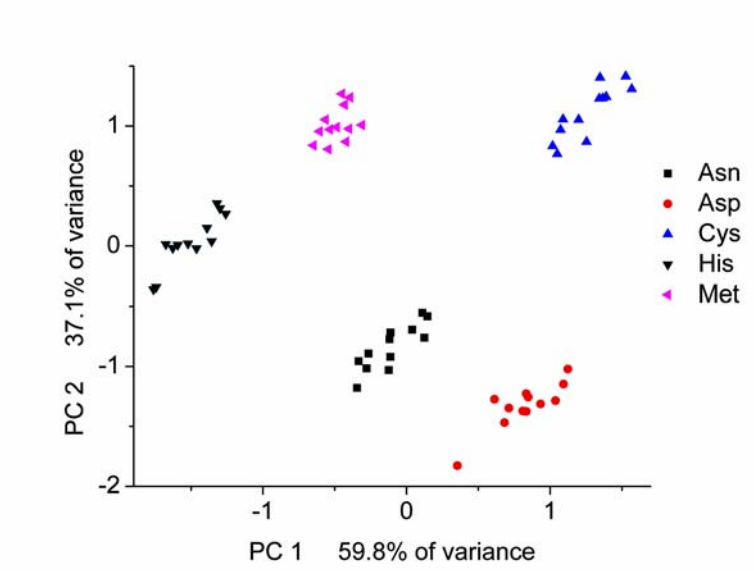

Figure 3.8 Principal component analysis plot for the identification of amino acids of group I.

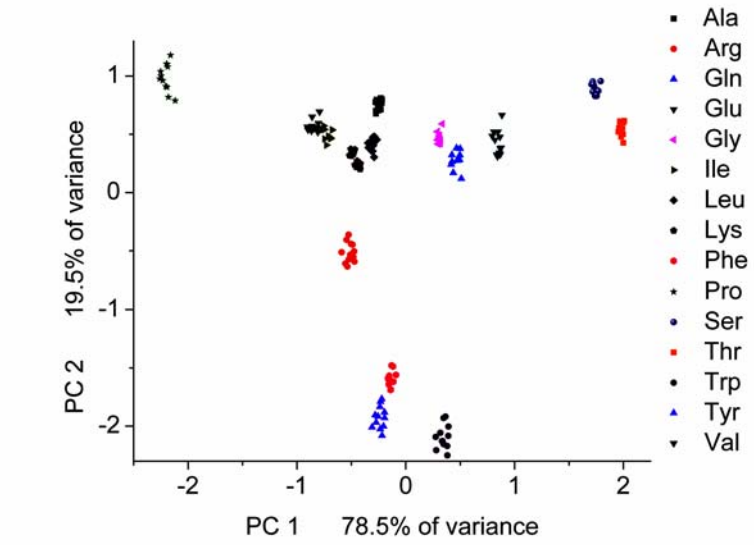

Figure 3.9 Principal component analysis plot for the identification of amino acids of group II.

The data appear in well-separated groups with the only overlap found for valine and isoleucine. To some extent, chemical and structural similarities are reflected by the relative

position of the group. The data of the hydroxy amino acids serine and threonine, for example, are positioned in proximity to each other as well as the data for the aromatic amino acids phenylalanine, tyrosine, and tryptophan. The only cyclic amino acid, proline, is well separated from the rest. We found that the affinity of fifteen amino acids without coordinating side-chains to Cp*Rh correlates with the PC 1 axis of the score plot (Figure 3.10). At the same time, no correlation between pK(NH_2) and PC 1 was observed. The second axis PC 2 separates aromatic amino acids from non-aromatic ones, which suggests that hydrophobic interactions contribute to the discrimination of amino acids as well.

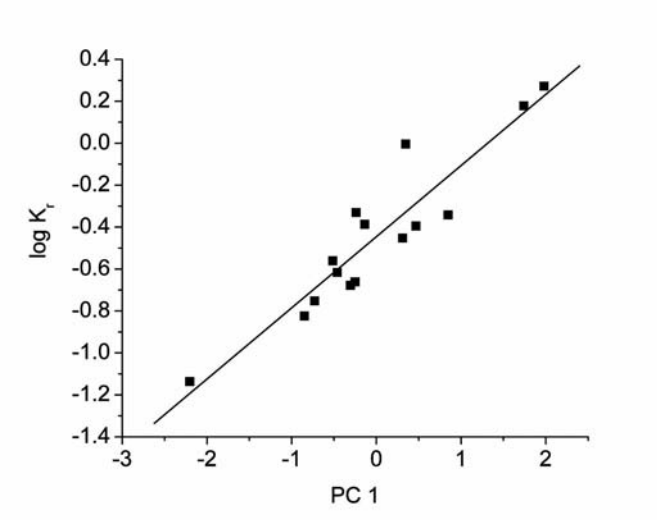

Figure 3.10 The correlation between the PC 1 axis of Figure 3.9 and the logarithm of relative binding constants of 15 amino acids to the Cp*Rh complex. Correlation coefficient R = 0.93.

3.3. Conclusion

The results described above demonstrate the analytical power of IDAs performed in an array format. Closely related analytes such as leucine and isoleucine are clearly distinguishable, a result which would be very difficult to achieve with a classical one sensor–one analyte approach. The IDA array used for our analysis is very easy to build because it just requires mixing of commercially available building blocks at different pH. It appears likely that similar assays can be constructed for the analysis of more complex analytes such as peptides and proteins.

Chapter 4

Pattern-based recognition of nucleotides with a multicomponent indicator displacement assay[101]

4.1. Introduction

Nucleotides are of prime importance for many biological processes. It is therefore not surprising that considerable efforts have been made to build artificial receptors and sensors for this class of compounds.

One example of a chemosensor for guanosine triphosphate (GTP) is shown in Figure 4.1. Kim *et al.* synthesized **43**, which represents a selective receptor for GTP over adenosine mono-, di - , and triphosphates (AMP, ADP, and ATP respectively).[102] Upon coordination to the sensor, the guanine base in GTP acts as a fluorescence quencher which results in chelation-induced fluorescence quenching, whereas a chelation-enhanced fluorescence is observed for AMP, ADP, and ATP. Thus, guanosine triphosphate can be detected selectively. It was found that the selectivity for GTP (K_a = 8.7*10^4 M^{-1}) is about 6 times higher than that for ATP, and over 100 times higher than those for ADP, AMP, and inorganic anions.

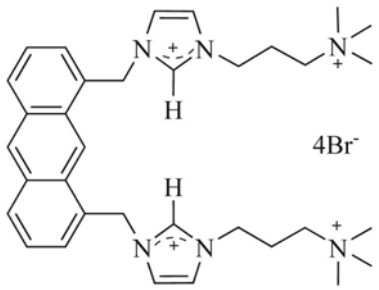

43

Figure 4.1 A fluorescent chemosensor for GTP.

Another example of a fluorescent chemosensor (**44**) which is able to detect ADP, ATP, and the pyrophosphate anion[a] in depicted in Figure 4.2.[103] Here, a macrocyclic polyamino-metal complex acts as anion host while a fluorescent aromatic amine acts as a fluorescent reporter. In the absence of anions, the 7-amino group of coumarin is weakly coordinated by the Cd^{2+} ion. By the addition of an appropriate anion, the amino group is displaced and the anion coordinates to Cd^{2+} instead. Consequently, changes in the emission spectrum of the fluorophore are generated so as functional substitution at the 7-position of the coumarin ring affects the fluorescence spectra of 7-substituted coumarins. The association constants for the nucleotides guanosine monophosphate (GMP), ADP, ATP and the

a. The sensor can be used for the detection of citrate as well.

pyrophosphate anion were found to be in the range (1.3-7.1)*10^4 M^{-1}. Lower association constants were found for inorganic anions and other nucleotides tested in the study (adenosine, uridine, and cytidine monophosphates). A few more recent examples of chemical sensors for nucleotides and the pyrophosphate anion can be found in the references [104-109].

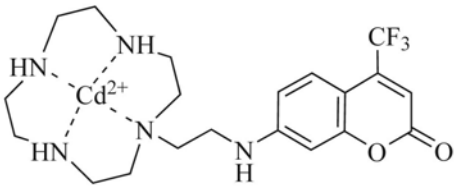

44

Figure 4.2 A fluorescent chemosensor for ADP, ATP, and the pyrophosphate anion.

Despite significant success in nucleotides' sensing, many of the systems described so far display limitations such as low sensitivity or selectivity, or require substantial synthetic efforts. In this chapter we describe a *multicomponent indicator displacement assay* (MIDA), which is based on an organometallic receptor and three dyes. In combination with statistical tools such as linear discriminant analyses or artificial neural networks, it is possible to sense nucleotides in aqueous solution by UV-Vis spectroscopy with high fidelity.

4.2. Results and discussion

For a classical indicator displacement assay a particular indicator is generally chosen in such a way that its affinity for the receptor is lower than that of the analyte of interest but higher than that of competing analytes.[10,23,25,44,110] The analysis is then performed at the wavelength, where the free and the bound indicator display the largest difference in absorption (colorimetric sensor) or emission (fluorescent sensor). Although the majority of IDAs have been performed according to this scheme, there are first reports, which suggest that the parallel utilization of multiple receptors and/or indicators in a single cuvette can be advantageous. Anslyn at al. have used a MIDA based on two receptors and two indicators to simultaneously sense malate and tartrate.[91] Subsequently, the same group has shown that citrate and calcium can be determined with an IDA, in which one analyte acts as a second receptor.[90] In chapter 5 we will describe a MIDA based on a dynamic mixture of several metal-dye complexes, which can be used to sense di- and tripeptides.[111,112]

A direct consequence of using multiple receptors/indicators is that the dynamic range of the assay can be enlarged. For a classical one receptor-one indicator IDA, analytes which show a significantly higher or lower affinity to the receptor than the indicator, give rise to the same all or nothing signal. In MIDAs, low-affinity analytes *and* high-affinity analytes may give rise to a signal. For a sensor based on one receptor and three different indicators, this is shown in Scheme 4-1.

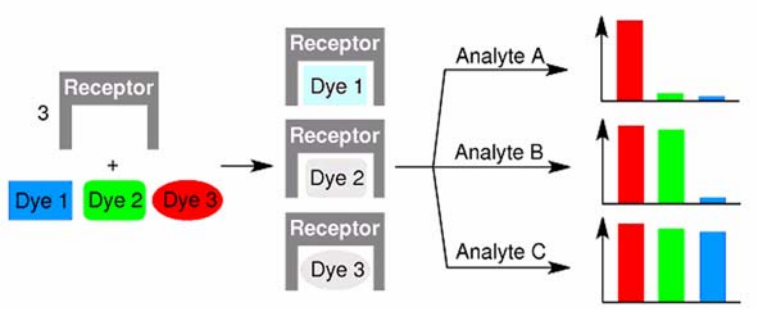

Scheme 4-1 Schematic representation of a MIDA based on one receptor and three different indicators (dyes 1-3). Analytes with a low affinity for the receptor lead to a partial displacement of the indicator whereas high-affinity analytes replace all indicators.

The assembly of the receptor with the dyes leads to the formation of three sensors, which give a differential response upon addition of analytes. One should note that the changes for the various indicator/receptor combinations need to occur in different regions of the spectrum in order to provide a good differentiation. As a consequence, the analysis is performed with the data of several wavelengths and pattern recognition protocols are valuable tools to assist the analysis. The MIDA approach is conceptually related to sensor arrays.[56,113] But contrary to sensor arrays with independent sensor units, the sensors used in a MIDA are connected by exchange reactions. Furthermore, the various sensors of an array are generally addressed separately whereas for a MIDA, a single measurement is sufficient as the read-out.

Previously, we have shown that the organometallic complex $[Cp^*RhCl_2]_2$ (**34**) can be used to construct IDAs for the sensing of His/Met containing peptides (Chapter 2), amino acids (Chapter 3), and aminosugars.[114] It had been reported that the Cp*Rh fragment is able to bind to nucleotides in aqueous solution.[115] This prompted us to investigate, whether **34** can be used to build a MIDA for nucleotides. Suited indicators for a MIDA should fulfil the following

criteria: a) they should bind to the Cp*Rh fragment with different affinities; b) the spectroscopic changes upon coordination should occur in different regions of the UV-Vis spectrum. From a small screening of commercially available dyes (see the Annex for other dyes tested), the following three indicators emerged as potential candidates: gallocyanine (**40**), mordant yellow 10 (**45**), and evans blue (**46**) (Figure 4.3).

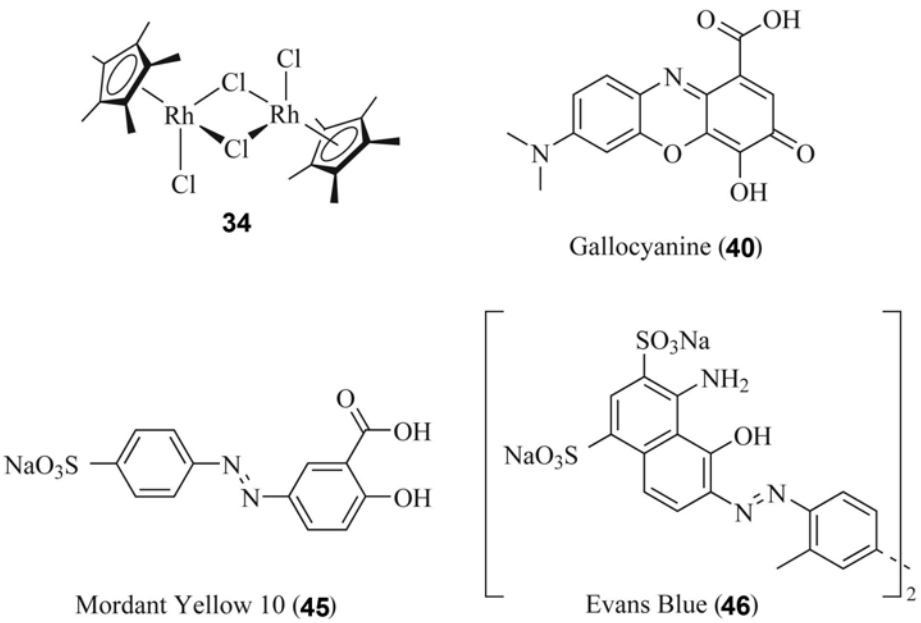

Figure 4.3 The Rh complex and the three dyes which were used to build the sensor.

To determine the association constant between the Rh complex and mordant yellow 10 (**45**), UV-Vis titration experiments were performed. The titration data were fitted to a 1:1 binding algorithm using the program DATAN 3.1, trial version.[116] The metal binding constant for mordant yellow 10 (**45**) was determined to be $K_{\mathbf{45}}$ = 3.7 (± 0.3)*10^4 M^{-1}, and major changes upon binding occur at 408 nm.[b] Gallocyanine shows an affinity of $K_{\mathbf{40}}$ = 2.3 (± 0.2)*10^6 M^{-1} and spectral changes occur at 625 and 720 nm (see Chapter 3, Figure 3.4). The affinity of evans blue to the Rh complex was found to be higher than that of gallocyanine but due to the presence of multiple metal binding sites, an association constant was not calculated. The most significant spectral changes occur at 601 nm. The titration curves for **45** (40 μM) and **46** (20 μM) by **34** (0-25 μM) are shown in Figure 4.4 and Figure 4.5 respectively.

*b. Experimental conditions: [**45**] = 25 μM, [**34**] = 0 – 25 μM, 50 mM phosphate buffer, pH 7.4*

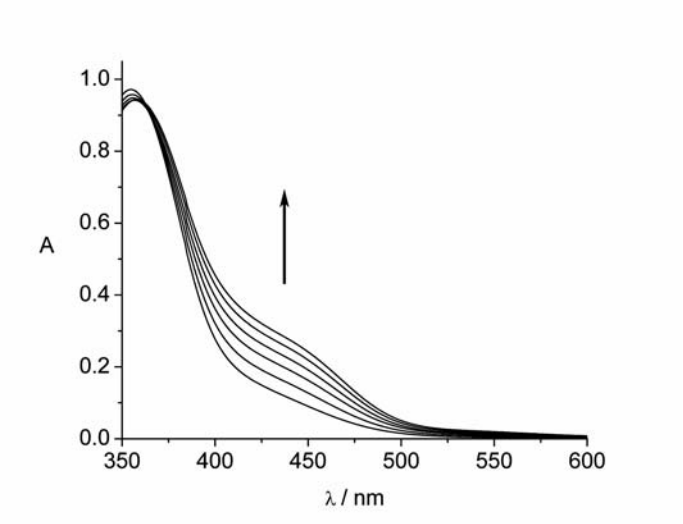

Figure 4.4 UV-Vis spectra of solutions of **45** (40 μM) upon addition of a variable amount of complex **34** (final Rh concentration: 0, 10, 20 30, 40, and 50 μM). The spectra were recorded in H_2O (50 mM phosphate buffer, pH 7.4) after equilibraion.

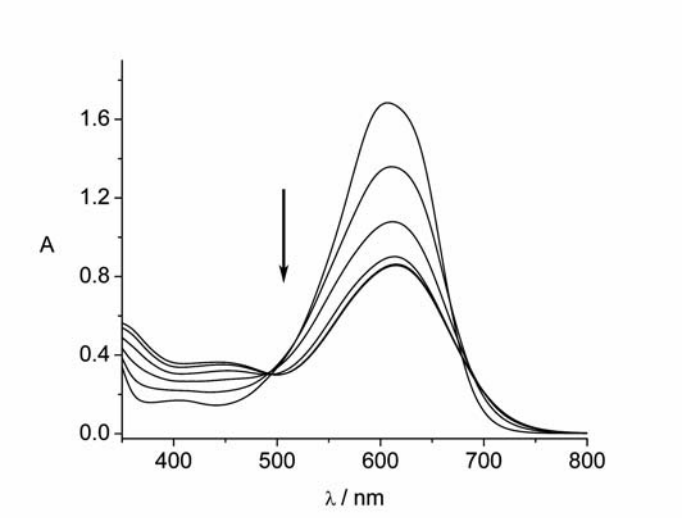

Figure 4.5 UV-Vis spectra of solutions of **46** (20 μM) upon addition of a variable amount of complex **34** (final Rh concentration: 0, 10, 20 30, 40, and 50 μM). The spectra were recorded in H_2O (50 mM phosphate buffer, pH 7.4) after equilibraion.

To reveal the spectroscopic changes generated upon coordination of the dyes **40**, **45**, and **46** to the Rh complex **34**, the following experiment was performed: the solutions of the respective dye (final concentrations: 40 μM for **40** and **45**, 20 μM for **46**) and **34** (final Rh concentration: 40 μM) were mixed in a cuvette and the UV-Vis spectrum was measured after an equilibration time of 1 hour. The same experiment was performed without complex **34**. The difference between the spectrum of the pure dye and the dye-Rh complex was calculated (Figure 4.6).

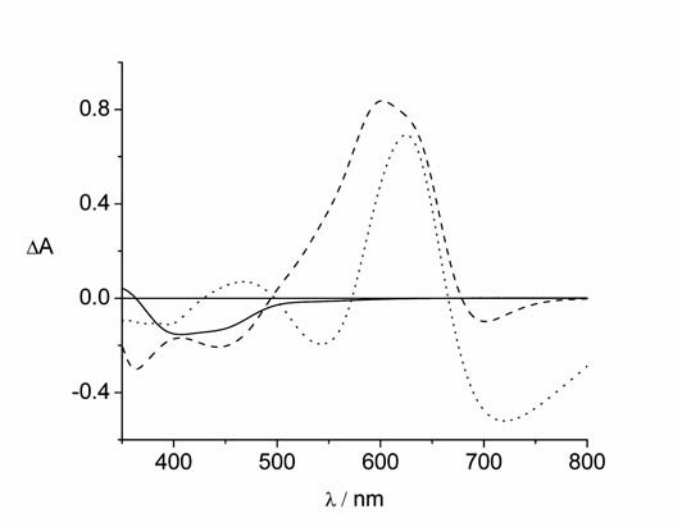

Figure 4.6 UV-Vis difference spectra obtained upon coordination of mordant yellow 10 (solid line), gallocyanine (dotted line) or evans blue (dashed line) to **34**. Concentrations: [mordant yellow 10] = 40 μM, [gallocyanine] = 40 μM, [evans blue] = 20 μM, [Rh] = 40 μM; 50 mM phosphate buffer, pH 7.4.

Next, we investigated the response of a sensor comprised of complex **34** and the dyes **40**, **45**, and **46** upon addition of the nucleotides adenosine diphosphate (ADP), adenosine triphosphate (ATP) or guanosine triphosphate (GTP). The respective analyte (final concentration: 0.5 mM) was mixed with the solution of the sensor (final concentrations: [mordant yellow 10] = [gallocyanine] = 40 μM, [evans blue] = 20 μM, [Rh] = 120 μM). A blank experiment was performed with no nucleotide being added. After an equilibration time of 1 hour the UV-Vis spectrum in the region 350-800 nm was recorded. The difference between the blank measurement and the respective analytes was calculated.

For ADP, the most pronounced changes occurred at 443 nm indicating that only the weakly bound mordant yellow 10 was displaced to a significant extend (Figure 4.7). For GTP, changes at 619 nm were observed in addition to changes at 436 nm. This showed that GTP has a higher affinity for the Rh complex than ADP, resulting in a replacement of mordant yellow 10 and gallocyanine. For ATP, the maximum changes in the UV-Vis spectrum occurred at 619 nm, which suggested that this analyte is also able to partially displace the high affinity dye evans blue.[c] A MIDA based on complex **34** and the dyes **40**, **45** and **46** therefore allows an easy distinction of these three nucleotides. In this case the different responces to the analytes come from the fact that all three nucleotides have a different affinity to the Rh-Cp* complex.[d]

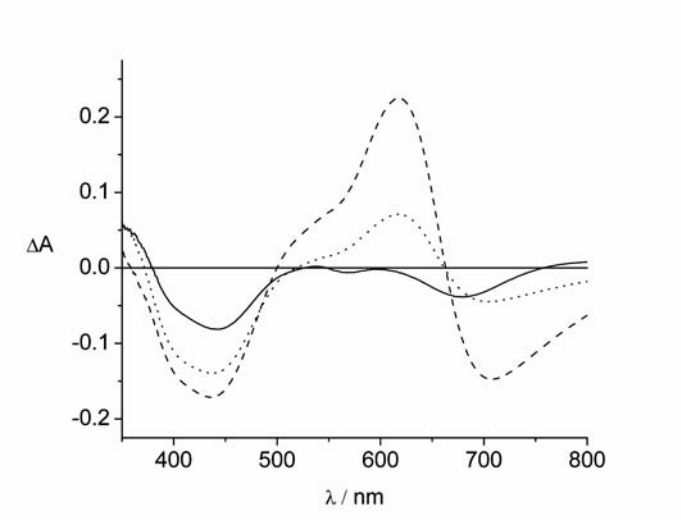

Figure 4.7 UV-Vis difference spectra obtained upon addition of ADP (solid line), GTP (dotted line) or ATP (dashed line) to a sensing ensemble composed of complex **34** and the dyes **40**, **45** and **46**. Concentrations: [mordant yellow] = [gallocyanine] = 40 μM, [evans blue] = 20 μM, [Rh] = 120 μM, [nucleotide] = 0.5 mM, 50 mM phosphate buffer, pH 7.4.

To test the scope of our sensor, we first extended the range of the analytes by adding cyclic adenosine monophosphate (cAMP), adenosine monophosphate (AMP) and the pyrophosphate anion (PPi). We then performed a similar experiment but this time we employed a linear discriminant analysis (LDA)[55] to identify the analytes. Six independent

*c. Control experiments with complex **34**, evans blue, and ATP confirmed that ATP can indeed displace evans blue to some extent.*

d. NMR experiments showed that several species are formed upon reaction of the nucleotides with the Cp-Rh complex so the exact constants could not be calculated.*

measurements were performed for each analyte ([nucleotide] = [PPi] = 1.0 mM, the sensor composition is the same as in Figure 4.7). The intensities at the wavelengths 720, 625, 600, 540 and 440 nm were chosen as the input variables for the LDA. These wavelengths correspond approximately to the maxima in the difference spectra for the dyes **40**, **45**, and **46** (Figure 4.6). A 100% classification accuracy was achieved. The final score plot is shown in Figure 4.8. The data appear in well-separated groups, which demonstrates that the six analytes can readily be discriminated.

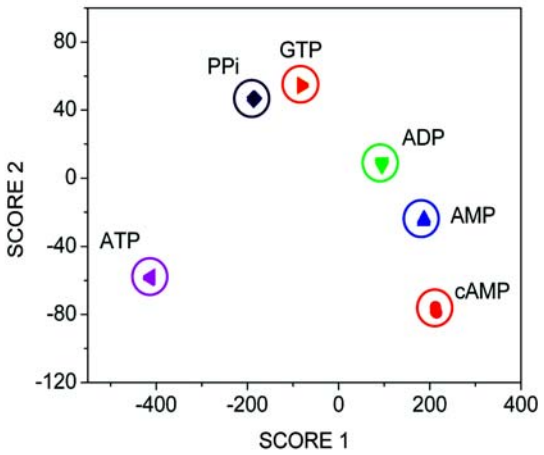

Figure 4.8 Two-dimensional LDA score plot for the analysis of five different nucleotides and pyrophosphate. Concentrations: [mordant yellow] = [gallocyanine] = 40 μM, [evans blue] = 20 μM, [Rh] = 120 μM, [nucleotide] = 1.0 mM, 50 mM phosphate buffer, pH 7.4.

The very good differentiation that was achieved prompted us to attempt a more difficult task: to determine simultaneously the concentrations of several analytes. For this purpose, we have focused on ATP, cyclic AMP (cAMP), and PPi. The hydrolysis of ATP to give cAMP and PPi is catalyzed by adenylate cyclase (AC). AC is an important enzyme, which participates in many signalling pathways.[117,118] Its activity is commonly measured by monitoring the conversion of [α-^{32}P]ATP to [α-^{32}P]cAMP using ion-exchange chromatography to separate the nucleotides.[119-121] To test whether our sensing ensemble could be used to measure the concentrations of ATP and cAMP/PPi simultaneously, we prepared two stock solutions: one with ATP and another one with equal concentrations of cAMP and PPi. By mixing these stock solutions, we then made a calibration set of 36 ternary

solutions with ATP and cAMP/PPi concentrations between 0.0 and 1.0 mM (0.2 mM increments). The calibration set was used to train an artificial neural network (ANN) employing a standard multi-layer perceptron (MLP) model.[122] MLP is one of the most popular models of ANNs. The main component of a MLP is the neuron, a unit which sums the inputs and performs a transformation *via* an activation function, which is responsible for non-linearity. In our case, the hyper-tangent transfer function was used. Neurons form a structure with some inputs representing exploratory variables, a variable number of hidden layers including the activation function, and the outputs corresponding to the target variable(s). The particular MLP structure used for our analysis contained five input neurons (the selected input wavelengths - 720, 625, 600, 540, and 440 nm), five hidden neurons arranged in one layer, and two output neuron which provide the values of target variables (concentrations). The structure of the MLP is presented in Figure 4.9.

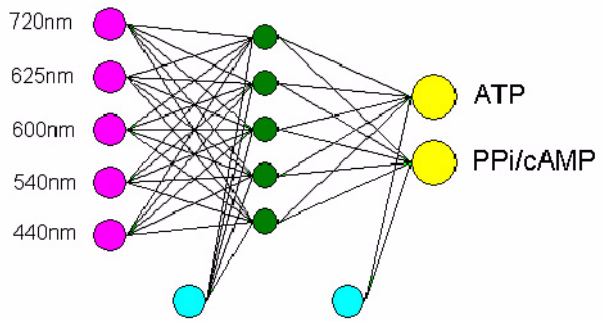

Figure 4.9 The structure of the MLP with five input neurons (purple), one layer of five hidden neurons (green), two constants (blue), and two outputs (yellow).

The number of hidden neurons is subject to optimal configuration for a particular case study. In general, the complexity of the MLP must be consistent with the amount of information for training – there should be enough data to match the dependence. Choosing too many hidden neurons may lead to over-fitting. The MLP then loses its ability to generalize the information from the samples. In the case of over-fitting, the complexity of the model is too high for the task. The model fits the training data precisely; however it can not generalize when new samples are introduced. To avoid the risk of an over-fitting, a 6-fold cross-validation error was considered. This is a standard and commonly used approach in the model selection. In the cross-validation procedure, a fraction of the available training data is not used for training but for the estimation of the validation error of the model. In a K-fold cross-validation, the data are

split into K parts, each of them being consequently excluded from the training set and used to calculate the mean square error of the model. The results are then averaged over all splits, and, if necessary, after several repetitions of the described procedure.

The application of MLP proceeded first through the described structure selection phase. Then the model with the optimized structure was trained on the data, i.e. the weights of the neurons were adapted to minimize the mean squared error. This training employed minimization of the quadratic mean square error (MSE) cost function for optimizing the summation weights at each neuron. An error back-propagation algorithm was applied to calculate the gradient of the MSE and to adapt the weights. The Levenberg-Marquardt algorithm was used for this purpose. After the MLP was trained and the optimal weights were found, the predictions were computed by presenting the intensities at the selected five wavelengths of the test samples to the MLP inputs. The results at the outputs were then computed using the trained MLP. The software which implements the described MLP was developed in the research group of the Institute of Geomatics and Analysis of Risk, University of Lausanne.[123],e

To test the predictive power of the trained artificial neural network, we prepared a validation set of ten samples with ATP and cAMP/PPi concentrations between 0.0 and 1.0 mM. The actual and predicted concentrations for the validation samples are shown in Figure 4.10. Root-mean-square errors were calculated to be 0.045 mM for ATP and 0.042 mM for cAMP/PPi. It is interesting to note that lower concentrations were predicted for ATP for each sample while that wasn’t the case for cAMP/PPi.

e. We are grateful to V. Timonin (Institute of Geomatics and Analysis of Risk, University of lausanne) for providing the software.

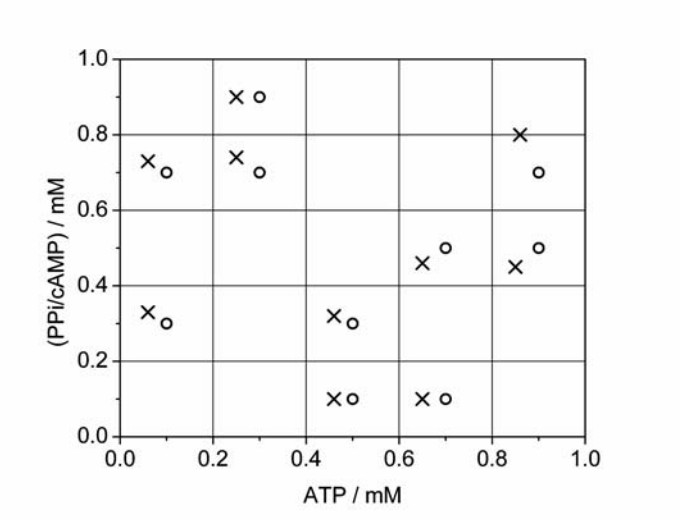

Figure 4.10 Actual (circles) and predicted (crosses) concentrations for ternary ATP/cAMP/PPi mixtures ([cAMP] = [PPi]). The intersections of the grid lines represent the 36 points used as the calibration set. The composition of the MIDA is the same as in Figure 4.6 and Figure 4.7.

4.3. Conclusion

In summary, we have shown that a sensing ensemble composed of a Rh complex **34** and three dyes **34**, **45**, and **46** can be used to sense low millimolar concentrations of nucleotides and pyrophosphate in buffered aqueous solution. Moreover, the MIDA allows to simultaneously determine the concentrations of ATP and PPi/cAMP with a single UV-Vis measurement. The sensor displays a very pronounced selectivity for nucleotides and PPi over phosphate as the analysis can be performed in 50 mM phosphate buffer. From an experimental point of view it is noteworthy that the sensor can be obtained by simply mixing four commercially available compounds. Overall, the results clearly demonstrate the analytical power of MIDAs in combination with pattern-recognition protocols.

Chapter 5

Dynamic combinatorial libraries of dye complexes as sensors[111,112]

5.1. Introduction

Mixtures of compounds, which are formed by the combinatorial assembly of molecular building blocks under thermodynamic control are generally referred to as "dynamic combinatorial libraries" (DCLs).[124-130] DCLs represent adaptive chemical networks. If a target molecule is added to such library, a re-equilibration will occur until thermodynamic minimum is established. Scheme 5-1 illustrates how the addition of a target molecule to the dynamic combinatorial library of receptors results in the amplification of the library member with the highest affinity for the target. Similarly, addition of a receptor to the dynamic combinatorial library of inhibitors can be used to amplify the inhibitor with the highest affinity for the corresponding receptor. Given that it is possible to detect this amplification by analytical techniques, a dynamic combinatorial library could be screened for molecules that bind to the target in a single experiment.

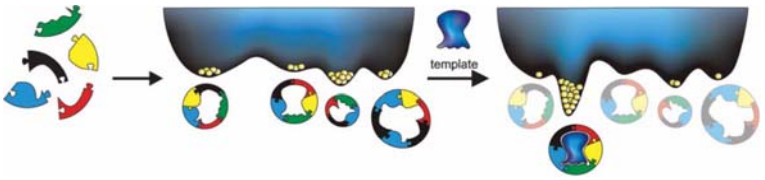

Scheme 5-1 Amplification of the best receptor for the target molecule in a DCL. Adopted from [124] @The Royal Society of Chemistry

In one of the early examples, Lehn *et. al.* screened a dynamic combinatorial library composed of 12 imines in order to find the best inhibitor for the enzyme carbonic anhydrase.[131] The DCL was prepared by mixing 4 amines with 3 aldehydes (Scheme 5-2). The exchange reactions were stopped by the irreversible reduction of the imine bond. The authors found that the addition of the carbonic anhydrase shifted the equilibrium population toward the product **47**, that was closest in structure to the known strong inhibitor of the enzyme (**48**) (Figure 5.1).

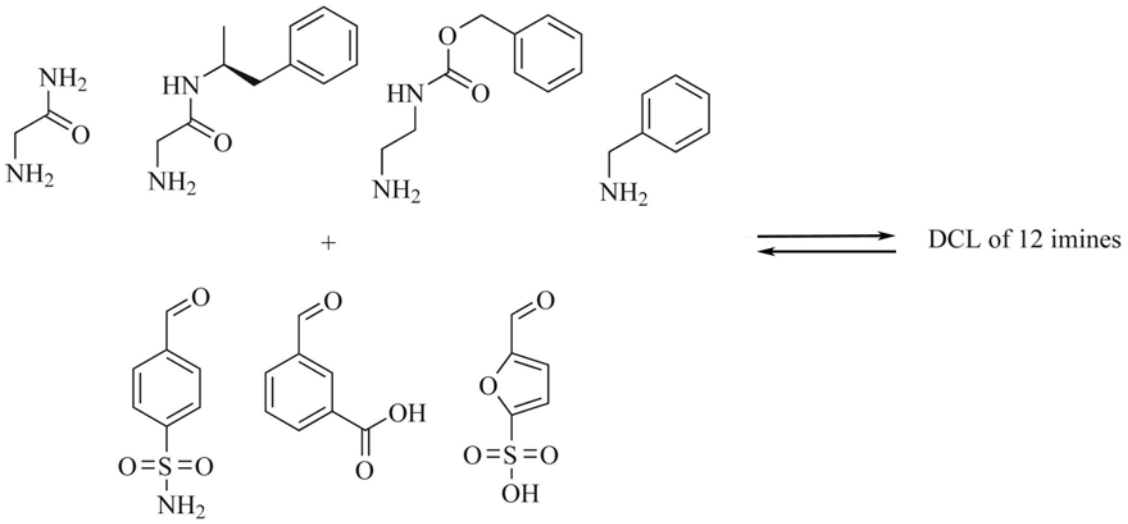

Scheme 5-2 The dynamic combinatorial library of 12 imines screened for the best inhibitor of the enzyme carbonic anhydrase.

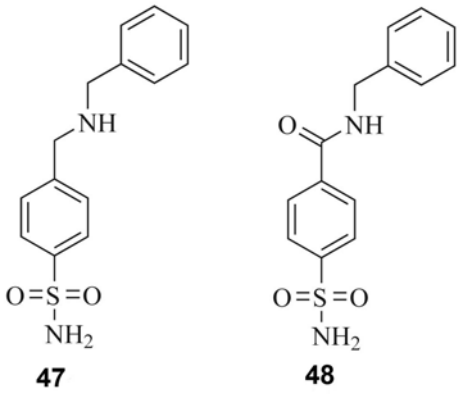

Figure 5.1 The library member amplified in the presence of carbonic anhydrase (**47**) and a known strong inhibitor of the enzyme (**48**).

This target-induced adaptation of DCLs has been employed to study receptors, catalysts, enzyme inhibitors and new materials.[124-141] But speaking more generally, the relative concentrations of the members of a DCL depend not only on the presence or absence of a target molecule, but also on the whole environment of the systems (solvent, pH etc.). A certain library composition is thus a characteristic feature of the respective environment. If the DCL composition can be transduced into a specific signal output, it is possible to use the DCL as a sensor. Up to now, DCLs have mainly been analyzed by HPLC, mass spectrometry and

NMR spectroscopy.[124-130] For sensing purposes, however, a fast and cheap analysis method such as fluorescence or UV-Vis spectroscopy would be advantageous.

It should be noted, that the utilization of dynamic combinatorial libraries for sensing purposes is still largely unexplored. Just a few examples, which can be considered as DCL sensors of low complexity (though not described as such), are known from the literature. Anslyn *et. al.* used a chemosensing ensemble comprised from two indicators and two receptors to simultaneously detect tartrat and malate[91] or citrate and calcium.[90] The multicomponent indicator displacement assay employed for the detection of nucleotides and described in Chapter 4 can be considered as a small library of 3 sensors. The first work where authors claimed utilization of a *dynamic polymer* for sensing purposes was accomplished in the group of Lehn.[141]

Lehn *et al*. investigated the condensation reaction of 2,7-fluorenebiscarboxaldehyde (**49**) with 2,7-diaminofluorene (**50**) and *trans*-1,4-diaminocycloxehane (**51**) in the presence of variable amounts of Zn salt (Scheme 5-3).

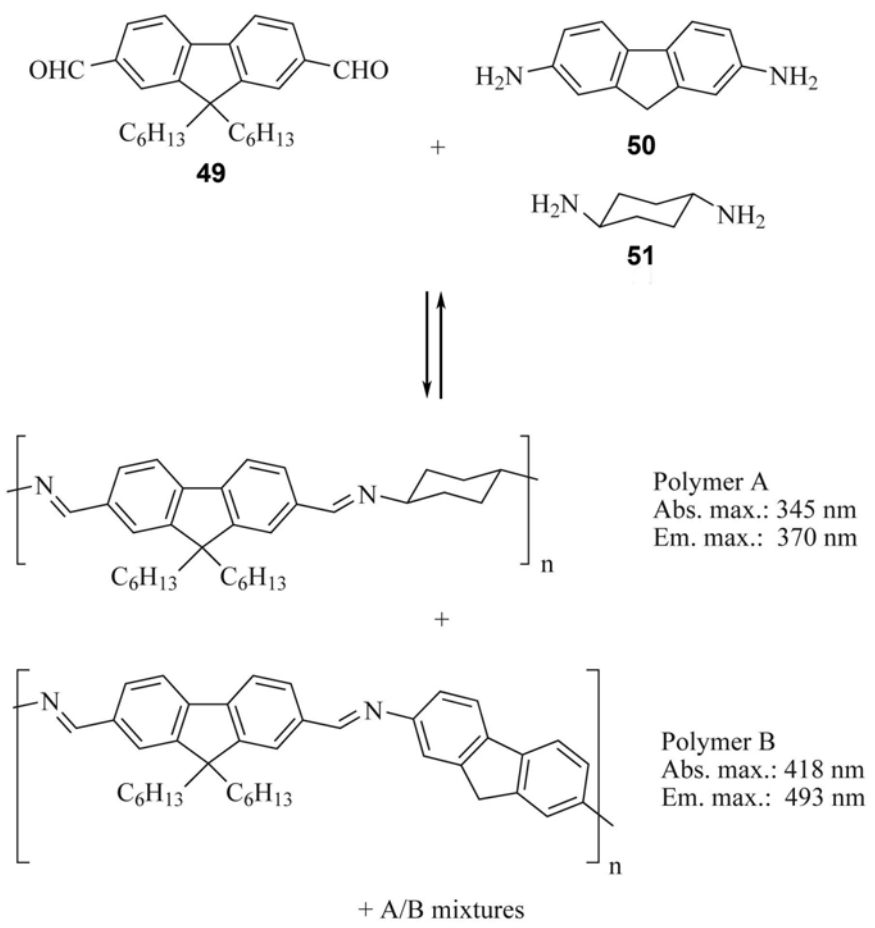

Scheme 5-3 Formation of a dynamic mixture of polymers by condensation of **49** with **51** and **52**. Upon addition of Zn^{2+}, the rearrangement towards polymer B accompanied by a change of color is observed.

In the absence of zinc, polymer A was found to be dominant product. The addition of increasing amounts of zinc shifted the equilibrium in favor of the polymers containing the aromatic monomer **50**. Polymer B was found to be the dominant species when the system was equilibrated in the presence of two equivalents of Zn^{2+}. This shift was explained by the preferential complexation of zinc salt to the more nucleophilic diamine **51**. Since the polymers A and B show different absorption spectra, the zinc-modulated change in polymer composition resulted in a change in color. Similarly, the fluorescence emission maximum was shifted from 370 nm to 493 nm with a concomitant increase in intensity. The dynamic polymer ("dynamer") can therefore be regarded as a system which is able to detect zinc due to an analyte-induced constitutional rearrangement.

To explore the utilization of dynamic combinatorial libraries for sensing purposes, we have constructed a DCL of metal-dye complexes, in which the library members have a different color. Any re-equilibration will therefore result in a variation of the UV-Vis spectrum of the mixture (Figure 5.2). In the following section we show that such a library can be used to identify dipeptides in aqueous solution with high selectivity (section 5.2.1). Moreover, we will show that the DCL composition can be optimized for a particular sensing problem (section 5.2.2).

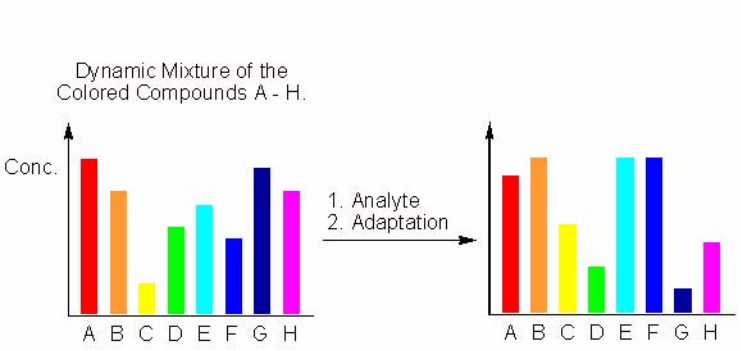

Figure 5.2 The adaptive behavior of a DCL upon addition of an analyte can be used to identify this analyte by UV-Vis spectroscopy given that the library members possess a characteristic color.

5.2. Results and discussion

5.2.1. Dynamic combinatorial libraries of dye complexes as sensors - proof of the concept

In order to generate a DCL, in which the library members have a characteristic color, we have used the commercially available dyes arsenazo I (**52**), methylcalcein blue (**53**) and glycine cresol red (**54**) in combination with the metal salts $CuCl_2$ and $NiCl_2$ (Scheme 5-4). In buffered aqueous solution (2-(N-cyclohexyl)aminoethansulfonic acid (CHES) buffer, pH 8.4), the dyes form stable complexes with Cu^{2+} and Ni^{2+} as evidenced by UV-Vis titration experiments. This is in agreement with reports about the high metal affinity of **52**,[142-144] **53**,[145-147] and **54**[148,149] To investigate the stoichiometry of the metal-dye complexes, Job's plot analyses[150] have been performed for each metal-dye combination ($[dye+metal]_{total}$ = 150 μM, 15 mM CHES buffer, pH 8.4). The experiments revealed that complexes with more than one ligand per metal were formed in addition to 1:1 complexes (see Figure 5.3-Figure 5.8).

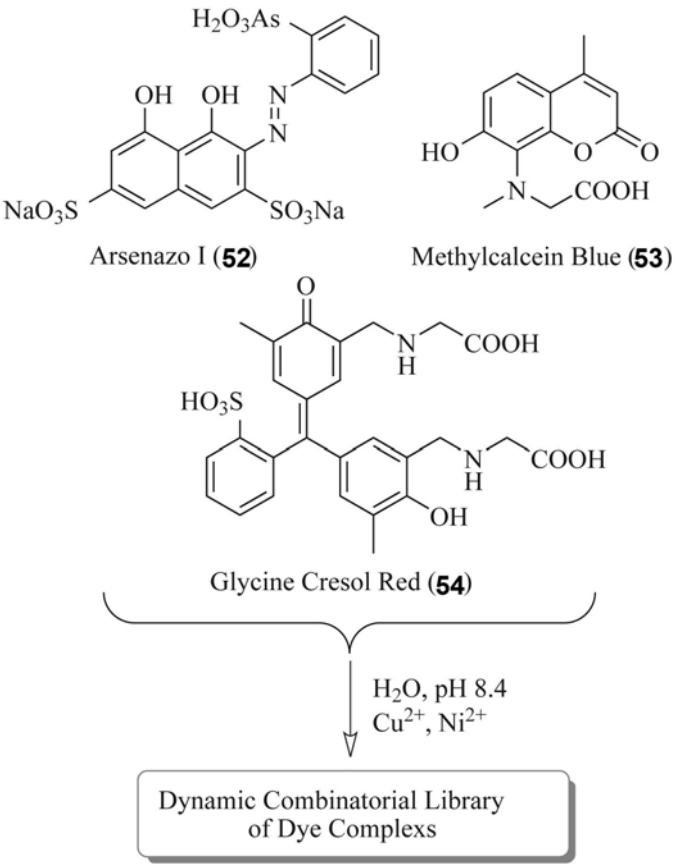

Scheme 5-4 Generation of a DCL of metal-dye complexes by mixing azsenazo I (**52**), methylcalcein blue (**53**), and glycine cresol red (**54**) with $CuCl_2$ and $NiCl_2$ in buffered aqueous solution.

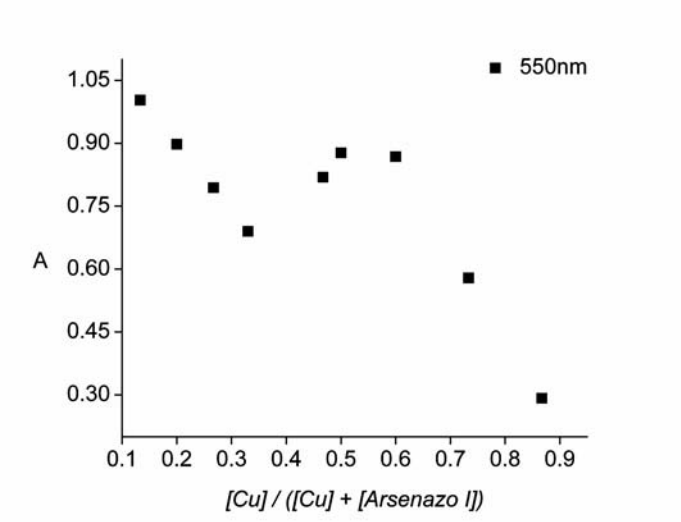

Figure 5.3 Job's plots for arsenazo I and $CuCl_2$. Concentrations: $[dye + metal]_{total}$ = 150 μM, 15 mM CHES buffer, pH 8.4.

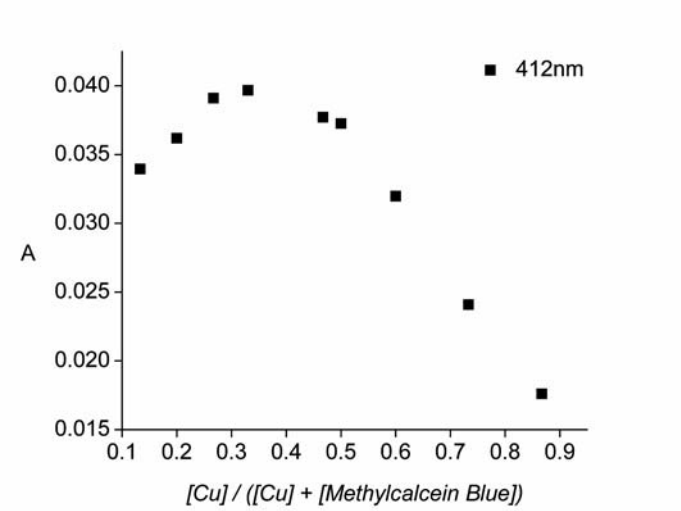

Figure 5.4 Job's plots for methylcalcein blue and $CuCl_2$. Concentrations: $[dye + metal]_{total}$ = 150 μM, 15 mM CHES buffer, pH 8.4.

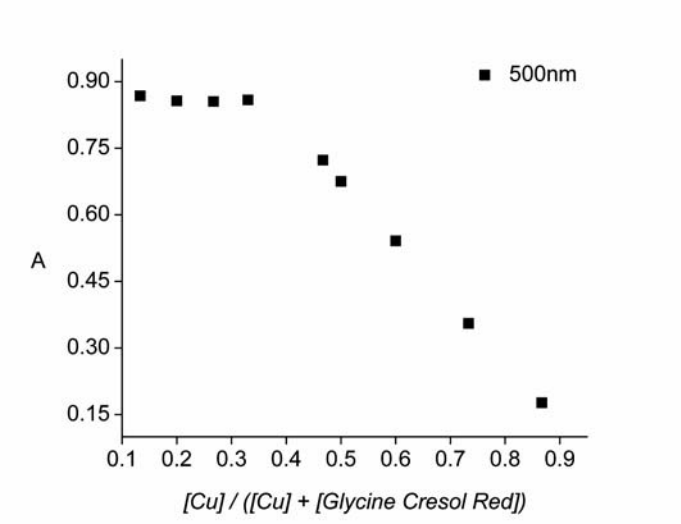

Figure 5.5 Job's plots for glycine cresol red and $CuCl_2$. Concentrations: $[dye + metal]_{total}$ = 150 μM, 15 mM CHES buffer, pH 8.4.

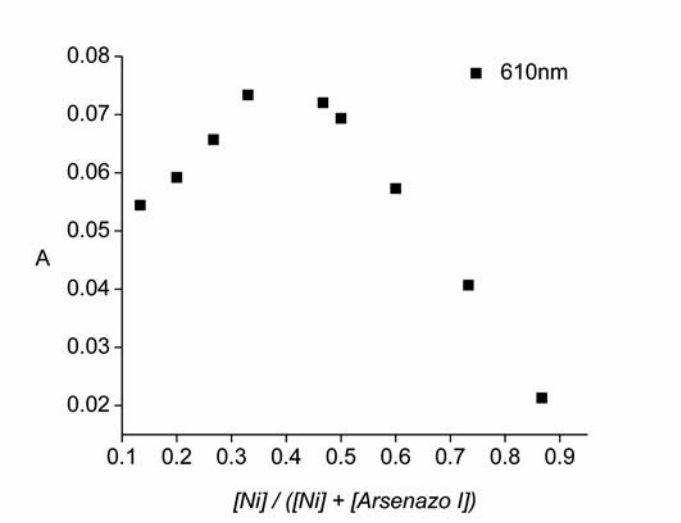

Figure 5.6 Job's plots for arsenazo I and $NiCl_2$. Concentrations: $[dye + metal]_{total}$ = 150 μM, 15 mM CHES buffer, pH 8.4.

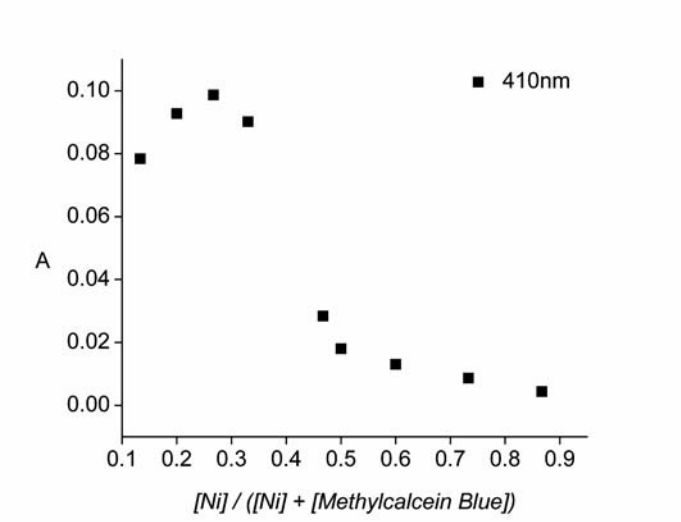

Figure 5.7 Job's plots for methylcalcein blue and $NiCl_2$. Concentrations: $[dye + metal]_{total}$ = 150 μM, 15 mM CHES buffer, pH 8.4.

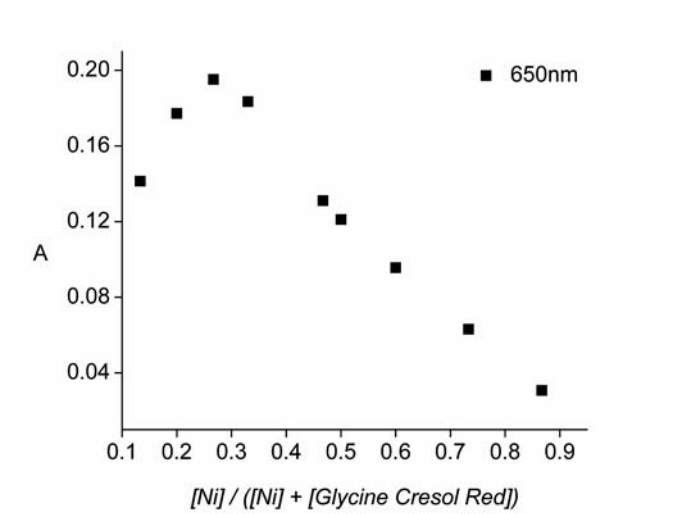

Figure 5.8 Job's plots for glycine cresol red and $CuCl_2$. Concentrations: $[dye + metal]_{total}$ = 150 μM, 15 mM CHES buffer, pH 8.4

To demonstrate that individual metal-dye complexes are able to undergo ligand exchange reactions, the following experiments have been performed: for each metal-dye combination, the UV-Vis spectrum was recorded (final concentrations: [dye] = 75 μM, [metal] = 50 μM, 37.5 mM CHES buffer, pH 8.4). Then the spectra of combinations of one metal and

two dyes or two metals and one dye (final concentrations: $[dye]_{total}$ = 150 μM, $[metal]_{total}$ = 100 μM, 37.5 mM CHES buffer, pH 8.4) were recorded (all spectra was recorded after equilibration for 30 min. at 60 °C). From this data, the sum of the spectra of the individual metal-dye combinations were subtracted. The resulting difference spectra are depicted in Figure 5.9, Figure 5.10, and Figure 5.11.

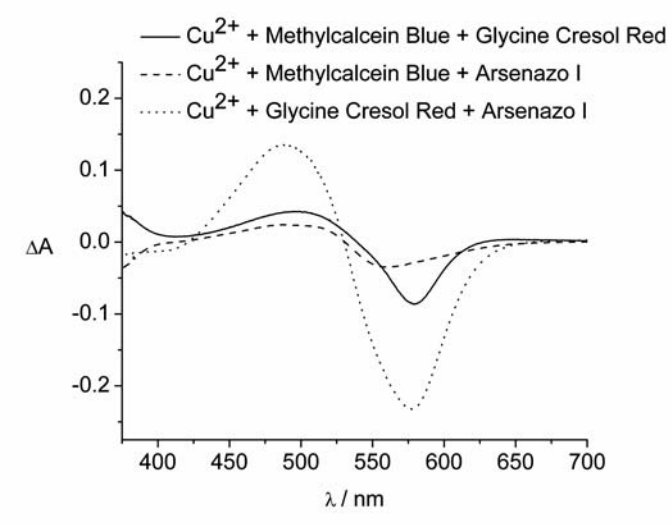

Figure 5.9 Difference spectra for the ligand exchange between copper-dye(s) complexes.

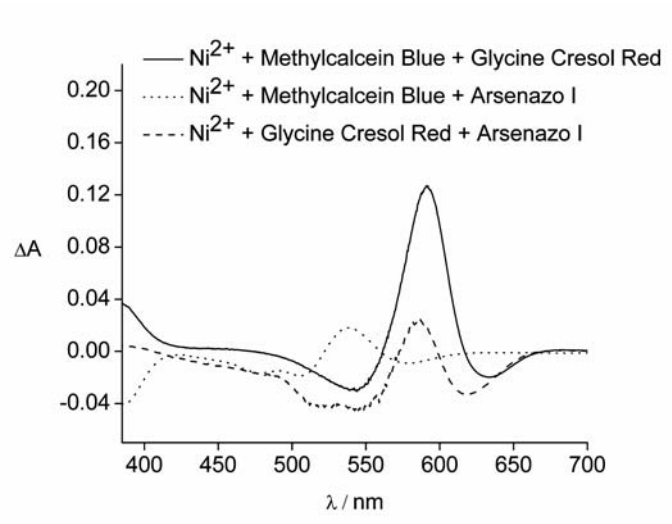

Figure 5.10 Difference spectra for the ligand exchange between nickel-dye(s) complexes.

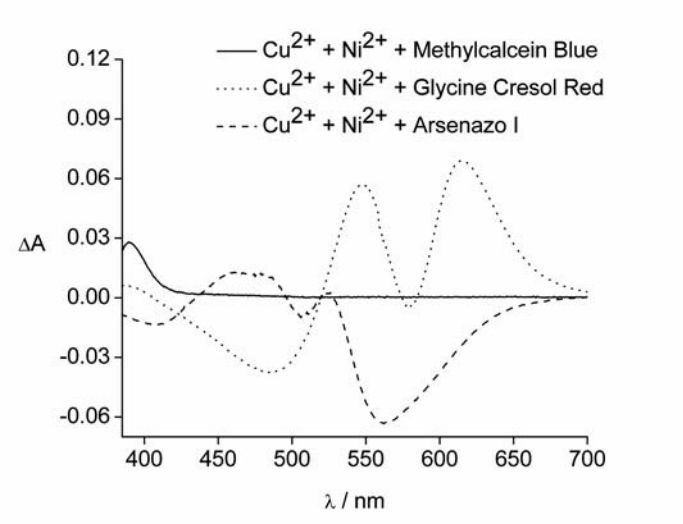

Figure 5.11 Difference spectra for the ligand exchange between dye-metal(s) complexes.

This data confirmed that solutions of the dyes **52 - 54** and the two metal salts contain a complex mixture of metal-dye complexes and that these complexes and small amounts of free metal ions and dyes are in a dynamic equilibrium with each other. Any disturbance of this equilibrium by addition of an analyte was expected to result in a characteristic change of color.

We decided to use dipeptides as analytes to demonstrate this proposal (for the sensors which are able to detect small peptides or amino acids in aqueous solution see Chapters 2 and 3, as well as the references: [32,45,151-156]). Dipeptides are known to form stable complexes with Cu^{2+} and Ni^{2+} ions[157] and may therefore displace some of the dyes from the metal ions.[9,10,110] This should lead to an increase of the free dye concentration as well as to a re-equilibration of the remaining metal-dye complexes. In the first experiment, we added aqueous solutions of the dipeptides Val-Phe, Gyl-Ala, His-Ala, Ala-His, Phe-Pro and Pro-Gly to a mixture of the three dyes and the two metal salts (final concentrations: [peptide] = 1.0 mM; [**52**] = [**53**] = [**54**] = 75 μM; [Cu] = [Ni] = 75 μM; 35 mM CHES buffer, pH 8.4). The changes of the UV-Vis spectra upon addition of the respective peptide are shown in Figure 5.12.

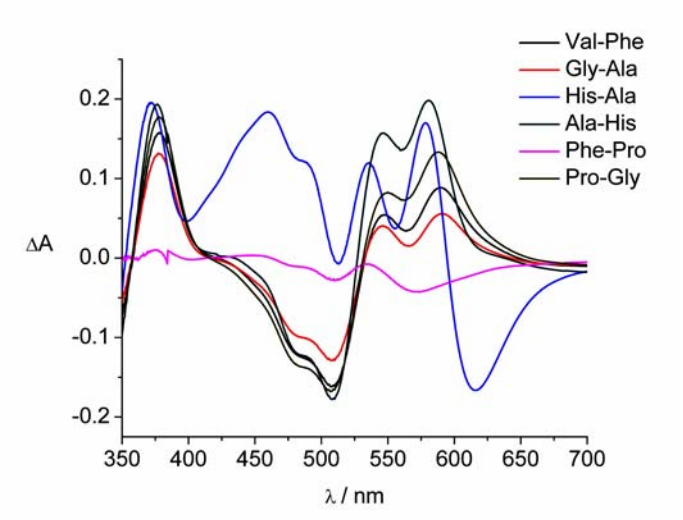

Figure 5.12 The changes in the UV-Vis spectra upon addition of different dipeptides (1.0 mM) to an aqueous solution containing a DCL sensor composed of the dyes **52-54** and the metal salts $CuCl_2$ and $NiCl_2$ ([**52**] = [**53**] = [**54**] = 75 μM, [Cu] = [Ni] = 75 μM, 35 mM CHES buffer, pH 8.4)

All six dipeptides can be easily distinguished by UV-Vis spectroscopy. An experiment of this kind can therefore be used to identify the respective dipeptide. It is interesting to note that His-Ala gave rise to a spectrum which was very different from that of the other peptides. This can be explained by the fact that the side chain of the N-terminal His residue is able to coordinate to the metal ions. The spectrum of Ala-His, on the other hand, was more similar to what was found for simple dipeptides such as Val-Phe. This suggests that the side chains of a His residue at the C-terminus is less important for metal coordination. Another distinct spectrum was found for Phe-Pro, for which rather weak color changes were observed. This highlights the importance of the amide bond for metal coordination.[157]

In order to test the scope of the DCL sensor, we have performed a second set of experiments with dipeptides, which are structurally more closely related (Gly-Ala, Val-Phe, Ala-Phe, Phe-Ala, and D-Phe-Ala). As expected, the UV-Vis difference spectra were similar to each other. We therefore used chemometrics[158-162] to classify the analytes. For each dipeptide, 15 UV-Vis measurements were performed. To verify that the discrimination between the analytes was not due to small differences in the concentrations of the peptide stock solutions, we varied the peptide concentration for each analyte on purpose by ± 5%. Thus, five

measurements were performed with a peptide concentration of 1.00 mM, five with a concentration of 0.95 mM, and five with a concentration of 1.05 mM (the sensor composition was the same as described in Figure 5.12). Data analysis was carried out with the help of the commercial statistics program SYSTAT (vers. 11.0).[163] In order to determine which wavelengths in the region between 350 and 700 nm were most relevant for the identification of the peptide, a pre-selection was performed using an automatic variable selection algorithm. The data of the eight wavelengths, which were selected, were then classified by a linear discriminant analysis (LDA).[55] A graphic representation of this analysis in the form of a score plot is given in Figure 5.13.

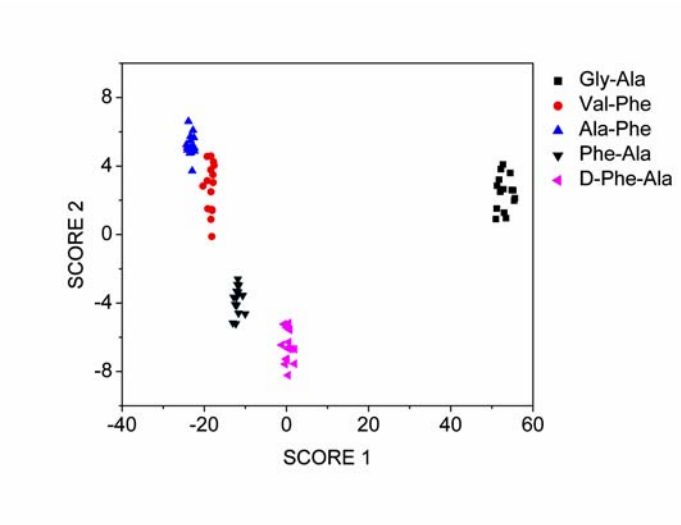

Figure 5.13 Two-dimensional LDA score plot for the analysis of five dipeptides.

A 100% discrimination was achieved for a “jack-knifed” classification matrix in which one measurement at a time was treated as an unknown and the rest of the data was used as the training set. A 97% discrimination was achieved in a cross-validation in which 50% of the measurements were taken out randomly and the rest of the data was used as the training set. The only misclassification was found for Phe-Ala, which was confused with D-Phe-Ala. This is quite remarkable, given the fact that none of the dipeptides contains coordinating side chains and that closely analytes such as the regioisomers Ala-Phe and Phe-Ala and the stereoisomers Phe-Ala and D-Phe-Ala were used.

When the complexity of the DCL was reduced by omitting one of the two metal salts, the discriminative power of the sensor was lower: for a DCL containing the dyes **52-54** and

only $CuCl_2$, 7 out of the 75 measurements were misclassified (Table 5.1) and for a DCL containing the dyes **52**-**54** and only $NiCl_2$, 17 misclassifications were obtained (Table 5.2). This shows that a certain library complexity is required to obtain a good differentiation.

Table 5.1 Jackknifed classification matrix for the DCL containing only $CuCl_2$.

	Ala-Phe	D-Ala-Phe	Gly-Ala	Phe-Ala	Val-Phe	% correct
Ala-Phe	14	0	0	0	1	93
D-Ala-Phe	0	15	0	0	0	100
Gly-Ala	0	0	15	0	0	100
Phe-Ala	0	0	0	12	3	80
Val-Phe	0	0	0	3	12	80
Total	14	15	15	15	16	91

Final concentrations: [**52**] = [**53**] = [**54**] = 75 μM, [Cu] = 150 μM, 35 mM CHES buffer, pH 8.4. For each dipeptide, five measurements were performed with a concentration of 0.95 mM, five with a concentration of 1.00 mM, and five with a concentration of 1.05 mM.

Table 5.2 Jackknifed classification matrix for the DCL containing only $NiCl_2$.

	Ala-Phe	D-Ala-Phe	Gly-Ala	Phe-Ala	Val-Phe	% correct
Ala-Phe	12	0	1	0	2	80
D-Ala-Phe	0	12	0	3	0	80
Gly-Ala	1	0	12	2	0	80
Phe-Ala	0	4	1	10	0	67
Val-Phe	3	0	0	0	12	80
Total	16	16	14	15	14	77

Final concentrations: [**52**] = [**53**] = [**54**] = 75 μM, [Ni] = 150 μM, 35 mM CHES buffer, pH 8.4. For each dipeptide, five measurements were performed with a concentration of 0.95 mM, five with a concentration of 1.00 mM, and five with a concentration of 1.05 mM.

5.2.2. Combinatorial optimization of a DCL sensor

In chapter 5.2.1 we have shown that the sensing of peptides with a DCL of metal-dye complexes is experimentally very simple because all that is required is to dissolve commercially available dyes together with transition metal salts in a buffer and to record a UV-Vis spectrum. Below we demonstrate that this approach has another major advantage: its inherent flexibility. A DCL sensor is generated by a self-assembly of multiple subunits. This allows to rapidly optimize the system for a specific sensing problem by the variation of the amounts and the relative ratios of the constituent building blocks in a combinatorial fashion. For the analysis of sequence isomeric tripeptides we will demonstrate that the best sensor composition is strongly dependent on the analytical problem that is addressed. With the optimized sensor, it is possible to discriminate mixtures of tripeptides from the samples and to obtain quantitative information.

For our experiments we focused on three different analytes: the sequence isomers His-Gly-Gly (**55**), Gly-His-Gly (**56**), and Gly-Gly-His (**57**). Our initial goal was to optimize a DCL sensor for the discrimination of the analytes **55** and **57** and of **56** and **57**. As building blocks, we used the same three dyes arsenazo I (**52**), methylcalcein blue (**53**), and glycine cresol red (**54**) together with $CuCl_2$ and $NiCl_2$ (Scheme 5-4). The peptides **55**, **56**, and **57** are known to coordinate to Cu^{2+} and Ni^{2+} in aqueous solution.[164] Depending on the nature of the peptide, the metal ion, and the pH, complexes with different stochiometries are formed. It was, thus, expected that the addition of the tripeptides to the mixture of metal-dye complexes would result in a partial liberation of dyes accompanied by a re-equilibration of the remaining metal-dye complexes and, hence, in changes in the UV-Vis spectrum.

For the screening, 20 different sensors were generated for each analyte pair by variation of the total (80, 160, 240, and 320 μM), and the relative metal concentration using a constant dye concentration of [methylcalcein blue] = [arsenazo I] = [glycine cresol red] = 75 μM in buffered aqueous solution (100 mM CHES, pH 8.4). Five independent measurements were performed for each DCL-peptide combination ([peptide] = 1.00 mM). The analytes gave rise to characteristic UV-Vis spectra, which were dependent on the DCL composition. To approximate the ability of the respective DCL sensor to discriminate between two peptides, we calculated the area between the UV-Vis curves obtained for the two analytes. The data for the peptides **56** and **57** using a DCL with a metal concentration of [Ni^{2+}] = 240 μM and [Cu^{2+}] = 80 μM are shown in Figure 5.14. The overall results of the screening are depicted in Figure 5.15.

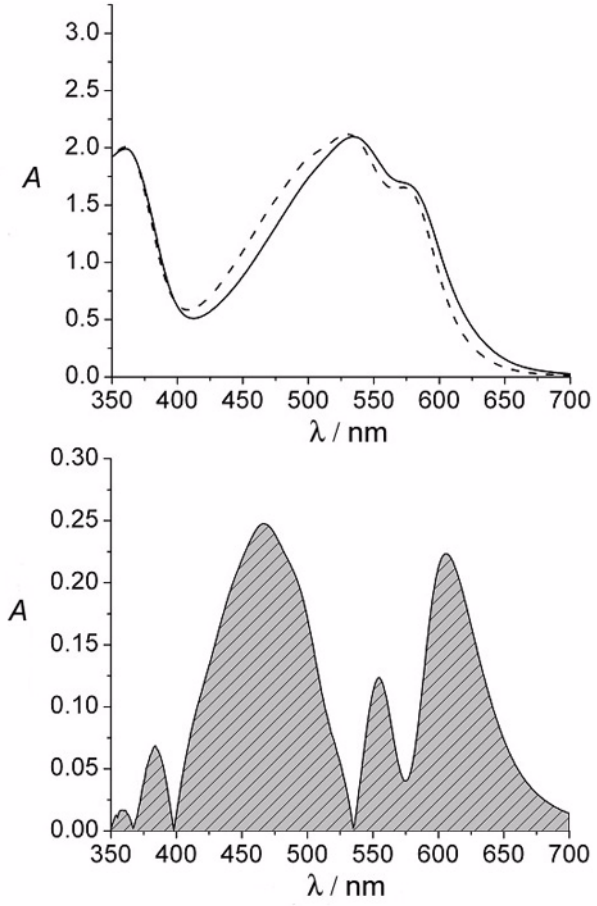

Figure 5.14 Top: UV-Vis spectra of a DCL of metal-dye complexes after addition of the tripeptides **56** (solid line) or **57** (dashed line); Bottom: absolute difference between the two curves. Conditions: [peptide] = 1.00 mM; [methylcalcein blue] = [arsenazo I] = [glycine cresol red] = 75 μM, $[Ni^{2+}]$ = 240 μM, $[Cu^{2+}]$ = 80 μM, 100 mM CHES buffer, pH 8.4. The data represent averaged values from 5 independent measurements.

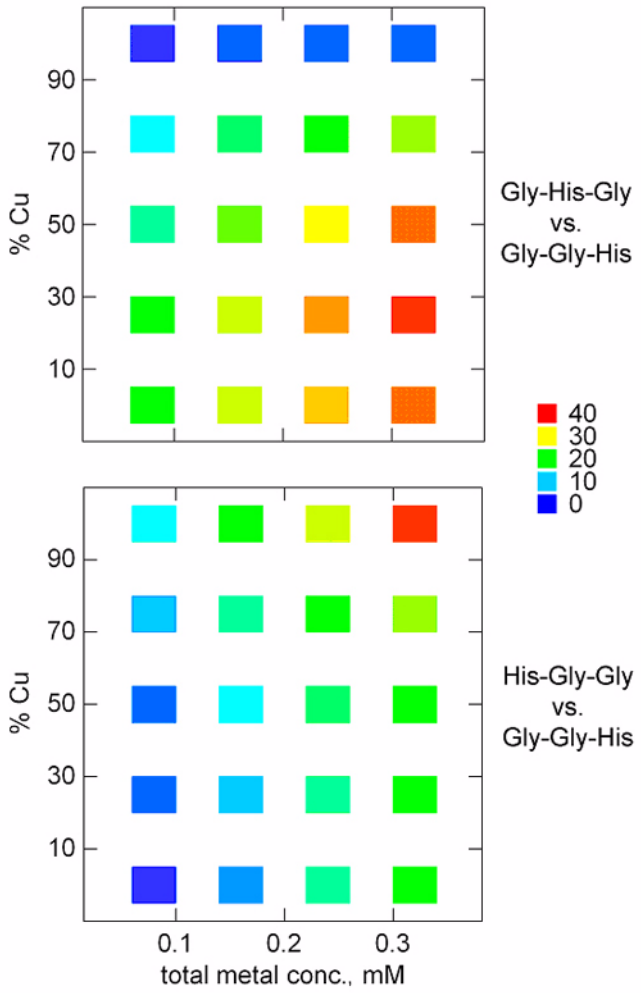

Figure 5.15 The ability of a DCL sensor to discriminate between the sequence isomers **56** and **57** (top) and **55** and **57** (bottom) as a function of the total metal concentration and Cu^{2+}/Ni^{2+} ratio. The color coding indicates the differentiation, which was achieved for the respective sensor composition. The data (arbitrary units) are based on five independent measurements; the errors are < 2 units.

For the discrimination of **56** and **57** as well as of **55** and **57**, a high total metal concentration of 320 μM was found to be advantageous. Interesting differences, however, were observed for the best Cu^{2+}/Ni^{2+} ratio. For the analyte pair **56** and **57**, a mixture of 25% Cu^{2+} and 75% Ni^{2+} resulted in the largest difference in the UV-Vis spectra. For the analyte pair **55** and **57**, on the other hand, a sensor containing exclusively copper gave the best result. This demonstrated that the optimal sensor composition can vary substantially, even for closely related analytes.

The small screening of 20 different sensors was not expected to result in the identification of the overall best sensor composition for a given analyte pair, since other important parameters, such as the total or relative dyes concentration, were not varied. Nevertheless, the best sensors identified in the screening already possess a remarkable analytical power, as demonstrated by the following results.

An interesting analytical problem is the discrimination of pure samples from mixtures. To address this issue, we used the optimized sensor containing 75% Ni^{2+} (240 μM) and 25% Cu^{2+} (80 μM) for the analyte pair **56** and **57**. Five different samples containing either the pure peptides **56** and **57** or mixtures of the two (**56**/**57** == 3:1, 1:1, and 1:3) were analyzed. The total peptide concentration in all cases was 1.0 mM. Five independent UV-Vis measurement were performed for each sample, and the resulting data were then classified by a linear discriminant analysis. Each spectrum consisted of 351 data points (350-700 nm, $\Delta\lambda$ = 1 nm), most of which are linearly dependent and, hence, contain no unique information about the analyte. We therefore employed a selection algorithm to choose the variables (wavelengths), which contribute the most to the differentiation between analytes. The selected variables were then used to calculate the classification functions and to generate score plots, which show the clustering of the data (Figure 5.16).

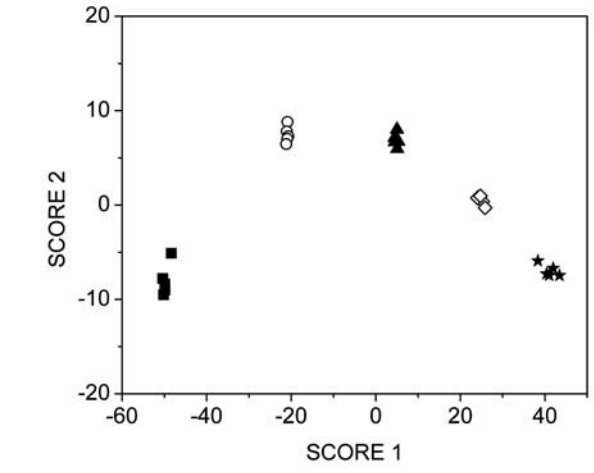

Figure 5.16 Two-dimensional LDA score plot for the analysis of the tripeptide **56** (stars), **57** (squares), and the mixture of the two peptides at the following ratios: **56**/**57** = 1:3 (circles), **56**/**57** = 1:1 (triangles), and **56**/**57** = 3:1 (diamonds).

The analysis evidenced that the sensor response permits the identification of the respective sample without any misclassification. It was, thus, possible to discriminate Gly-His-Gly (**56**) from Gly-Gly-His (**57**) and from mixtures of the two by a simple UV-Vis measurement. From Figure 5.16, it is also apparent that the resulting data can be used as a "calibration curve" to estimate the **56**/**57** ratio of samples with unknown composition.

In a second set of experiments, we investigated the possibility to simultaneously identify and quantify samples containing the peptide either **56** or **57**. For each peptide, four samples with a total concentration of 0.25, 0.5, 0.75, and 1.00 mM were analyzed by five independent UV-Vis measurements. The data were treated as described above. From the resulting LDA score plot (Figure 5.17), it is evident that the DCL sensor is, indeed, able to provide information about the nature *and* the amount of the respective peptide. The accuracy of a quantitative determination is estimated to be ± 10 μM.

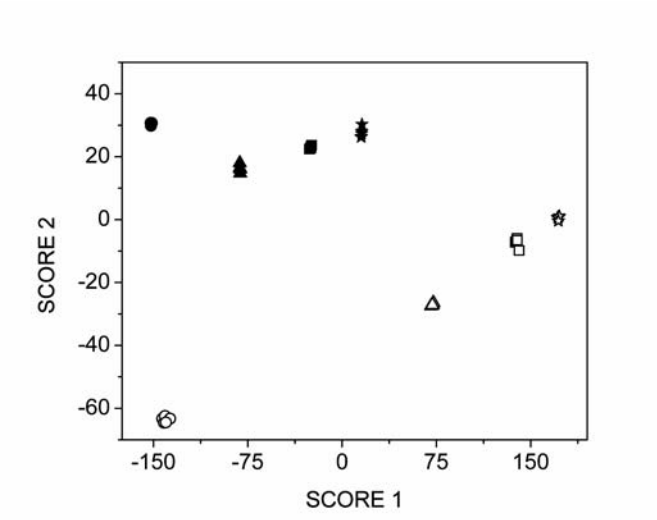

Figure 5.17 Two-dimensional LDA score plot for the analysis of the tripeptides **56** (filled symbols) and **57** (closed symbols) at various concentrations (0.25 mM, circles; 0.50 mM, triangles; 0.75 mM, squares; 1.00 mM, stars).

5.3. Conclusion

The results described above clearly demonstrate the potential of DCLs as sensors. The dynamic combinatorial library used in this study was obtained by mixing commercially available dyes with two transition-metal salts. Despite this simplicity, it was possible to differentiate closely related analytes such as stereoisomers Phe-Ala and D-Phe-Ala. It should

be noted that other adaptive systems which show a detectable response upon addition of an analyte can easily be envisioned. DCL based on compounds with a distinct redox potential or fluorescence, for example, are potentially well suited. The response could then be used to identify a single component or to classify a complex matrix.

DCL sensors are by definition complex chemical systems. Consequently, it is difficult to predict the sensor response for a given analyte. The lack of control is compensated by the fact that DCL sensors can easily be modified, and thus optimized. This key advantage is demonstrated by the results described in the section 5.2.2. A DCL sensor consisting of three dyes and two metal salts was optimized for the differentiation of sequence-isomeric tripeptides by screening the response of 20 sensors with a variable composition. The identity of the best sensor was found to depend on the problem that was addressed. The analytical power of the optimized sensor was sufficient to differentiate aqueous solutions containing a variable ratio of the tripeptides Gly-His-Gly and Gly-Gly-His and to obtain quantitative information about these analytes.

Chapter 6

Experimental part

6.1. General

6.1.1. Instruments

All UV-Vis spectra were recorded with a *Lambda 40* spectrometer (Perkin Elmer) with a 1 nm data interval. The spectra were recorded after an equilibration period (specified for each receptor-dye combination in the respective section). A *Spectra Max 340* (Molecular Devices) microplate reader was used to read 96-well microplates. A *692 pH/Ion Meter* (Metrohm) was used to measure the pH.

6.1.2. Reagents

The complex $[Cp^*RhCl_2]_2$ was synthesized in our laboratory using conventional methods.[165] Ligand **36** was synthesized using a published method.[88] All other reagents (buffers, dyes, peptides, amino acids, nucleotides, dansyl chloride, 8-aminoquinoline, copper and nickel chlorides, and sodium pyrophosphate) were commercially available and used as received without further purification. All stock solutions were prepared either in buffered or in pure aqueous solution. The details about the buffers used to prepare the stock solution of a particular reagent are provided in the respective section.

6.1.3. Buffers

Bidistilled water was used to prepare all solutions. To prepare stock solutions of the 2-(N-morpholino)ethansulfonic acid (MES) and 2-(N-cyclohexyl)aminoethansulfonic acid (CHES) the appropriate acid was dissolved in bidistilled water and the pH was adjusted with a 1.0 M solution of NaOH. The phosphate buffers with specific pHs were prepared by dissolving appropriate amounts of sodium dihydrogen phosphate and disodium hydrogenphosphate salts in bidistilled water.

6.1.4. Software

Gepasi (version 3.30)[99,100] and DATAN[116] software were used to calculate binding constants. Systat[163] (version 11.0) and Minitab (version 14.0) were used to perform linear discriminant and principal component analyses respectively. The software used to perform multi-layer perceptron neuronal network analysis was developed in the Institute of Geomatics and Analysis of Risk, University of Lausanne.[123]

6.2. Sequence-selective detection of histidine- and methionine-containing peptides

100 mM pH 7.0 phosphate buffer was used to prepare the stock solutions of the Rh-Cp* complex (**34**), azophloxine dye (**35**) and peptides. For competition experiments, the solution of a peptide was mixed with the solution of the **34** and then the solution of the dye **35** was added. All UV-Vis spectra were recorded after 10 minutes equilibration at 50^0 C. Gepasi software (version 3.30) was used to calculate the binding constants.

6.3. A chemosensor ensemble for the identification of 20 natural amino acids

6.3.1. General

Phosphate buffer (100 mM, pH 7.0) was employed for the stock solutions of complex **34** and the dyes **40**-**42**. Stock solutions of the amino acids were prepared in pure water. All UV-Vis measurements were performed after 1 hour equilibration time (r. t.).

6.3.2. UV-Vis analysis

For group I, solutions of respective amino acid (final concentration 0.05 mM), of complex **34** (final concentration 0.05 mM), of the buffer (CHES, MES, or phosphate; final concentration 90 mM) and of the dye (**41** or **42**, final concentration 0.15 mM) were mixed in a compartment of a 96-well plate. The absorbance at 345 nm (**41**) or 400 nm (**42**) was determined after equilibration. For group II, solutions of the respective amino acids (final concentration 0.75 mM), of complex **34** (final concentration 0.05 mM), of the respective buffer (CHES, MES, or phosphate; final concentration 85 mM) and of the dye **40** (final concentration 0.10 mM) were mixed in a compartment of a 96-well plate. The absorbance at 750 nm was determined after equilibration. For each amino acid, 12 measurements were carried out.

6.3.3. Data processing

The UV-Vis data was normalized in the following way: $A_{norm} = (A - A_{dye})/(A_{\mathbf{34}/dye} - A_{dye})$, where A corresponds to the measured absorption of an observation, A_{dye} to the adsorption of the pure dye solution (dye = **40**, **41** or **42**) and $A_{\mathbf{34}/dye}$ to the adsorption of the Rh-

Cp* complex of the dye **40**, **41** or **42** (Rh to dye ratio 1:1). This type of normalization gave values between 0 and 1 for all measurements. The normalized data have been used to perform a linear discriminant analysis or a principal component analysis using the statistical software Minitab (version 14.0) and Systat (version 11.0).

6.4. Pattern-based recognition of nucleotides with a multicomponent indicator displacement assay

Phosphate buffer (50 mM, pH 7.4) was used for all experiments. Stock solution were prepared with the buffer. All spectra were measured after 1 hour equilibration time.

6.5. Dynamic combinatorial libraries of dye complexes as sensors

CHES buffer (pH 8.4) was employed for stock solutions of the dyes **52-54**. Stock solutions of the peptides and metal salts were prepared in pure water. UV-Vis spectra were recorded after 30 minutes equilibration at 60^0 C (for the experiments with dipeptides) or after 2 hours equilibration at room temperature (for the experiments with tripeptides). The linear discriminant analysis was performed with the SYSTAT software. For each measurement, 351 data points (absorbance values in the region λ = 350-700 nm) were used as input. To determine the wavelengths, which contribute most to the differentiation, a variable selection algorithm was applied. The selected variables were then utilized to calculate the classification functions and to generate the score plots.

Chapter 7 *Annex*

7.1. Other dyes tested as potential indicators

Below we present the results of a small screening of commercially available dyes, which were tested as potential indicators (in combination with complex **34** as a receptor) for the displacement assay of nucleotides and the pyrophosphate anion. The dyes **40**, **45** and **46** were used in the final experiments (see Figure 4.3, Chapter 4). To be used as an indicator in the displacement assay, the dye(s) should fulfil the following criteria:

a) be soluble in the solvent to be used for the analysis (50 mM pH 7.4 phosphate buffer in our case)

b) have a reasonably high extinction coefficient

c) coordinate to the receptor (complex **34** in our case) with a concomitant change in color and with relatively fast exchange kinetics

d) the dye and its complex with the receptor should be stable in solution so as reproducible results can be obtained

e) be displaced by the analyte(s) of interest.

We used the amino acid phenylalanine as a "test" analyte as its affinity to the receptor (complex **34**) was expected to be in the same range as that of the nucleotides. The structures of the dyes (**58-74**) which, finally, were not used for the analysis, are depicted in Figure 7.1 and Figure 7.2. The particular reasons why these dyes were not used are given below.

Celestine blue (**61**) and alizarin (**68**) were not soluble in water. The extinction coefficient of aurintricarboxylic acid (**71**) was found to be too low. The dyes **58** and **59** produce no significant color change if mixed with the solution of the receptor **34**. Azomethine-H (**74**) was found to decompose in the buffer solution. The same was true for complexes of the dyes **63**, **69**, **70** with the Rh complex **34**. The dyes **60**, **64-66**, and **73** coordinated to **34**, but no displacement of the dye by the test analyte (phenylalanine) was observed. The dye **72** was potentially suitable for the analysis of nucleotides, but due to its similarity to **45**, it was not employed.

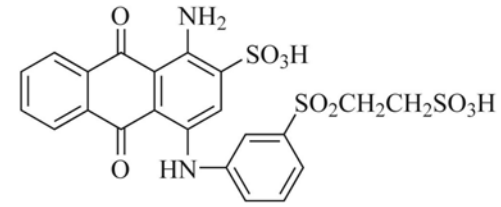

Remazol Brilliant Blue R (**58**)

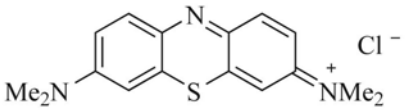

Methylene Blue (**59**)

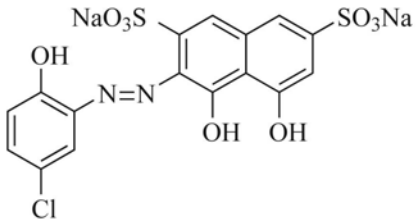

Mordant Blue 13 (**60**)

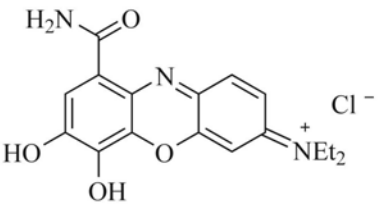

Celestine Blue (**61**)

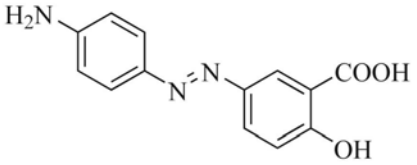

Mordant Yellow 12 (**62**)

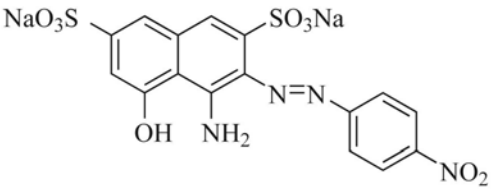

Nitro Red (**63**)

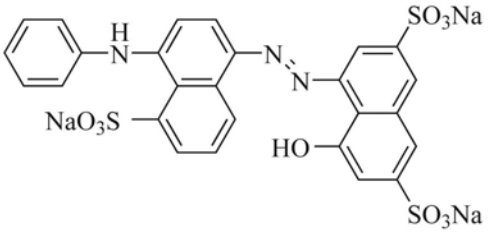

Acid Blue 92 (**64**)

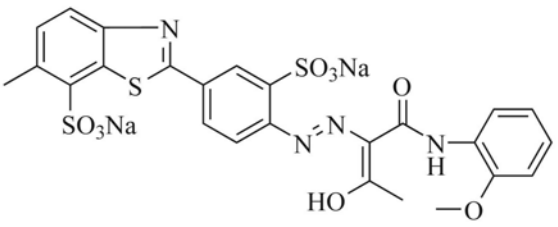

Direct Yellow 27 (**65**)

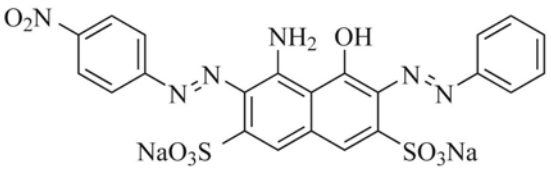

Naphtol Blue Black (**66**)

Figure 7.1 Commercially available dyes, which were tested in combination with the Cp*-Rh complex **34** for the analysis of nucleotides and the pyrophosphate anion (Chapter 4).

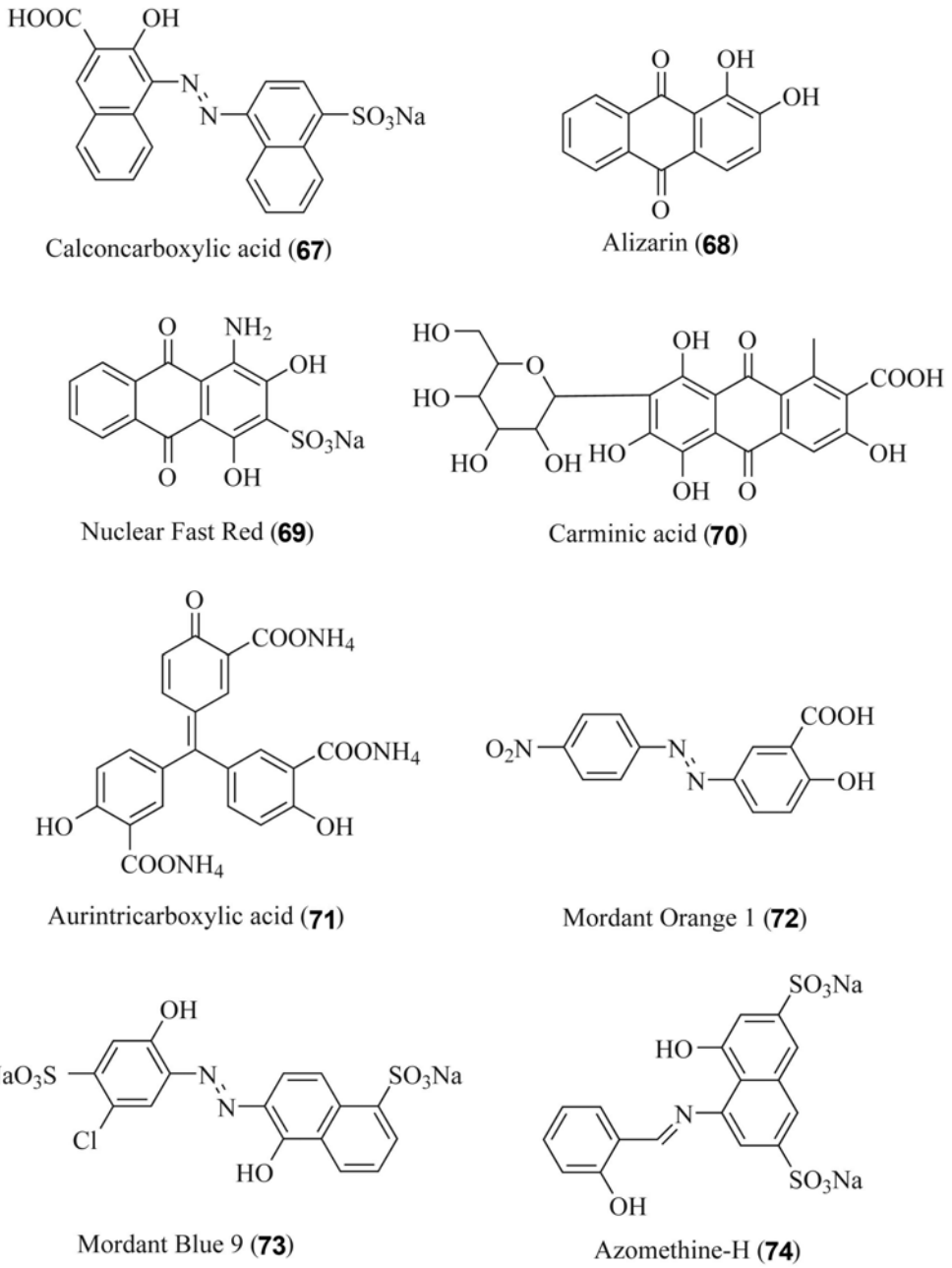

Figure 7.2 Commercially available dyes, which were tested in combination with the Cp*-Rh complex **34** for the analysis of nucleotides and the pyrophosphate anion (Chapter 4).

7.2. Fluorescent chemosensor for the pyrophosphate anion

In the course of our studies we found that the dye methylcalcein blue (**53**) can be used, together with the Rh complex **34**, as the fluorescent sensor for the pyrophosphate anion. The fluorescence of **53** is quenched to a substantial extent upon addition of **34**. In the presence of pyrophosphate, the fluorescence is restored proportionally to the concentration of the anion. However, we found that this can be explained from a kinetic point of view: the presence of the pyrophosphate anion slows down the formation of the complex between **53** and **34** (Figure 7.3). Further investigations are needed to explore this phenomenon.

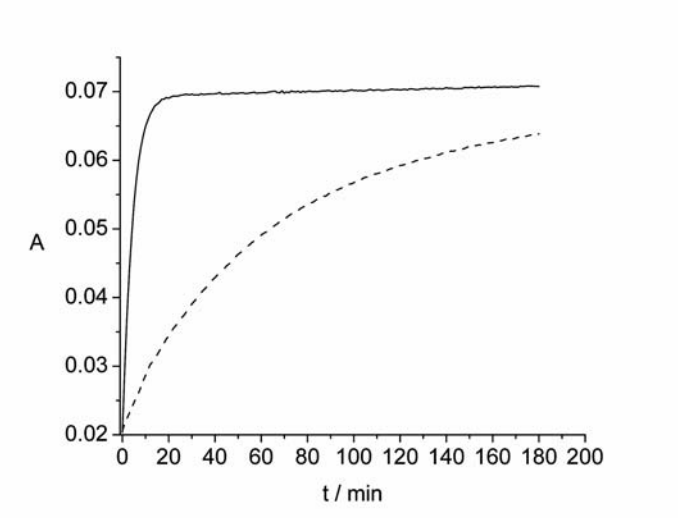

Figure 7.3 Absorbance at 410 nm for the reaction between Rh complex **34** (12.5 μM Rh) and the dye **53** (12.5 μM) with (dashed line) and without (solid line) pyrophosphate (250 μM). Conditions: 50 mM pH 7.4 MOPS buffer.

7.3. Crystallographic data

7.3.1. General

For data collection, a Mo Kα radiation on different equipment has been used: a marresearch mar345 IPDS (**75**) or KUMA CCD (**76**). Cell refinement and data reduction has been carried out with the aid of CrysAlis RED 1.7.1 β release.[166] All structures were refined using the full-matrix least-squares on F^2 with all non-H atoms anisotropically defined. The hydrogen atoms were placed in calculated positions using the "rigid model". Structure refinement and geometrical calculations were carried out on all structures with SHELXTL 5.1.[167,168]

7.3.2. Crystal structures of complexes 75 and 76

X-Ray structures of complexes **75** and **76** are presented in Figure 7.4 and Figure 7.5 respectively. Crystallographic data for these two complexes are given in Table 7.1.

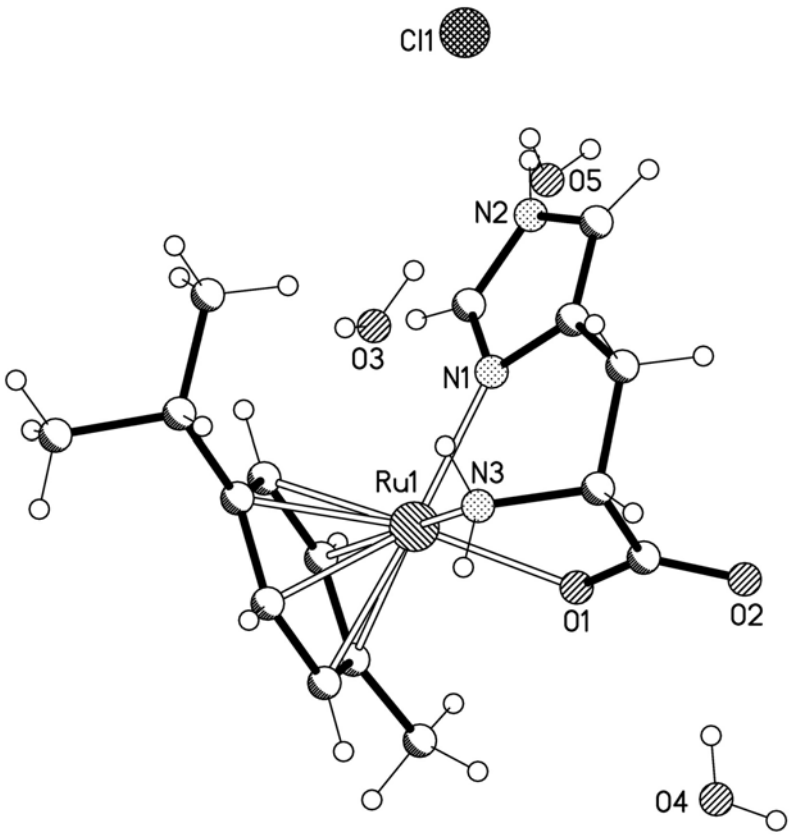

Figure 7.4 [(p-cymene)Ru(His)]Cl (**75**).

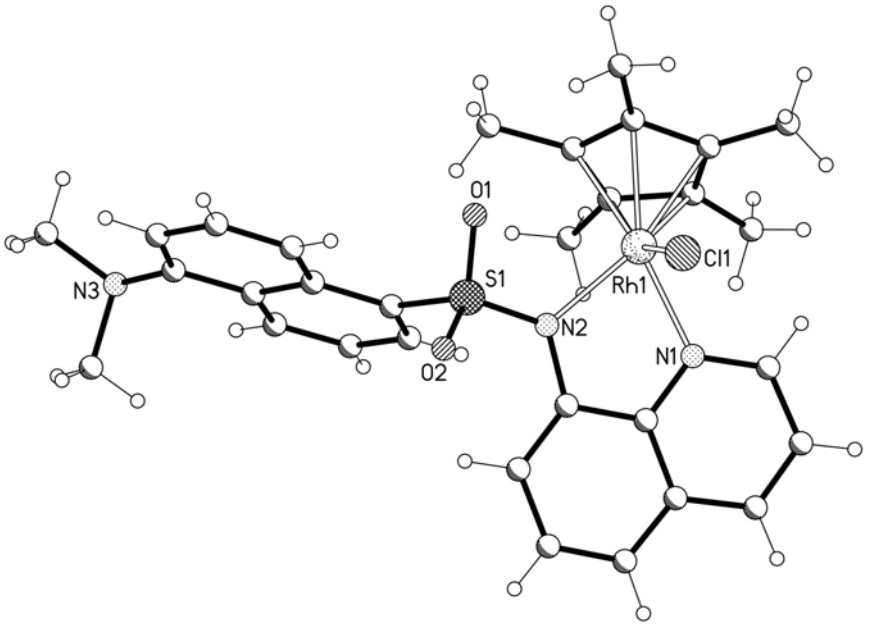

Figure 7.5 Complex **76**.

Table 7.1 Crystallographic data for complexes **75** and **76**.

	75	**76**
empirical formula	$C_{16}H_{28}ClN_3O_5Ru$	$C_{32}H_{37}ClN_3O_3RhS$
molecular weight / g*mol^{-1}	478.93	682.07
crystal system	monoclinic	monoclinic
space group	P2(1)	P2(1)/c
a / Å	9.110(4)	23.2012(12)
b / Å	11.9352(17)	15.3809(8)
c / Å	9.928(7)	8.6627(3)
α / º	90	90
β / º	110.07(4)	95.392(4)
γ / º	90	90
V / Å^3	1013.9	3077.6(2)
Z	2	4
d / g*cm^3	1.569	1.472

Table 7.1 Crystallographic data for complexes **75** and **76**.

	75	**76**
absorption coefficient / mm^{-1}	0.935	0.747
Θ range / ^{o}	2.93 to 25.02	3.18 to 25.03
index ranges	-10 => 10	-27 => 27
	-11 => 11	-17 => 18
	-13 => 13	-10 => 10
reflections collected	6118	17840
independent reflections	3348 [R_{int} = 0.0256]	5424 [R_{int} = 0.0417]
adsorption correction	semi-empirical from equivalents	none
max and min transmission	0.9051 and 0.8438	
data / restrains / parameters	3348 / 10 / 254	5424 / 0 / 370
goodness of fit on F^2	1.096	0.961
final R indices [$I > 2\sigma(I)$]	R_1 = 0.0311	R_1 = 0.0275
	wR_2 = 0.0659	wR_2 = 0.0590
R indices (all data)	R_1 = 0.0372	R_1 = 0.0431
	wR_2 = 0.075710	wR_2 = 0.0625
largest diff. peak / hole / e*$Å^{-3}$	1.222 / -0.537	0.395 / -0.743

In complex **75**, the Ru(1)-N(1) and Ru(1)-N(3) distances (2.130 and 2.124 Å) were found to be similar to the distances in complexes of the (cymene)Ru fragment with N,N[169] or N,O[80] chelates (with the ligands being an amino-oxazoline and 3-hydroxy-2-pyridone respectively). Contrary, the Ru(1)-O(1) bond length (2.115 Å) was found to be slightly longer than in (cymene)Ru complexes with N,O[80] or O,O[170] chelates (with the ligands being 3-hydroxy-2-pyridone and pyrocatechol respectively). In complex **76**, the Rh(1)-N(1) distance (2.086 Å) was found to be 0.05 Å shorter than Rh(1)-N(3) distance (2.134 Å) with the latter being very close to the Rh-N bond length in similar complexes between the Cp*Rh fragment and N,O[80] or N,N[171] chelating ligands (with the ligands being 3-hydroxy-2-pyridone and pyridyloxazoline respectively).

Chapter 8 *References*

[1] A. W. Czarnik, *Advances in supramolecular chemistry*, Vol. 3, JAI Press, Greenwich, Connecticut, **1993**.

[2] H.-G. Lohr, F. Vogtle, *Acc. Chem. Res*. **1985**, *18*, 65-72.

[3] M. Takagi, K. Ueno, *Top. Curr. Chem.* **1984**, *121*, 39-65.

[4] A. W. Czarnik, *Acc. Chem. Res*. **1994**, *27*, 302-308.

[5] P. D. Beer, J. Cadman, *Coord. Chem. Rev.* **2000**, *205*, 131-155.

[6] L. Fabbrizzi, M. Licchelli, G. Rabaioli, A. Taglietti, *Coord. Chem. Rev.* **2000**, *205*, 85-108.

[7] T. W. Bell, N. M. Hext, *Chem. Soc. Rev.* **2004**, *33*, 589-598.

[8] R. Martinez-Manez, F. Sancenon, *Chem. Rev.* **2003**, *103*, 4419-4476.

[9] C. Suksai, T. Tuntulani, *Chem. Soc. Rev.* **2003**, *32*, 192-202.

[10] B. T. Nguyen, E. V. Anslyn, *Coord. Chem. Rev.* **2006**, *250*, 3118-3127.

[11] A. P. de Silva, H. Q. N. Gunaratne, T. Gunnlaugsson, A. J. M. Huxley, C. P. McCoy, J. T. Rademacher, T. E. Rice, *Chem. Rev.* **1997**, *97*, 1515-1566.

[12] T. W. Bell, Z. Hou, Y. Luo, M. G. B. Drew, E. Chapoteau, B. P. Czech, A. Kumar, *Science* **1995**, *269*, 671-674.

[13] G. R. Deviprasad, F. D'Souza, *Chem. Comm.* **2000**, 1915-1916.

[14] N. B. Sankaran, S. Nishizawa, M. Watanabe, T. Uchida, N. Teramae, *J. Mat. Chem*. **2005**, *15*, 2755-2761.

[15] M. E. Huston, E. U. Akkaya, A. W. Czarnik, *J. Am. Chem. Soc*. **1989**, *111*, 8735-8737.

[16] K. Sook Kyung, B. Mi Yeon, L. Sang-Hyeon, N. Kensuke, C. Seon-Woog, Y. Juyoung, *J. Incl. Phenom. Macrocyc. Chem.* **2002**, *43*, 71-75.

[17] S. Mann, *Chem. Commun.* **2004**, 1-4.

[18] R. H. Yang, W. H. Chan, A. W. M. Lee, P. F. Xia, H. K. Zhang, K. A. Li, *J. Am. Chem. Soc.* **2003**, *125*, 2884-2885.

[19] D. Y. Sasaki, B. E. Padilla, *Chem. Commun.* **1998**, 1581-1582.

[20] B. C. Roy, B. Chandra, D. Hromas, S. Mallik, *Org. Lett.* **2003**, *5*, 11-14.

[21] D. R. Shnek, D. W. Pack, F. H. Arnold, D. Y. Sasaki, *Angew. Chem. Int. Ed. Engl.* **1995**, *34*, 905-907.

[22] S. Wiskur, H. Ait-Haddou, E. Anslyn, J. Lavigne, *Acc. Chem. Res.* **2001**, *34*, 963-972.

[23] E. V. Anslyn, *J. Org. Chem.* **2007**, *72*, 687-699.

[24] M. J. Perry, in *Monoclonal Antibody: Principles and Applications*, Wiley-Liss, New-York, **1995**.

[25] A. M. Piatek, Y. J. Bomble, S. L. Wiskur, E. V. Anslyn, *J. Am. Chem. Soc.* **2004**, *126*, 6072-6077.

[26] M. Inouye, K.-I. Hashimoto, K. Isagawa, *J. Am. Chem. Soc.* **1994**, *116*, 5517-5518.

[27] K. N. Koh, K. Araki, A. Ikeda, H. Otsuka, S. Shinkai, *J. Am. Chem. Soc.* **1996**, *118*, 755-758.

[28] A. Metzger, E. V. Anslyn, *Angew. Chem. Int. Ed.* **1998**, *37*, 649-652.

[29] J. J. Lavigne, E. V. Anslyn, *Angew. Chem. Int. Ed.* **1999**, *38*, 3666-3669.

[30] K. Niikura, A. Metzger, E. V. Anslyn, *J. Am. Chem. Soc.* **1998**, *120*, 8533-8534.

[31] S. E. Schneider, S. N. O'Neil, E. V. Anslyn, *J. Am. Chem. Soc.* **2000**, *122*, 542-543.

[32] H. Ait-Haddou, S. L. Wiskur, V. M. Lynch, E. V. Anslyn, *J. Am. Chem. Soc.* **2001**, *123*, 11296-11297.

[33] Z. Zhong, E. V. Anslyn, *J. Am. Chem. Soc.* **2002**, *124*, 9014-9015.

[34] S. L. Tobey, E. V. Anslyn, *Org. Lett.* **2003**, *5*, 2029-2031.

[35] A. T. Wright, E. V. Anslyn, *Org. Lett.* **2004**, *6*, 1341-1344.

[36] L. Zhu, E. V. Anslyn, *J. Am. Chem. Soc.* **2004**, *126*, 3676-3677.

[37] T. Zhang, E. V. Anslyn, *Tetrahedron* **2004**, *60*, 11117-11124.

[38] J. F. Folmer-Andersen, V. M. Lynch, E. V. Anslyn, *J. Am. Chem. Soc.* **2005**, *127*, 7986-7987.

[39] P. A. Gale, L. J. Twyman, C. I. Handlin, J. L. Sessler, *Chem. Commun.* **1999**, 1851-1852.

[40] S. Atilgan, E. U. Akkaya, *Tetrahedron Lett.* **2004**, *45*, 9269-9271.

[41] S. A. Hilderbrand, M. H. Lim, S. J. Lippard, *J. Am. Chem. Soc.* **2004**, *126*, 4972-4978.

[42] C. Yin, F. Gao, F. Huo, P. Yang, *Chem. Commun.* **2004**, 934-935.

[43] M. Boiocchi, M. Bonizzoni, L. Fabbrizzi, G. Piovani, A. Taglietti, *Angew. Chem. Int. Ed.* **2004**, *43*, 3847-3852.

[44] L. Fabbrizzi, N. Marcotte, F. Stomeo, A. Taglietti, *Angew. Chem. Int. Ed.* **2002**, *41*, 3811-3814.

[45] M. A. Hortala, L. Fabbrizzi, N. Marcotte, F. Stomeo, A. Taglietti, *J. Am. Chem. Soc.* **2003**, *125*, 20-21.

[46] W. N. Lipscomb, N. Strater, *Chem. Rev.* **1996**, *96*, 2375-2434.

[47] L. Fabbrizzi, F. Foti, A. Taglietti, *Org. Lett.* **2005**, *7*, 2603-2606.

[48] L. Fabbrizzi, A. Leone, A. Taglietti, *Angew. Chem. Int. Ed.* **2001**, *40*, 3066-3069.

[49] M. Bonizzoni, L. Fabbrizzi, G. Piovani, A. Taglietti, *Tetrahedron* **2004**, *60*, 11159-11162.

[50] F. F. Robert, *Angew. Chem. Int. Ed.* **1999**, *38*, 1870-1880.

[51] D. A. Wink, Y. Vodovotz, J. Laval, F. Laval, M. W. Dewhirst, J. B. Mitchell, *Carcinogenesis* **1998**, *19*, 711-721.

[52] C. Vittorio, B. Timothy Edward, S. Anna Maria Giuffrida, Neurochemical Research 2000, 25, 1315-1341.

[53] B. Malnic, J. Hirono, T. Sato, L. B. Buck, *Cell* **1999**, *96*, 713-723.

[54] D. Lancet, N. Ben-Arie, *Curr. Biol.* **1993**, *3*, 668-674.

[55] P. C. Jurs, G. A. Bakken, H. E. McClelland, *Chem. Rev.* **2000**, *100*, 2649-2678.

[56] K. J. Albert, N. S. Lewis, C. L. Schauer, G. A. Sotzing, S. E. Stitzel, T. P. Vaid, D. R. Walt, *Chem. Rev.* **2000**, *100*, 2595-2626.

[57] T. Nakamoto, K. Fukunishi, T. Moriizumi, *Sensors and Actuators B*, **1990**, *1*, 473-476.

[58] T. Nakamoto, A. Fukuda, T. Moriizumi, *Sensors and Actuators B,* **1993**, *10*, 85-90.

[59] J. A. J. Brunink, C. Di Natale, F. Bungaro, F. A. M. Davide, A. D'Amico, R. Paolesse, T. Boschi, M. Faccio, G. Ferri, *Anal. Chim. Acta* **1996**, *325*, 53-64.

[60] P. Corcoran, H. V. Shurmer, J. W. Gardner, *Sensors and Actuators B*, **1993**, *15*, 32-37.

[61] J. W. Gardner, A. Pike, N. F. De Rooij, M. Koudelka-Hep, P. A. Clerc, A. Hierlemann, W. Gopel, *Sensors and Actuators B,* **1995**, *26*, 135-139.

[62] M. C. Lonergan, E. J. Severin, B. J. Doleman, S. A. Beaber, R. H. Grubbs, N. S. Lewis, *Chem. Mater.* **1996**, *8*, 2298-2312.

[63] K. C. Persaud, *Trends Anal. Chem.* **1992**, *11*, 61-67.

[64] J. V. Hatfield, P. Neaves, P. J. Hicks, K. Persaud, P. Travers, *Sensors and Actuators B,* **1994**, *18*, 221-228.

[65] L. Baldini, A. J. Wilson, J. Hong, A. D. Hamilton, *J. Am. Chem. Soc.* **2004**, *126*, 5656-5657.

[66] C. Zhang, K. S. Suslick, *J. Am. Chem. Soc.* **2005**, *127*, 11548-11549.

[67] N. T. Greene, S. L. Morgan, K. D. Shimizu, *Chem. Comm.* **2004**, 1172-1173.

[68] N. T. Greene, K. D. Shimizu, *J. Am. Chem. Soc.* **2005**, *127*, 5695-5700.

[69] A. Buryak, K. Severin, *Angew. Chem. Int. Ed.* **2004**, *43*, 4771-4774.

[70] H.-J. Schneider, *Angew. Chem. Int. Ed. Engl.* **1993**, *32*, 848-850.

[71] M. W. Peczuh, A. D. Hamilton, *Chem. Rev.* **2000**, *100*, 2479-2494.

[72] T. Mizutani, K. Wada, S. Kitagawa, *Chem. Comm.* **2002**, 1626-1627.

[73] M. Sirish, H.-J. Schneider, *Chem. Comm.* **1999**, 907-908.

[74] C. Schmuck, M. Heil, *ChemBioChem* **2003**, *4*, 1232-1238.

[75] C. Schmuck, M. Heil, *Chem. Eur. J.* **2006**, *12*, 1339-1348.

[76] C. Schmuck, M. Heil, J. Scheiber, K. Baumann, *Angew. Chem. Int. Ed.* **2005**, *44*, 7208-7212.

[77] Z. Grote, M.-L. Lehaire, R. Scopelliti, K. Severin, *J. Am. Chem. Soc.* **2003**, *125*, 13638-13639.

[78] M.-L. Lehaire, R. Scopelliti, H. Piotrowski, K. Severin, *Angew. Chem. Int. Ed.* **2002**, *41*, 1419-1422.

[79] H. Piotrowski, K. Polborn, G. Hilt, K. Severin, *J. Am. Chem. Soc.* **2001**, *123*, 2699-2700.

[80] H. Piotrowski, G. Hilt, A. Schulz, P. Mayer, K. Polborn, K. Severin, *Chem. Eur. J.* **2001**, *7*, 3196-3208.

[81] H. Piotrowski, K. Severin, *Proc. Nat. Ac. Sci.* **2002**, *99*, 4997-5000.

[82] K. Severin, *Coord. Chem. Rev.* **2003**, *245*, 3-10.

[83] F. A. Dunand, L. Helm, A. E. Merbach, in *Advances in Inorganic Chemistry*, Vol. Volume 54, Academic Press, **2003**, pp. 1-69.

[84] F. Hintermaier, F. Kühlwein, C. Robl, W. Beck, *Zeitschrift für anorganische und allgemeine Chemie* **1995**, *621*, 829-836.

[85] K. Severin, R. Bergs, W. Beck, *Angew. Chem. Int. Ed.* **1998**, *37*, 1634-1654.

[86] D. V. Deubel, *J. Am. Chem. Soc.* **2004**, *126*, 5999-6004.

[87] J. C. Miller, J. N. Miller, in *Statistics for Analytical Chemistry*, Ellis Horwood Limited, Chichester, **1984**, pp. 96-100.

[88] P. Jiang, L. Chen, J. Lin, Q. Liu, J. Ding, X. Gao, Z. Guo, *Chem. Commun.* **2002**, 1424-1425.

[89] A. Buryak, K. Severin, *J. Am. Chem. Soc.* **2005**, *127*, 3700-3701.

[90] S. C. McCleskey, P. N. Floriano, S. L. Wiskur, E. V. Anslyn, J. T. McDevitt, *Tetrahedron* **2003**, *59*, 10089-10092.

[91] S. L. Wiskur, P. N. Floriano, E. V. Anslyn, J. T. McDevitt, *Angew. Chem. Int. Ed.* **2003**, *42*, 2070-2072.

[92] S. C. McCleskey, M. J. Griffin, S. E. Schneider, J. T. McDevitt, E. V. Anslyn, *J. Am. Chem. Soc.* **2003**, *125*, 1114-1115.

[93] S.-Y. Liu, L. Fang, Y.-B. He, W.-H. Chan, K.-T. Yeung, Y.-K. Cheng, R.-H. Yang, *Org. Lett.* **2005**, *7*, 5825-5828.

[94] M. S. Han, D. H. Kim, *Tetrahedron* **2004**, *60*, 11251-11257.

[95] D. Zhang, M. Zhang, Z. Liu, M. Yu, F. Li, T. Yi, C. Huang, *Tetrahedron Lett.* **2006**, *47*, 7093-7096.

[96] N. Shao, J. Y. Jin, S. M. Cheung, R. H. Yang, W. H. Chan, T. Mo, *Angew. Chem. Int. Ed.* **2006**, *45*, 4944-4948.

[97] J. F. Folmer-Andersen, V. M. Lynch, E. V. Anslyn, *Chem. Eur. J.* **2005**, *11*, 5319-5326.

[98] M. Fokkens, T. Schrader, F.-G. Klarner, *J. Am. Chem. Soc.* **2005**, *127*, 14415-14421.

[99] P. Mendes, *Trends Biochem. Sci.* **1997**, *22*, 361-363.

[100] P. Mendes, *Comp. Appl. Biosci.* **1993**, *9*, 563-571.

[101] A.Buryak, K. Severin, *Chem.Comm.*, **2007**, 2366-2368.

[102] J. Y. Kwon, N. J. Singh, H. N. Kim, S. K. Kim, K. S. Kim, J. Yoon, *J. Am. Chem. Soc.* **2004**, *126*, 8892-8893.

[103] S. Mizukami, T. Nagano, Y. Urano, A. Odani, K. Kikuchi, *J. Am. Chem. Soc.* **2002**, *124*, 3920-3925.

[104] A. Ojida, S.-k. Park, Y. Mito-oka, I. Hamachi, *Tetrahedron Lett.* **2002**, *43*, 6193-6195.

[105] D. H. Lee, S. Y. Kim, J.-I. Hong, *Angew. Chem. Int. Ed.* **2004**, *43*, 4777-4780.

[106] C. Li, M. Numata, M. Takeuchi, S. Shinkai, *Angew. Chem. Int. Ed.* **2005**, *44*, 6371-6374.

[107] S. Yamaguchi, I. Yoshimura, T. Kohira, S. Tamaru, I. Hamachi, *J. Am. Chem. Soc.* **2005**, *127*, 11835-11841.

[108] C. Bazzicalupi, A. Bencini, L. Bussotti, E. Berni, S. Biagini, E. Faggi, P. Foggi, C. Giorgi, A. Lapini, A. Marcelli, B. Valtancoli, *Chem. Comm.* **2007**, 1230-1232.

[109] H. W. Rhee, H. Y. Choi, K. Han, J. I. Hong, *J. Am. Chem. Soc*. **2007**, *129*, 4524-4525.

[110] L. Fabbrizzi, M. Licchelli, A. Taglietti, *Dalt. Trans.* **2003**, 3471-3479.

[111] A. Buryak, K. Severin, *Angew. Chem. Int. Ed.* **2005**, *44*, 7935-7938.

[112] A. Buryak, K. Severin, *J. Comb. Chem* **2006**, *8*, 540-543.

[113] A. T. Wright, E. V. Anslyn, *Chem. Soc. Rev.* **2006**, 14-28.

[114] F. Zaubitzer, A. Buryak, K. Severin, *Chem. Eur. J.* **2006**, *12*, 3928-3934.

[115] R. H. Fish, *Coord. Chem. Rev.* **1999**, *185-186*, 569-584.

[116] www.multid.se.

[117] R. K. Sunahara, C. W. Dessauer, A. G. Gilman, *Ann. Rev. Pharmacol. Toxicol.* **1996**, *36*, 461-480.

[118] J. L. Bos, *Nat. Rev. Mol. Cell Biol.* **2003**, *4*, 733-738.

[119] Y. Salomon, C. Londos, M. Rodbell, *Anal. Biochem.* **1974**, *58*, 541-548.

[120] M. D. Smigel, *J. Biol. Chem.* **1986**, *261*, 1976-1982.

[121] R. K. Sunahara, C. W. Dessauer, R. E. Whisnant, C. Kleuss, A. G. Gilman, *J. Biol. Chem.* **1997**, *272*, 22265-22271.

[122] S. Haykin, *Neural Networks: A Comprehensive Foundation*, Prentice Hall Int., **1999**.

[123] M. Kanevski, A. Pozdnoukhov, V. Timonin, *Machine Learning Algorithms for Spatial Data Analysis and Modelling. Theory and Case Studies*, Press Polytechnique et Universitaires Romandes, Lausanne, **2007** (in press).

[124] S. Otto, *J. Mat. Chem.* **2005**, *15*, 3357-3361.

[125] J. D. Cheeseman, A. D. Corbett, J. L. Gleason, R. J. Kazlauskas, *Chem. Eur. J.* **2005**, *11*, 1708-1716.

[126] J.-L. Reymond, *Angew. Chem. Int. Ed.* **2004**, *43*, 5577-5579.

[127] O. Ramstrom, T. Bunyapaiboonsri, S. Lohmann, J.-M. Lehn, *Biochim. Biophys. Acta* **2002**, *1572*, 178-186.

[128] J.-M. Lehn, *Proc. Nat. Ac. Sci.* **2002**, *99*, 4763-4768.

[129] S. J. Rowan, S. J. Cantrill, G. R. L. Cousins, J. K. M. Sanders, J. F. Stoddart, *Angew. Chem. Int. Ed.* **2002**, *41*, 898-952.

[130] S. Otto, R. L. E. Furlan, J. K. M. Sanders, *Curr. Op. Chem. Biol.* **2002**, *6*, 321-327.

[131] I. Huc, J.-M. Lehn, *Proc. Nat. Ac. Sci.* **1997**, *94*, 2106-2110.

[132] T. Hotchkiss, H. B. Kramer, K. J. Doores, D. P. Gamblin, N. J. Oldham, B. G. Davis, *Chem. Comm.* **2005**, 4264-4266.

[133] R. T. S. Lam, A. Belenguer, S. L. Roberts, C. Naumann, T. Jarrosson, S. Otto, J. K. M. Sanders, *Science* **2005**, *308*, 667-669.

[134] S. Zameo, B. Vauzeilles, J.-M. Beau, *Angew. Chem. Int. Ed.* **2005**, *44*, 965-969.

[135] A. Bugaut, J.-J. Toulmé, B. Rayner, *Angew. Chem. Int. Ed.* **2004**, *43*, 3144-3147.

[136] M. Albrecht, I. Janser, J. Runsink, G. Raabe, P. Weis, R. Fröhlich, *Angew. Chem. Int. Ed.* **2004**, *43*, 6662-6666.

[137] R. Larsson, Z. Pei, O. Ramström, *Angew. Chem. Int. Ed.* **2004**, *43*, 3716-3718.

[138] K. Severin, *Chem. Eur. J.* **2004**, *10*, 2565-2580.

[139] P. T. Corbett, L. H. Tong, J. K. M. Sanders, S. Otto, *J. Am. Chem. Soc.* **2005**, *127*, 8902-8903.

[140] Z. Grote, R. Scopelliti, K. Severin, *Angew. Chem. Int. Ed.* **2003**, *42*, 3821-3825.

[141] N. Giuseppone, J. M. Lehn, *J. Am. Chem. Soc.* **2004**, *126*, 11448-11449.

[142] J. S. Fritz, M. Johnson-Richard, *Anal. Chim. Acta* **1959**, *20*, 164-171.

[143] B. Budesinsky, *Fres. J. Anal. Chem.* **1965**, *207*, 247-256.

[144] H. Khalifa, Y. M. Issa, *Microchem. J.* **1975**, *20*, 287-291.

[145] H. Yoshida, T. Ozawa, K. Jitsukawa, H. Einaga, *Polyhedron* **1993**, *12*, 1319-1328.

[146] G. M. Huitink, H. Diehl, *Talanta* **1974**, *21*, 1193-1202.

[147] H. G. Brittain, *Anal. Chem.* **1987**, *59*, 1122-1125.

[148] B. Budesinsky, J. Gurovic, *Collect. Czech. Chem. Commun.* **1963**, *28*, 1154-1161.

[149] I. V. Pyatnitskii, L. L. Kolomiets, V. S. Barshchevskaya, *J. Anal. Chem. (Moscow)* **1989**, *44*, 450-454.

[150] P. MacCarthy, *Anal. Chem.* **1978**, *50*, 2165-2165.

[151] P. K. Sudeep, S. T. S. Joseph, K. G. Thomas, *J. Am. Chem. Soc.* **2005**, *127*, 6516-6517.

[152] M. Kruppa, C. Mandl, S. Miltschitzky, B. Konig, *J. Am. Chem. Soc.* **2005**, *127*, 3362-3365.

[153] C.-F. Chow, B. K. W. Chiu, M. H. W. Lam, W.-Y. Wong, *J. Am. Chem. Soc.* **2003**, *125*, 7802-7803.

[154] Chung-Yin Lin, D.-F. Tai, T.-Z. Wu, *Chem. Eur. J.* **2003**, *9*, 5107-5110.

[155] K. E. S. Dean, G. Klein, O. Renaudet, J.-L. Reymond, *Bioorg. Med. Chem. Lett.* **2003**, *13*, 1653-1656.

[156] G. Klein, J.-L. Reymond, *Angew. Chem. Int. Ed.* **2001**, *40*, 1771-1773.

[157] H. Sigel, B. Martin, *Chem. Rev.* **1982**, *82*, 385-426.

[158] B. K. Lavine, J. J. J. Workman, *Anal. Chem.* **2004**, *76*, 3365-3372.

[159] A. de Juan, R. Tauler, *Anal. Chim. Acta* **2003**, *500*, 195-210.

[160] P. Geladi, S*pectrochim. Acta B* **2003**, *58*, 767-782.

[161] P. Geladi, B. Sethson, J. Nystrom, T. Lillhongad, T. Lestander, J. Burger, S*pectrochim. Acta B* **2003**, *59*, 1347-1357.

[162] P. K. Hopke, *Anal. Chim. Acta* **2003**, *500*, 365-377.

[163] SYSTAT, vesrion 11, Systat Software Inc., Richemond, California, USA.

[164] H. Kozlowski, W. Bal, M. Dyba, T. Kowalik-Jankowska, *Coord. Chem. Rev.* **1999**, *184*, 319-346.

[165] C. White, A. Yates, P.M. Maitlis, *Inorg. Synth.* **1992**, *29*, 228-234.

[166] Oxford Diffraction Ltd.:Abingdon, Oxfordshire, U.K., **2005**.

[167] G. M. Sheldrick, SHELXTL, University of Gottingen: Gottingen, Germany, **1997**.

[168] BrukerAXS, Inc.: Madison, WI, **1997**.

[169] M. Gomez, S. Jansat, G. Muller, G. Aullon, M. A. Maestro, *Eur. J. Inorg. Chem.* **2005**, 4341-4351.

[170] M. Melchart, A. Habtemariam, S. Parsons, S. A. Moggach, P. J. Sadler, *Inorg. Chim. Acta* **2006**, *359*, 3020-3028.

[171] D. L. Davies, J. Fawcett, S. A. Garratt, D. R. Russel, *Dalton Trans*. **2004**, 3629-3634.

Curriculum Vitae

Andrey BURYAK

26 years old - Single - Russian

andrey.buryak@epfl.ch

Cotes de la Bourdonnette 8

CH - 1007 Lausanne

+41 77 412 74 26

----------EDUCATION ----------

2003-2007 Ph. D. in Chemistry (in progress) at the **École Polytechnique Fédérale de Lausanne** (EPFL) - Institut des Sciences et Ingénierie Chimiques, advisor: **Prof. Kay Severin** - *Metal-Based Chemosensors for Amino Acids, Peptides, and Nucleotides.*

1998-2003 Master of Science in Chemistry with honor at the **Moscow State University**, Moscow, Russia. Diploma work - *Moleclar Imprinting Effect on Silica Gel Modified with Alkoxysilanes* - supervisor **Prof. Lisichkin G. V.**

1998 School Diploma with honor at the School no. 68, Ryazan, Russia

----------RESEARCH AND TEACHING SKILLS----------

SCIENTIFIC TECHNIQUES:

- Handling air and moisture sensitive chemical products using Schlenk glassware and glovebox techniques
- Standard ^{1}H, ^{13}C NMR; UV-Vis, IR and fluorescent spectroscopy
- High performance liquid chromatorgaphy (HPLC)
- Multivariate analysis (principal component and linear discriminant analyses)

ASSISTANTSHIP:

Practical work for the 1st and 3rd years students in chemistry

----------CONFERENCED ATTENDED----------

- Poster at the CHUV Research day, 2007, Lausanne
- Oral presentation at the SCS Fall Meeting, 2006, Zurich
- Flash poster presentation at the 3rd International Symposium on Bioorganometallic Chemistry, 2006, Milan
- Poster at the SCS Fall Meeting , 2005, Lausanne

- Poster at the 4th COST Chemistry Symposium, 2005, Lausanne

- Poster at the SCS Fall Meeting, 2004, Zurich

----------PUBLICATIONS----------

xx. Agent-Based Modeling of Self-Assembled Molecular Macrocycles
Grégory Mermoud, Nikolaus Correll, Andrey Buryak, Alcherio Martinoli, Kay Severin
in preparation.

8. Pattern-Based Sensing of Nucleotides in Aqueous Solution with a Multicomponent Indicator Displacement Assay
A. Buryak, K. Severin
Chem. Comm. **2007**, 2366-2368.

7. Combinatorial Optimization of a Colorimetric Sensor for Tripeptides
A. Buryak, K. Severin
J. Comb. Chem. **2006**, 8, 540-543.

6. Cp*Rh-Based Indicator Displacement Assays for the Identification of Amino Sugars and Aminoglycosides
F. Zaubitzer, A. Buryak, K. Severin
Chem. Eur. J. **2006**, 12, 3928-3934.

5. Dynamic Combinatorial Libraries of Dye Complexes as Sensors (VIP PAPER)
A. Buryak, K. Severin
Angew. Chem. Int. Ed. **2005**, 44, 7935-7938.

4. A Chemosensor Array for the Colorimetric Identification of 20 Natural Amino Acids
A. Buryak, K. Severin
J. Am. Chem. Soc., **2005**, 127, 3700-3701.

3. An Organometallic Chemosensor for the Sequence-Selective Detection of Histidine- and Methionine-Containing Peptides in Water at Neutral pH
A. Buryak, K. Severin
Angew. Chem. Int. Ed. **2004**, 43, 4771-4774.

2. [η^6-2-(2-Methylbenzoyloxy)ethylmethacrylate]bis(η^6-1,2,4,5-tetramethylbenzene)tri-μ-hydrido-μ^3-oxo-triruthenium(II)(3 Ru-Ru) tetrafluoroborate
L. Vieille-Petit, B. Therrien, A. Buryak, K. Severin, G. Süss-Fink
Acta Cryst. **2004**, E60, m1909-m1911

1. Synthesis of a Metallamacrocyclic $Re(CO)_3$ Complex Using a Tridentate Bridging Ligand
T. Brasey, A. Buryak, R. Scopelliti, K. Severin
Eur. J. Inorg. Chem. **2004**, 964-967.